



FAKULTÄT MASCHINENBAU

Master of Science in Manufacturing Technology

Fachgebiet Werkstoffprüftechnik

Prof. Dr.-Ing. habil. Frank Walther

M a s t e r T h e s i s

The effects of grain refinement on the mechanical properties of aluminium cast alloys used in automotive industry

by

Onur Özaydın

Registration Number: 162924

Supervisors:

Prof. Dr.-Ing. habil. Frank Walther

Asisst. Prof. Dr. Mehmet İpekoğlu

Submitted on 18.06.2015

Master Thesis

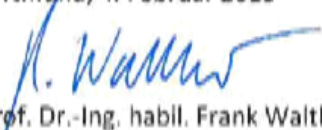
Name: Onur Ozaydin
Supervisor: Dipl.-Wirt.-Ing. Sebastian Myslicki, M.Sc. Shafaqat Siddique
Title: The effects of grain refinement on the mechanical properties of aluminium cast alloys used in automotive industry

Microstructural parameters like secondary dendrite arm spacing (SDAS) strongly influence the quasistatic and, especially, fatigue properties of aluminium castings. The size of these parameters, in turn, depends on different refining elements like Ti and B. To control these microstructural parameters, the influence of grain refinement must be investigated. This master thesis will analyze the influence of grain refinement on the mechanical properties of cast aluminium alloy (AlSi6Cu4) used in automotive industry for cylinder heads.

After literature survey, the current state of the art in the optimum percentage of refining elements will be determined and a framework for improving the mechanical properties will be developed. Refining elements will be added at different levels to check their influence on SDAS values. After grain refinement, stress relief will be carried out over half of the specimens, so that the influence of post-refinement stress relief on the mechanical properties could also be investigated. The specimens will be extracted from the cylinder heads from the critical areas. Microscopic analysis would be carried out to measure the SDAS values. The optimum percentage of the refining elements for the required SDAS values will be determined. Quasistatic mechanical properties as well as fatigue properties will be investigated so that optimum percentage of Ti and B can be determined for highest ultimate tensile strength and yield strength values. Woehler curves will be generated and the resulting life will be compared with the predetermined life cycles required for the product for conformance to the performance criteria.

All the practical work will be carried out at CEVHER Aluminium Foundry in Turkey.

Dortmund, 4. Februar 2015


(Prof. Dr.-Ing. habil. Frank Walther)

Eidesstattliche Versicherung

Özaydin, Onur

162924

Name, Vorname

Matr.-Nr.

Ich versichere hiermit an Eides statt, dass ich die vorliegende Bachelorarbeit/Masterarbeit* mit dem

Titel The effects of grain refinement on the mechanical
properties of aluminium cast alloys used in automotive
industry

selbstständig und ohne unzulässige fremde Hilfe erbracht habe. Ich habe keine anderen als die angegebenen Quellen und Hilfsmittel benutzt sowie wörtliche und sinngemäße Zitate kenntlich gemacht. Die Arbeit hat in gleicher oder ähnlicher Form noch keiner Prüfungsbehörde vorgelegen.

İzmir, 18.06.2015



Ort, Datum

Unterschrift

*Nichtzutreffendes bitte streichen

Belehrung:

Wer vorsätzlich gegen eine die Täuschung über Prüfungsleistungen betreffende Regelung einer Hochschulprüfungsordnung verstößt, handelt ordnungswidrig. Die Ordnungswidrigkeit kann mit einer Geldbuße von bis zu 50.000,00 € geahndet werden. Zuständige Verwaltungsbehörde für die Verfolgung und Ahndung von Ordnungswidrigkeiten ist der Kanzler/die Kanzlerin der Technischen Universität Dortmund. Im Falle eines mehrfachen oder sonstigen schwerwiegenden Täuschungsversuches kann der Prüfling zudem exmatrikuliert werden. (§ 63 Abs. 5 Hochschulgesetz - HG -)

Die Abgabe einer falschen Versicherung an Eides statt wird mit Freiheitsstrafe bis zu 3 Jahren oder mit Geldstrafe bestraft.

Die Technische Universität Dortmund wird gfls. elektronische Vergleichswerkzeuge (wie z.B. die Software „turnitin“) zur Überprüfung von Ordnungswidrigkeiten in Prüfungsverfahren nutzen.

Die oben stehende Belehrung habe ich zur Kenntnis genommen:

İzmir, 18.06.2015
Ort, Datum


Unterschrift

Abstract

Microstructural parameters like secondary dendrite arm spacing (SDAS) strongly influence the quasistatic and, especially, fatigue properties of aluminium castings. The size of these parameters, in turn, depends on different refining elements like Ti and B. To control these microstructural parameters, the influence of grain refinement must be investigated. This study analyzes the influence of grain refinement on the mechanical properties of cast aluminium alloy (AlSi6Cu4) used in automotive industry for cylinder heads.

After literature survey, the current state of the art in the optimum percentage of refining elements has been determined and a framework for improving the mechanical properties has been developed. Refining elements have been added at different levels to check their influence on SDAS values. Microscopic analysis would be carried out to measure the SDAS values. The optimum percentage of the refining elements for the required SDAS values has been determined.

Three new refining element levels are determined and applied to related aluminium cylinder head groups. First refining element level gave 23.11 μm SDAS value which is insufficient SDAS level for the related product. Second refining element level gave 19.74 μm SDAS value which is sufficient level and it gave appropriate mechanical properties. Third refining element level gave 15.71 μm SDAS value which gave the best mechanical properties.

After grain refinement, stress relief has been carried out over half of the specimens, so that the influence of post-refinement stress relief on the mechanical properties could also be investigated. The specimens have been extracted from the cylinder heads from the critical areas and they showed around 10% UTS and around 25% YS better values after stress relief.

Quasistatic mechanical properties as well as fatigue properties have been investigated so that optimum percentage of Ti and B can be determined for highest ultimate tensile strength and yield strength values. Woehler curves have been generated and the resulting life has been compared with the predetermined life cycles required for the product for conformance to the performance criteria.

Keywords: Aluminium, Cylinder head, Grain refiner, Mechanical properties, SDAS.

Acknowledgement

This study is the Master thesis of Joint Degree Master Program in Master of Science in Manufacturing Technology (MMT). The Joint Degree Master Program was carried out in cooperation between Turkish-German University and TU Dortmund University.

First, I would like to acknowledge DAAD (Deutscher Akademischer Austausch Dienst - German Academic Exchange Service) for financial support throughout my Master degree study.

Second, I would like to gratefully acknowledge to my supervisors Prof. Dr.–Ing. habil. Frank Walther from TU Dortmund and Asisst. Prof. Dr. Mehmet İpekođlu from Turkish-German University. Their support, constructive criticism, encouragement and evaluation lead this study. In addition to this, I would like to express my appreciation to M.Sc. Shafaqat Siddique and Dipl.-Wirt.-Ing. Sebastian Myslicki for their cooperations and constructive criticisms in this thesis. Their guidances, suggestions and supports are valuable for me. At last, I would like acknowledge to Prof. Dr. Yücel Birol and Prof. Dr. Remzi Varol.

All practical works in this thesis are carried out at Cevher Aluminium Foundry in İzmir/Turkey. I am very grateful being a part of Cevher Aluminium Foundry. I would like to acknowledge to Mr. Atif Eralp, Mr. Neşet Kiremitçi and all colleagues in Cevher Aluminium Foundry.

Finally, I would like to say my special thanks to my parents Emel Özaydın - Osman Özaydın, to my sister Sevil Özaydın Turkay, and to my dear friends Elif Şener, Mehmet Kargı and Esmeray Üstünyağız.

Table of Contents

Table of Contents	i
List of Figures	iii
List of Tables	viii
Abbreviations and Formula Symbols	x
1 Introduction	1
1.1 Objective and goals	1
1.2 Motivation	1
1.3 Outline	2
2 State of the Art	4
2.1 Background	4
2.2 Application in the automotive industry	12
2.2.1 Cylinder head	12
2.3 Foundry technology	15
2.3.1 Casting of aluminium cylinder heads	15
2.4 Material: Aluminium and aluminium alloys	19
2.4.1 Aluminium and aluminium alloys	19
2.4.2 Effect of alloying elements	21
2.4.3 Al-Si-Cu (3xx.x) system	22
2.5 Solidification	23
2.5.1 Solidification of Al-Si-Cu systems	23
2.5.2 Casting defects	24
2.5.3 Dendrite arm spacing (DAS)	27
2.6 Grain refinement	30
2.6.1 Mechanism of grain refinement	31
2.6.2 Methods of grain refinement	33
2.6.3 Advantages and disadvantages	34

2.6.4	Gas content	34
2.7	Stress relieving	36
2.7.1	Stress relieving and annealing (TS condition)	36
3	Experimental Methods	37
3.1	Casting	37
3.1.1	Casting the cylinder head	37
3.1.2	Design of all tests	42
3.1.3	Casting cylinder head with different additions	43
3.1.4	Specimen preparation.....	45
3.1.5	Stress relieved cylinder heads	51
3.2	Metallurgical approach.....	51
3.2.1	Chemical composition.....	51
3.2.2	Macrostructure.....	53
3.2.3	Grain size	54
3.2.4	Microstructure.....	59
3.3	Brinell hardness test	64
3.4	SDAS measurement.....	65
3.5	Tensile test	66
3.6	Fatigue test.....	67
4	Results	70
4.1	Results of Brinell hardness test.....	70
4.2	Results of SDAS measurement	71
4.3	Results of tensile test.....	79
4.4	Results of fatigue test	86
4.4.1	Woehler (S-N) curve.....	88
5	Discussion	92
6	Summary and Outlook	94
7	References	95

List of Figures

Figure 1.1: Dendritic structure [Pav10].....	1
Figure 2.1: The effect of SDAS on UTS-YS of cast cylinder heads in 319 alloys [Zha05].....	5
Figure 2.2: The effect of microstructure on the fatigue behaviour of 319 alloys [Zhu06].....	8
Figure 2.3: Chronological overview of damage mechanism leading to failure [Kli12], [Rie04]	11
Figure 2.4: Detailed aluminium cylinder head [NN15].....	12
Figure 2.5: Cylinder head with cross-section [Bec11].....	13
Figure 2.6: Trends in market share of casting methods for aluminium cylinder heads [NN02]	15
Figure 2.7: a) Top casting method, b) Bottom casting method, c) Tilt casting method [Pav08]	16
Figure 2.8: Filling of mould cavity in tilt gravity casting [Sme14].....	17
Figure 2.9: a) Lading and dosing, b) Transporting of casting basin, c) Docking of casting basin, d) Starting of casting, e) Ending of casting, f) Undocking of casting basin [Sme14].....	18
Figure 2.10: a) Exogenous solidification type (1) Smooth wall, (2) Rough wall, (3) Spongy, b) Endogenous solidification type (4) Pulpy or mushy, (5) Shell forming [Bas07]	23
Figure 2.11: a) Higher solidification speed (Rough wall type) (x10 Magnification), b) Lower solidification speed (Spongy) (x10 Magnification).....	24
Figure 2.12: Macrostructure pictures of gas porosity. a) x10 Magnification, b) x10 Magnification.....	25
Figure 2.13: Macrostructure pictures of gas porosity. a) x40 Magnification, b) x63 Magnification.....	25
Figure 2.14: a) Primary and secondary macro porosity [Cam94], b) Primary and secondary macro porosity.....	25
Figure 2.15: Macrostructure pictures of shrinkage. a) x10 Magnification, b) x10 Magnification	26
Figure 2.16: a) Optical micrographs of gas porosity in cylinder head casting [Bir08], b) Optical micrographs of gas porosity in cylinder head casting	26

Figure 2.17: a) Optical micrographs of shrinkage in cylinder head casting [Bir08], b) Optical micrographs of shrinkage in cylinder head casting	26
Figure 2.18: a) Optical micrographs of oxide in engine head casting [Kon14], b) Optical micrographs of oxide in cylinder head casting	27
Figure 2.19: Primary and secondary dendrite arm spacing [Dju12]	27
Figure 2.20: a) Microscope view sample (Magnification x100), b) SDAS measurement method (Linear interception method).....	29
Figure 2.21: The measurement area of SDAS values on the combustion chamber [NN12]..	30
Figure 2.22: a) Ti content of grain refinement samples b) B content of grain refinement samples.....	31
Figure 2.23: a) Macroscopic picture of No.1.1 (Grain size: 500 μm), b) Picture of No.1.2 (Grain size: 315 μm), c) Picture of No.2.2 (Grain size: 200 μm).....	31
Figure 2.24: a) The nucleation of TiAl_3 [Bac83], b) The effect of grain refiner on the cooling curve [Sig07]	32
Figure 2.25: a) Macrostructure before inoculation, b) Macrostructure after inoculation.....	33
Figure 2.26: a) Weighing machine MK2200, b) Vacuum machine, c) Pressure gauge (640 mmHg)	35
Figure 2.27: a) Before degassing in the vacuum (Group A), b) After degassing in the vacuum (Group B)	36
Figure 3.1: The production line [NN15]	37
Figure 3.2: Transferring the liquid metal from melting furnace to transfer ladle [NN15]	38
Figure 3.3: a) Positions of sand cores in the mould [Sme14], b) Named sand cores [NN12]	39
Figure 3.4: Gathered sand cores in the mould [NN15]	39
Figure 3.5: a) Water jacket 1, b) Water jacket 2 and outlet sand core, c) Side oil channel 2, d) Side oil channel 1 and inlet sand core, e) Top sand core and oil gallery [NN12]	40
Figure 3.6: Solidification of cast in tilt casting process [Sme14]	41
Figure 3.7: Design of all measurements and tests	42
Figure 3.8: Temperature measurement points on the combustion chambers	44
Figure 3.9: Drawing of tensile test bar in DIN 50125 [DIN91]	46

Figure 3.10: a) Tensile test bar mould, b) Uncut specimen, c) Sawed specimen, d) Machined to $d_0=12$ mm tensile test bar.....	46
Figure 3.11: a) CAD picture of $d_0=5$ mm tensile test bar under the combustion chamber, b) CAD picture of $d_0=5$ mm tensile test bar under the combustion chamber with zoom.....	47
Figure 3.12: a) Combustion chamber and tensile test bar, b) Sawed cylinder head, c) Perspective view of critical region, d) Separated critical region, e) Machined $d_0=5$ mm tensile test bar.....	47
Figure 3.13: Roughness test machine [NN12].....	48
Figure 3.14: a) X-Ray inspection [NN12], b) X-Ray photograph of two $d_0=12$ mm tensile test specimens.....	48
Figure 3.15: a) Measured area on the first and third combustion chamber region, b) Sample for microstructure and SDAS measurement.	49
Figure 3.16: Used fatigue specimen [Rob01]	49
Figure 3.17: a) Combustion chamber and specimen region, b) Perspective view of cylinder head, c) Sawed specimen, d) Machined fatigue specimen.	50
Figure 3.18: X-Ray pictures of two fatigue specimens.....	50
Figure 3.19: a) Furnace, b) Screen of furnace.....	51
Figure 3.20: Optical emission spectrometer [NN15].....	52
Figure 3.21: Chemical composition is determined from three different points.....	52
Figure 3.22: a) Streuers Unitom – 2 Cutting machine, b) Ostas grinding machine	54
Figure 3.23: Reference pictures of grain size under x10 Magnification [Cen80].	55
Figure 3.24: a) 1 st Step of sample in group 1, b) 2 nd Step of sample in group 1, c) 3 rd Step of sample in group 1, d) 4 th Step of sample in group 1.....	56
Figure 3.25: a) 1 st Step of sample in group 1 (x10 Magnification) (Grain size: 315 μm), b) 2 nd Step of sample in group 1 (x10 Magnification) (Grain size: 500 μm), c) 3 rd Step of sample in group 1 (x10 Magnification) (Grain size: 315 μm), d) 4 th Step of sample in group 1 (x10 Magnification) (Grain size: 315 μm).....	56
Figure 3.26: Freezing direction of cylinder heads [NN12].....	57
Figure 3.27: Macrostructure of different regions on group 2 sample (Non-stress relieved) ...	57
Figure 3.28: Macrostructure of different regions on group 2 sample (Stress relieved)	58

Figure 3.29: Macrostructure of different regions on group 3 sample (Non-stress relieved) ...	58
Figure 3.30: a) Aluminium cylinder head, b) Cross-section of related area, c) Sample for microstructure and SDAS measurement, d) Software interface	59
Figure 3.31: Four different areas of cross section and microscopic photos	60
Figure 3.32: Micrographs of AlSi6Cu4	61
Figure 3.33: a) Micrographs of the structure, b) Typical phases in a cast AlSi6Cu4	61
Figure 3.34: Chinese script samples in the structure.....	63
Figure 3.35: β (Al-Fe-Si) samples in the structure	63
Figure 3.36: Fine round shaped silicon in the structure	63
Figure 3.37: a) Emco-Test test machine, b) Hardness measurement of cylinder head.....	64
Figure 3.38: a) Hardness measurement regions [NN14], b) 1 st Region, c) 2 nd Region, d) 3 rd Region	65
Figure 3.39: SDAS measurement sample	66
Figure 3.40: Zwick ZS 100 tensile test machine	67
Figure 3.41: Rotating bending fatigue test machines	68
Figure 3.42: Dial inducator	68
Figure 3.43: Fatigue machine setting up [Rob01].....	69
Figure 3.44: a) Counterbalance weight and load on the fatigue testing machine [Rob01], b) Counterbalance weight and load on the fatigue testing machine	69
Figure 4.1: a) Brinell hardness results of non-stress relieved cylinder heads, b) Brinell hardness results of stress relieved cylinder heads	70
Figure 4.2: Comparing the Brinell Hardness (HB) values of different regions.....	71
Figure 4.3: Secondary dendrite arm spacing values of AlSi6Cu4 aluminium cylinder head in different regions	74
Figure 4.4: a) 1 st group cylinder head without stress relief, b) 1 st group cylinder head with stress relief, c) 2 nd group cylinder head without stress relief, d) 2 nd group cylinder head with stress relief, e) 3 rd group cylinder head without stress relief, f) 3 rd group cylinder head with stress relief.	78
Figure 4.5: Clean fracture surface. a) x10 Magnification, b) x15 Magnification, c) [Das04]...	80
Figure 4.6: Small oxide flakes. a) x10 Magnification, b) x15 Magnification, c) [Das04].....	80
Figure 4.7: Medium oxide flakes. a) x10 Magnification, b) x20 Magnification, c) [Das04]	80

Figure 4.8: Large oxide flakes. a) x10 Magnification, b) x20 Magnification, c) [Das04].....	80
Figure 4.9: Comparing UTS and YS of $d_0=5$ mm specimens.....	82
Figure 4.10: Comparing ϵ of $d_0=5$ mm specimens.....	82
Figure 4.11: UTS/YS-SDAS values of specimens from AISi6Cu4 cylinder heads.....	83
Figure 4.12: Elongation-SDAS values of specimens from AISi6Cu4 cylinder heads.....	83
Figure 4.13: Comparing UTS and YS of $d_0=12$ mm specimens.....	84
Figure 4.14: Comparing ϵ of $d_0=12$ mm specimens.....	84
Figure 4.15: Comparing the UTS and YS of $d_0=5$ mm and $d_0=12$ mm specimens.....	86
Figure 4.16: Comparing the ϵ of $d_0=5$ mm and $d_0=12$ mm specimens.....	86
Figure 4.17:Fracture surface a) x20 Magnification, b) x40 Magnification, c) x63 Magnification	87
Figure 4.18:Fracture surface a) x20 Magnification, b) x40 Magnification, c) x63 Magnification	87
Figure 4.19:Fracture surface a) x20 Magnification, b) x40 Magnification, c) x63 Magnification	87
Figure 4.20:Fracture surface a) x20 Magnification, b) x40 Magnification, c) x63 Magnification	88
Figure 4.21: a) Rotating bending fatigue test, b) Fractured specimen.....	89
Figure 4.22: S-N values of 1 st group with and without stress relief process.....	90
Figure 4.23: S-N values of 2 nd group with and without stress relief process.....	90
Figure 4.24: S-N values of 3 rd group with and without stress relief process.....	91
Figure 4.25: S-N values of all groups with and without stress relief process.....	91

List of Tables

Table 2.1: Mechanical properties of critical areas of cylinder head [Sme14]	4
Table 2.2: Chemical composition of AlSi6Cu4 [EN10].....	19
Table 2.3: Mechanical properties of AlSi6Cu4 [EN10].....	20
Table 2.4: Major, minor and modifier elements of aluminium alloys [Ran12]	20
Table 2.5: Classification of casting aluminium alloys [Pav10].....	22
Table 2.6: Ti, B values and grain size of 8 samples	30
Table 2.7: Ti, B values of the structure before and after inoculation.....	33
Table 2.8: Density in air, density in vacuum and density index.....	35
Table 2.9: Mechanical properties of AlSi7Cu3Mg0.35Fe with and without stress relief process [Ren14]	36
Table 3.1: Sand cores properties	40
Table 3.2: Manufacturing parameters of all groups	45
Table 3.3: Chemical content of melting furnace material and material of the three groups...	53
Table 3.4: Chemical reactions in the structure and temperature [Bel05]	62
Table 3.5: Inputs of tensile tests	67
Table 4.1: Arranged results of Brinell hardness test.....	70
Table 4.2: Measured distance, dendrite count and mean SDAS values of measuring point 1 and 2.....	72
Table 4.3: Measured distance, dendrite count and mean SDAS values of measuring point 3 and 4.....	72
Table 4.4: Equations of SDAS calculations [Pav10].....	73
Table 4.5: Averaged SDAS, median of mean SDAS and standard deviation	73
Table 4.6: SDAS values of different measuring points in cross-section of aluminium cylinder head.....	75
Table 4.7: Measured distance, dendrite count and mean SDAS values of 1 st group	75
Table 4.8: Measured distance, dendrite count and mean SDAS values of 2 nd group.....	76
Table 4.9: Measured distance, dendrite count and mean SDAS values of 3 rd group	76
Table 4.10: Averaged SDAS (<i>xSDAS</i>), median of mean SDAS (<i>xSDAS</i>) and standard deviation.....	77

Table 4.11: The effects of oxide flakes on the mechanical properties	79
Table 4.12: Tensile test results of $d_0=5$ mm specimens which are extracted from combustion chamber region	81
Table 4.13: Tensile test results of $d_0=12$ mm specimens which are poured into the tensile test bar mould.....	84
Table 4.14: The effects of stress relief on the UTS and YS.....	85
Table 4.15: Different fractured samples in different cycle number.....	86
Table 4.16: Different failure samples with fractured cycle number.....	89

Abbreviations and Formula Symbols

Abbreviation	Illustration
DAS	Dendrite Arm Spacing
SDAS	Secondary Dendrite Arm Spacing
UTS	Ultimate Tensile Strength
YS	Yield Strength
ϵ %	Elongation
ppm	Parts per Million
MPI	Multi Point Injection
GDC	Gravity Die Casting
LPDC	Low Pressure Die Casting
HPDC	High Pressure Die Casting
EN	Europe Norm
DIN	Deutsches Institut für Normung (German Institute for Standardization)
T_{LIQ}	Liquidus Temperature
T_{SOL}	Solidus Temperature
T_n	Nucleation Temperature
T_g	Growth Temperature
kgf	Kilogram Force
d_0	Diameter of Specimen
d_1	Diameter of Grip
h	Height of Grip
L_0	Gauge Length
L_c	Parallel Length

L_t	Total Length
d_{vacuum}	Density in the Vacuum
d_{air}	Density in the Air
DI	Density Index
CNC	Computer Numerical Control
rpm	Revolution per Minute
HSS	High Speed Steel
AFS	American Foundrymen's Society
LOM	Light Optical Microscope
AVG	Average
SD	Standard Deviation
HB	Hardness Brinell

Formula symbol	Unit	Illustration
G_L	K/mm	Thermal Gradient
R	mm/s	Interface Velocity
t_s	s	Solidification Time
d_{air}	g/cm ³	Density in Air
d_{vacuum}	g/cm ³	Density in Vacuum
DI	%	Density Index
F	N	Test Load
D	mm	Steel Ball Diameter
d	mm	Average Indentation Diameter
d_1	mm	First Indentation Diameter
d_2	mm	Second Indentation Diameter (Perpendicular to First)

1 Introduction

1.1 Objective and goals

Casting defects such as hot tear and gas porosity are reduced by grain refinement. In addition, shrinkage porosity is redistributed by grain refinement. Grain refinement is obtained with adding titanium (Ti), particularly in association with boron (B), to aluminium alloys and Ti and B are widely used as grain refiners. Additionally, many other manufacturing parameters could affect the grain size. Grain size of cast aluminium is dependent on solidification and cooling rate. For instance, if the cooling rate is increased, grain size is decreased [Bro99].

DAS values are measured with using microscope and special software. In the literature, three different dendrite arm spacing which are called primary (λ_1), secondary (λ_2) and tertiary (λ_3) dendrite arm spacing are defined [Pav10]. SDAS values are limited for critical areas on the cylinder heads. Supplier must guarantee the SDAS values are under the limits.

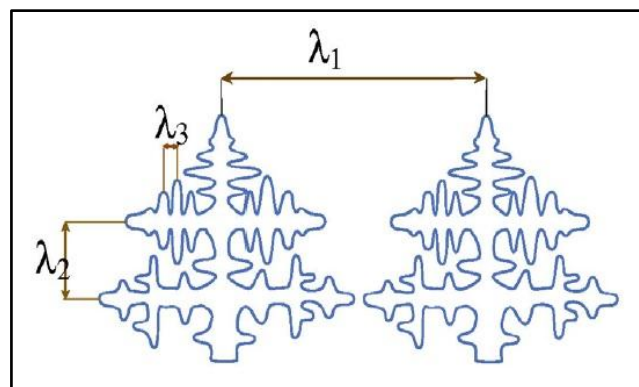


Figure 1.1: Dendritic structure [Pav10]

Firstly, tensile tests will be carried out on the specimens to determine UTS (ultimate tensile strength), YS (yield strength), and $\epsilon\%$ (elongation) values. Then, fatigue tests will be carried out to determine the S-N values.

The correlation between mechanical properties and SDAS values is already evident; if SDAS values increase, mechanical properties will worsen. The first goal of this study is to investigate the extent of this relationship between values. Next, this study will try to determine the effects of grain refinement on the mechanical properties and fatigue behaviour.

1.2 Motivation

Automotive companies define SDAS limit in their specification for cast aluminium parts such as cylinder head and cylinder block. The critical area for SDAS is combustion chamber surface. The limit of SDAS values depends on the automotive companies and the design of cylinder head.

Pavlovic-Krstic (2010) noted that the SDAS values range from 20 μm to 40 μm on the critical area of aluminium cylinder head. The critical areas on the combustion chamber which may be located in the center of combustion chamber or between the valve guides are defined by automotive companies in detail. In addition, it is noted that the control of the solidification rate, and parallelly the SDAS values, is difficult because the parts used in automotive industry have very complex geometry with many cavities and different wall thickness [Pav10]. The optimum percentage of grain refiner will be defined for minimum SDAS values with used casting methods.

In this study, grain refiner is used to get finer microstructure and lower SDAS values. Finer microstructure will give better mechanical properties so it is important for automobile manufacturers. The percentage of grain refiner plays vital importance in casting process. The optimum percentage will be determined with experimental studies. There are many different parameters which affect the results.

In addition to quasistatic mechanical properties, fatigue behaviour of specimens will be investigated. The optimum percentage of grain refiner additive will be determined for optimized fatigue life time for appropriate SDAS values.

This master thesis will integrate the results to Cevher Aluminium Foundry which supplies different engine components to main automotive companies. The biggest motivation of this study is trying to find a solution for an engineering problem and present the solution to industry. This study represent to industry new options which can be used to get better mechanical properties. These new options can use not only for today, but also for the future. Beside this, the test samples are taken from final product so that the results satisfy the need of related industry.

1.3 Outline

This study consists of six basic sections.

1. Introduction: General definitions about the subject are given. The aims and the motivations of this study are presented.
2. State of the Art: First, similar studies in the literature are investigated. Theoretical knowledge about the fundamental concepts addressed in this study such as casting process, cylinder heads, aluminium (Al) and alloys, grain refinement, SDAS measurement are presented.

3. Experimental Methods: Appropriate manufacturing method for this study is determined after comparing all methods. Grain refined cylinder heads are cast with Ti and B additions. All tests and measurements are designed and quasistatic mechanical properties and fatigue life are determined under predetermined conditions and SDAS values are obtained.

4. Results: The results and measurements are collected and compared with each other.

5. Discussion: The results and trends are described in comparison to similar studies in the literature. The results are compared with expected values and trends.

6. Summary and Outlook: The thesis is summarized and the recommendations are presented. Present condition and possible application in the future will be noted.

The flow of thesis is started with literature survey. The application of cylinder head is investigated. Appropriate manufacturing method is determined as tilt gravity casting. In the industry application, aluminium is widely used for cylinder heads. After material research, the material of aluminium cylinder is determined as AlSi6Cu4 alloys. Before the experimental study, the parameters which can affect the mechanical properties are investigated. These parameters are solidification (cooling conditions), casting defects and microstructure. In this study, microstructure effects are determined. To improve the mechanical properties, grain refinement and stress relieving are applied. Grain refinement is done with three different level of grain refiner. In the experimental side, the effects of grain refinement on the mechanical properties are studied. SDAS values are measured and the effects on the mechanical properties are investigated. Not only SDAS values, but also cooling condition is investigated. Beside SDAS values, the effect of stress relief is studied on half of samples. The effect of stress relief on mechanical properties and hardness value are determined. Finally, rotating bending fatigue tests are carried out and S-N (Woehler) values are determined.

2 State of the Art

2.1 Background

Djurđević and Grzinčić (2012) studied the effects of major elements on the secondary dendrite arm spacing (SDAS) in the Al-Si-Cu alloys. They listed the phenomena which can affect the structure and mechanical properties. Chemical composition and cooling (solidification) rate from these phenomena play a vital role. Authors state that the effect of varying cooling rate on the SDAS values is widely investigated in the literature. Thus, they concentrated on the chemical composition. 20 samples are poured with different Si and Cu alloys percentage. The authors determined that SDAS values decreased with increasing Si and Cu percentage. High solubility was found less effective on grain refinement, and solubility of Cu is higher than Si. Therefore, higher Si content gives lower SDAS values. In conclusion, they reported that there is no significant change in SDAS values after adding 6 - 8% Si and 3 - 4% Cu in content [Dju12].

Smetan et al. (2014) have investigated the mechanical properties of aluminium cylinder heads which are made from three different materials (Table 2.1). Especially, they concentrated on the effects of heat treatment on samples. This study is important to identify the mechanical properties of critical areas such as center of combustion chamber, between combustion chambers and sealing surface of cylinder head gasket [Sme14].

Table 2.1: Mechanical properties of critical areas of cylinder head [Sme14]

Alloy AlSi6Cu4	Center combustion chamber			Between combustion chamber			Seal surface of cylinder head gaskets		
	UTS (MPa)	YS (MPa)	ϵ (%)	UTS (MPa)	YS (MPa)	ϵ (%)	UTS (MPa)	YS (MPa)	ϵ (%)
As-Cast	239	163	3.3	239	142	3.3	226	153	3.0
T6 Water Quenched	384	347	2.2	393	352	2.7	369	332	2.1
T6 Air Quenched	327	263	2.7	323	266	2.4	314	249	2.3
T7 Air Quenched	312	222	3.5	310	224	2.3	293	209	3.3

Zhang et al. (2003) investigated the influence of process parameters such as chemical composition, solidification rate, pouring temperature and mould temperature on the DAS values of cast aluminium cylinder heads. Three set of experiments were utilized. First, the effect of chemical composition is studied with three different alloys. Second, pouring / mould temperature and solidification rate is changed for samples. Third, geometrical changes are examined with using different feeding approaches. The authors noted that finer structure which is related to lower DAS values gives better mechanical properties in tensile test and shows better fatigue behaviour for cast aluminium alloys. The results of the first set show that increasing the concentration of alloying elements like Si and Cu cause reduction of DAS values. Results of the second set state that lower pouring temperature is more effective than lower local mould temperature to reduce DAS values. Nevertheless, low temperature in the combustion chamber on the mould gives significant reduction in DAS values (all DAS values measured from combustion chamber area). Finally, the third set shows the feeding region can affect the DAS values [Zha03].

Another study of Zhang et al. (2005) is about the effect of SDAS on mechanical properties of cylinder heads and engine blocks. Two different groups of aluminium alloys, A356 and 319, are used with and without heat treatment. Heat treatment such as T6-T7 or T6 is carried out on specimens which are taken from cylinder heads. In the first group, 319 alloy without heat treatment are used and UTS and YS show similar trends both decrease with increasing SDAS. But there are no significant differences in elongation (%) and hardness with different SDAS values. 319 alloys with T6/T7 heat treatment are used in the second group and A356 with T6 heat treatment is used in the third group. The authors observed that the trend of change in YS is not as steep as for UTS for all group samples. Besides this they used heat treated specimens which are taken from cylinder head so that they did not heat treat all cylinder heads. Figure 2.1 shows the effects of SDAS values on the ultimate tensile strength and yield strength for as-cast 319 alloys [Zha05].

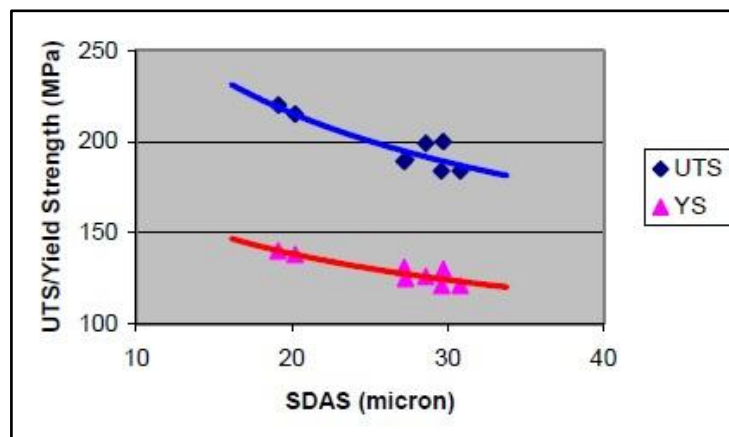


Figure 2.1: The effect of SDAS on UTS-YS of cast cylinder heads in 319 alloys [Zha05]

A number of studies concentrate on the effect of Ti and B on grain size and dendrite arm spacing of aluminium alloys. Hu and Li (1997) investigated the effect of grain refiner on aluminium alloys. Main material is AlSi8Cu2 (standardized in DIN 226S) with 0.11, 0.13, 0.15 and 0.17 wt % Ti additive levels. They presented microstructure pictures without inoculation and with different inoculation percentages. The differences in the microstructure can be observed easily. The authors noted that the grain size is reduced nearly to 60% with Ti until 0.13 wt %. Addition of Ti above 0.13 wt % has no significant effect on grain size. Grain size and DAS value may increase with addition of Ti and B in higher level to DIN226S. The reason of this is explained with the complicated interactions between Ti, Al, Si and B in the melt by the authors. Different form phases such as $TiAl_3$, AlB_2 and TiB_2 can nucleate the α -Al for grain refinement. In addition, $TiAl_3$ and TiB_2 can reduce the active Ti and it can decrease the effect of DAS refinement. Finally, they noted that optimum levels of Ti depend on the material content [Hu97].

In the following study, Hu and Li (1998) added more results to their previous study. They investigated the effects of B on grain size and DAS values. Main material is AlSi8Cu2 (standardized in DIN 226S) with 0.01, 0.03, 0.05 and 0.07 wt % B additive levels. The authors found out that the grain size is reduced almost 45% with B until 0.03 wt %. The optimum wt % B is determined as 0.01. In conclusion, alloys such as Al-Ti, Al-B are beneficial for grain refinement with determined levels which are mentioned above [Hu98].

Yu et al. (2005) studied the grain refinement efficiency of AlTiC ($Al_5Ti_{0.25}C$) and AlTiB (Al_5Ti_{1B}) in the A356. Master alloy such as $Al_5Ti_{0.25}C/Al_5Ti_{1B}$ level is arranged as 0.2, 0.5, 2.0, 5.0 wt %. The optimum level is determined as 0.5 wt %, the down trend is not steep when the additive level is above 0.5 wt %. According to their results, Al_5Ti_{1B} master alloy is a better grain refiner than $Al_5Ti_{0.25}C$ [Yu05].

Suharno et al. (2007) investigated the influence of grain refiner on the results of aluminium alloy ADC 12 (Al-Si10Cu2Fe). Al_5Ti_{1B} is used as grain refiner and grain refiner level is arranged as 0, 0.05, 0.1, 0.15, 0.2 wt %. In result, use of 0.15 wt % Al_5Ti_{1B} reduced the DAS values 50% in comparison to the case in which no grain refinement was used. If the Al_5Ti_{1B} percentage increases more, complex intermetallic phases such as $TiAl_3$ and TiB_2 occur and growth of the existing phase dominates the formation of the new nuclei [Suh07].

Serbino et al. (2011) investigated the SDAS refining in cylinder head. They planned two different manufacturing strategies which are used by suppliers widely. These strategies are: first, using modifier and/or grain refiners, and second, altering a distance of the cooling and tooling temperature. The experiments are carried on the Magmasoft® software and concentrate on SDAS values on the combustion chamber. They concluded that the best SDAS results can be taken from near the combustion chamber area at 150 °C [Ser11].

Zhang et al. (2003) figured out the linear relationship between DAS and pouring temperature. Lower pouring temperature gives lower DAS values as mentioned before. The optimum pouring temperature is determined around 705°C-720°C. The lowest pouring temperature limit is determined by casting quality. The optimum mould temperature in the combustion chamber is determined around 150°C. Mould temperature in combustion chamber is examined between 50°C - 250°C [Zha03].

Similarly, Pavlovic-Krstic (2010) used same approach with the previous study. First, the author listed four main parameters which Zhang et al. (2003) mentioned are chemical composition, solidification rate, pouring temperature and mould temperature. These parameters may affect the SDAS values. Solidification rate is leading to these parameters but chemical content cannot be neglected. SDAS values are decreased nearly 6 µm from 750°C to 650°C of pouring temperature. The mould temperature is varied from 250°C to 350°C and SDAS values are obtained around 19 µm – 25 µm respectively [Pav10].

Çolak and Kayıkcı (2009) studied the grain refinement effect of AlTiB master alloys on the ETIAL160 casting alloys. AlTiB master alloy is used as Al5Ti1B to obtain finer grains. Authors underlined that alongside the complex grain refinement mechanism, general acceptance states $TiAl_3$ and TiB_2 nucleate on heterogenous nucleation sites in the alloy to facilitate grain refinement [Çol09]. Similarly, this approach is mentioned also by Hi and Li's study (2005) [Hu97]. Çolak and Kayıkcı [Çol09] noticed aluminium alloy with finer grain shows better fluidity and feeding, higher strength and fatigue values and then lower porosity and homogeneous structure. After adding Al5Ti1B, nucleation takes time in the crucible and the optimum time must be determined. Shorter or longer holding times could give higher SDAS values. Correlatively, Hu and Li [Hu98] arranged their experiments to find out the optimum holding time for DIN 226S with Ti and B and they reported the optimum holding time to be 10 minutes for 0.13 wt % Ti alloys. Çolak and Kayıkcı [Çol09] reported the optimum holding time around 25 min. for Al5Ti1B additive to related aluminium alloy. These results show that the optimum holding time could vary according to aluminium alloys and grain refiner percentage.

Sigworth and Kuhn (2007) notified that grain refinement has a positive effect on mechanical properties, improved feeding, resulted in better fatigue strength, lower porosity ratio and finer porosity [Sig07].

Titanium has to be divided into two different groups. First one being 'soluble titanium' which is titanium aluminides ($TiAl_3$) dissolves quickly in alloys that contain less than 0.15% Ti. $TiAl_3$ particle sizes are 10-20 µm in master alloys without boron. Second one being 'insoluble titanium' which is titanium diboride (TiB_2) has low solubility in alloy [Sig07].

In their work, Djurdjević and Grzinčić (2012) [Dju12] stated that ‘high solubility is less effective on grain refinement’ and according to this approach TiB_2 has to be a better grain refiner than $TiAl_3$. Sigworth and Kuhn corrected this approach in their paper and noted that TiB_2 particles are excellent nuclei. Nevertheless, authors point out that the best combination of Ti and B for grain refinement depends on the alloy [Sig07].

Sigworth and Kuhn (2007) advised around 0.10% Ti (dissolved) in the alloy and 10-20 ppm B (insoluble) for Al-Si-Cu casting alloys such as 319 alloys. Finer grain size cannot be obtained without this quantity of Ti and the best grain size occurs around this B additive level. Other researchers who study this topic should keep in mind that this level is suggestive and it depends on the main aluminium alloy. As mentioned before, grain refinement helps to obtain lower porosity and finer pore size. Finer porosity affects the fatigue life positively. In conclusion, recommendations are given for each aluminium alloy by the authors. Al-Cu and Al-Zn-Mg alloys give the best results with low Ti percentage which is around 0.05%. Al-Si, Al-Si-Mg and Al-Mg alloys are affected by Ti slightly [Sig07].

Zhu et al. (2006) investigated the effects of microstructure on fatigue life. The main material is E319-T7. The key factor to control the fatigue life is pore size. They noted that SDAS controls the pore size and distribution of porosity and then the porosity effects the fatigue life time. They compared two different specimens with different SDAS values which are 30 μm and 70 μm , respectively. According to experimental results, the specimen with lower SDAS value has better fatigue strength. Important to note is that the porosity percentages are 0.26% and 0.87%, respectively. Porosity percentage could affect the fatigue results alongside SDAS values. The authors carried out the experiments at room temperature and frequency is 20 kHz so that they test the samples in very long cycle numbers. Cycle number extends up to 10^{10} cycles [Zhu06]. Under mentioned conditions, the trends of curves are changing between 10^6 - 10^7 cycles in Woehler curve. (Figure 2.2)

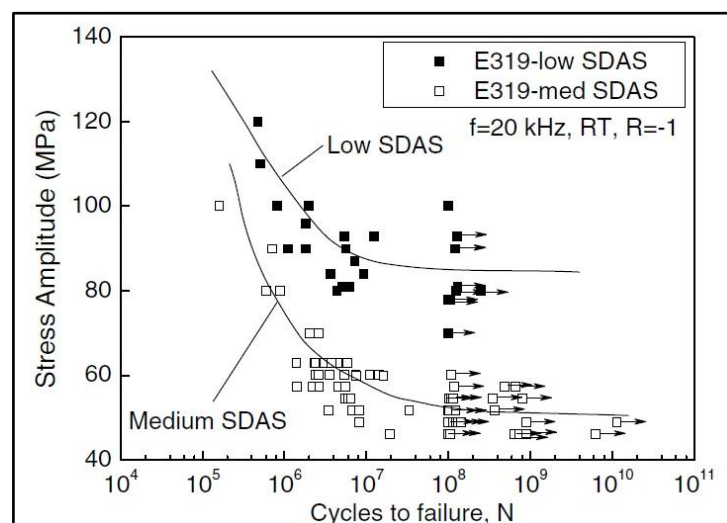


Figure 2.2: The effect of microstructure on the fatigue behaviour of 319 alloys [Zhu06]

In conclusion, they noted a decrease of the endurance limit around 25% from room temperature to 250°C. However, they compared the effects of microstructure and temperature on the fatigue strength and concluded that microstructure affects the fatigue strength more than temperature. As mentioned before, other researchers should keep in mind that the porosity percentage of samples is different and this parameter could affect the fatigue strength [Zhu06].

Firouz et al. (2007) studied the similar topic. Their results supported the previous study and they noted that the sample with lower SDAS values, finer grain size and lower porosity level showed better thermal fatigue strength. In addition, heat treatments such as T6 / T7 gave beneficial effects to the fatigue strength. T6 heat treatment shows better effect on the thermal fatigue life time of A319 alloy than T7 heat treatment. In addition, they noted that finer SDAS, lower porosity volume, lower brittle inter metallic contents and higher Sr modification could give better fatigue strength [Fir07].

On the other side, Bonollo and Tovo (1999) obtained results similar to previous studies in the literature about the effects of finer grain and lower SDAS on the mechanical properties. Beside this, they pointed out that the effects of porosity and SDAS on the fatigue behaviour of aluminium alloys is not same. According to them, SDAS plays vital role at low cycle fatigue [Bon99].

Boromei et al. (2010) studied the influence of the microstructure and porosity on the fatigue strength of Al-Si-Mg alloys. Specimens are extracted from engine heads. Engine heads are produced by gravity casting, refined by Ti-B, modified by Sr and degassed by high purity Ar. Inevitably, solidification defects such as gas porosity, shrinkage cavities and oxide films effect the fatigue strength. They determined that the main factor is porosity. If the porosity levels are similar to each other, micro structural parameters such as SDAS, size and shape of the Si and Fe based inter metallic compounds play role on the fatigue strength. In conclusion, they noted that solidification conditions of the complex parts such as engine head vary by region. Different SDAS values on the critical or non-critical areas could occur in the same part. In addition, there is no direct relation between SDAS and porosity according to them [Bor00].

Mattos et al. (2010) investigated the diesel engine cylinder head. First, they determined the UTS, YS and $\epsilon\%$ of specimens which are extracted from diesel engine cylinder head. In addition, they carried out the fatigue test according to ASTM 466-07. After the tests, they determined the average cycle around 10^6 cycles at predetermined stress amplitude level. In the results, they explained that the porosity is the main factor effecting fatigue strength [Mat10].

Major (2002) assessed the impact of porosity and micro structural parameters on the fatigue life. Porosity is the main parameter which can affect the fatigue life directly. Porosity tolerances could be defined according to the product. There is no porosity tolerance for cast parts which are used in aerospace industry. Commercial automotive cylinder heads may tolerate predetermined porosity levels and non-critical automotive parts have large tolerances about porosity. Parameters are classified into two groups consisting of direct and indirect parameters. Direct parameters are largest pore size, DAS and stress amplitude; whereas indirect parameters are modifier and grain refiner. The major parameter which affects the fatigue life is largest pore size. Impact of DAS on fatigue life is weaker than largest pore size but the impact of DAS could be distinguished at the similar pore size levels. Grain refinement influences the porosity, because the largest pores may locate at the grain boundaries. Indirect parameters such as modifier and grain refiner affect the fatigue life indirectly, but it is not to mean that these parameters are not important. They affect the pore size directly hence they affect the fatigue life indirectly. In conclusion, the author noted that smallest pore size and smallest DAS give best fatigue life. In addition, when the pore size and DAS values are increased, similarly, the deviation of results is increasing. That means the samples with lower pore size and DAS values could give more reliable results. Finally, the author noted that there is no significant effect of Sr modification on the fatigue life [Maj02].

Meyer et al. (1997) investigated the influence of microstructure on the static and thermal fatigue properties of 319 alloys. The effects of alloy grade, DAS which is influenced by cooling rate directly and heat treatment on the tensile and thermo-mechanical fatigue are studied. Two different alloy compositions which have different DAS values as 20 μm , 30 μm and 50 μm and two different heat treatment conditions as cast (without heat treatment) and T64 have been studied. In conclusion, UTS is increased with lower DAS values. Elongation and YS showed similar results with UTS. When comparing the alloy composition, YS is increasing and elongation is decreasing with impurities. The underlying reason for this is needle shaped or Chinese script shaped impurities such as iron and manganese. They cause brittle fracture in the structure. According to thermo-mechanical fatigue results, cycle of fracture is increased with lower DAS. Heat treatment such as T64 gives better fatigue strength [Mey97].

Wickberg et al. (1984) studied the effects of microstructure on the fatigue properties of a Cast Al7SiMg alloy. In addition, T6 heat treatment is applied to all specimens. They determined the relationship between SDAS and fatigue behaviour. The authors noted that lower SDAS values result in higher strength. Beside this, they figured out the effect of SDAS on the mechanical properties and the effect of porosity on the fatigue behaviour [Wic84].

Wang et al. (2001) studied the effect of micro structural constituents of A356/357 on the fatigue behaviour. They minimized the casting defects to see the influence of micro structural

constituents such as SDAS and content. The influence of SDAS or content on the fatigue behaviour becomes more appreciable. Normally, the size of casting defects is larger than microstructure defects. Thus, porosity has a more significant effect on fatigue. However, improved casting technology minimizes casting defects. In the present case, micro structural effects are getting more and more important on the fatigue behaviour. In the results, three different levels are described such as lower SDAS values level, intermediate SDAS values level and higher SDAS values level. Lower level is between 30 μm - 40 μm , intermediate level is between 40 μm - 60 μm and higher level is > 60 μm . At the lower and higher levels, fatigue life is decreasing with higher SDAS values as expected. But at the intermediate level, there is no significant difference on the fatigue life cycle. This result shows that, reducing SDAS values from around 60 μm to 40 μm is not sufficient to enhance the fatigue life. On the other hand, reducing SDAS values from 60 μm to 30 μm or 20 μm could show distinguished differences on the fatigue behaviour [Wan01].

According to Rie and Schmidt (1984) fatigue damage starts with strain location, crack initiation and crack propagation [Rie04].

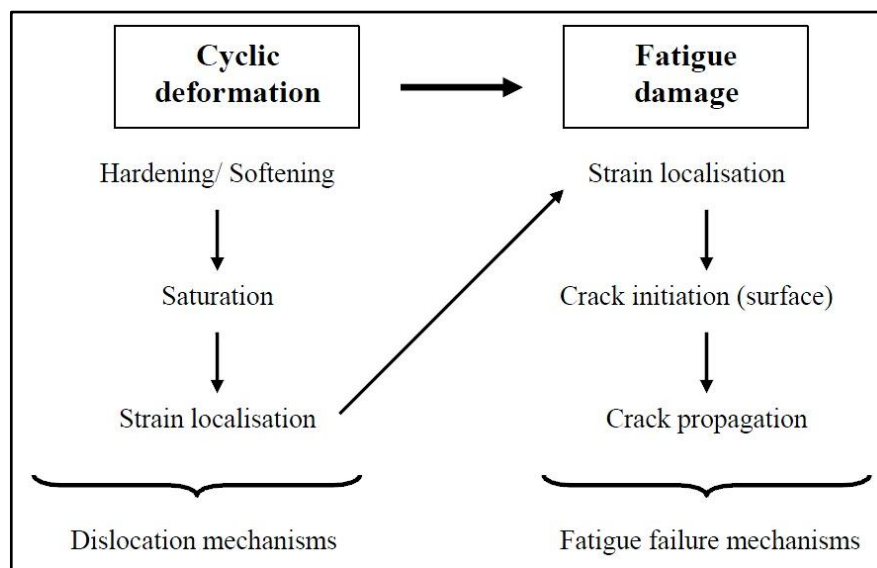


Figure 2.3: Chronological overview of damage mechanism leading to failure [Kli12], [Rie04]

Kliment (2012) shows the chronological steps of fatigue failure. First, cyclic deformation causes hardening and softening in the structure, as seen in Figure 2.3. After dislocation mechanism is active, crack initiation starts on the surface in micro scale. These micro cracks propagate to macro cracks and the failure occurs [Kli12].

2.2 Application in the automotive industry

2.2.1 Cylinder head

Main function of cylinder head is housing the cylinders under mechanical and thermal stresses. As known, air and gasoline are mixed in the combustion chamber and cylinder head conveys air and gasoline to the combustion chamber.

Cylinder head is one of the most complex parts in the engine. Combustion chamber areas and camshaft bearing supports or seats are critical parts and subjected to high stresses [Kor08].

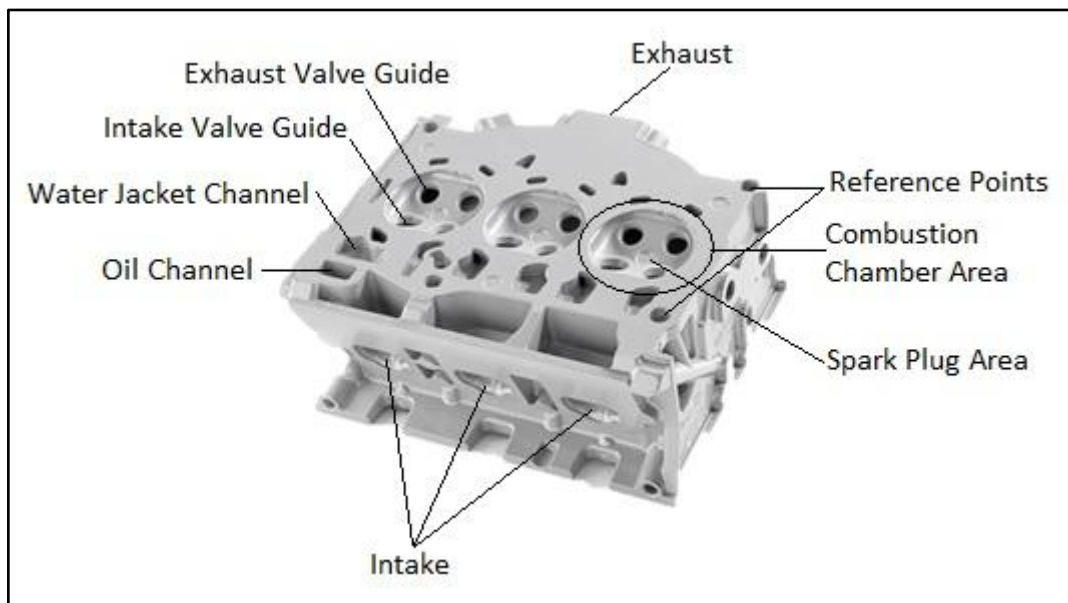


Figure 2.4: Detailed aluminium cylinder head [NN15]

In this study, aluminium cylinder head which is shown in detail in Figure 2.4 is used. This cylinder head is part of 1.0 lt MPI (Multi Point Injection) engine which has 3 cylinders and 4 valves per cylinder. In different designs of cylinder heads, intake – exhaust valves, oil and water jacket channels and spark plugs could be located on different regions. Similarly, number of the combustion chamber or intake – exhaust valve guides may vary. Based on practical knowledge, the most critical area is determined to be the combustion chamber which is affected by mechanical loads. In this study, specimens which are used for Brinell Hardness measurement, SDAS measurement, tensile and fatigue tests are extracted from the critical areas.

As mentioned earlier, Zhang et al. (2005) studied the aluminium cylinder heads. They paid attention to the effects of heat treatment on the mechanical properties of cylinder blocks and cylinder heads. They applied heat treatment on the specimens which are extracted from non-heat treated cylinder heads instead of whole heat treated cylinder heads. In results, the authors noted that the mechanical properties could be different if specimens are extracted

from whole heat treated cylinder heads [Zha05]. Similarly, additional samples prepared by pouring liquid metal to tensile test bar mould which is shaped with respect to standard test specimen dimensions instead of being extracted from cylinder head could give different results. The main reason of this situation is to see the effects of cooling (solidification) conditions. Surely, cylinder head moulds and tensile test bar mould have different solidification characters. Thus, the mechanical properties show differences in different shaped moulds.

In addition, different regions of same part could be affected by solidification condition and may show different mechanical properties. It is clear that extracted specimens from cylinder head for tensile and fatigue tests give closer results to real conditions. For this reason, the specimens which are used in measurements and tests will be extracted from aluminium cylinder head in this study.

The cylinder head is located between cylinder block and cylinder head covers. Cylinder head creates the combustion chamber after sitting on the cylinder block. Cylinder head is fastened to cylinder block with head bolts. Seaming is provided by cylinder head gaskets. Cylinder head gaskets inhibit the leakage of cooling water and engine oil. In addition, it blocks the mixing cooling water and engine oil with each other. Figure 2.5 shows the cross-section.

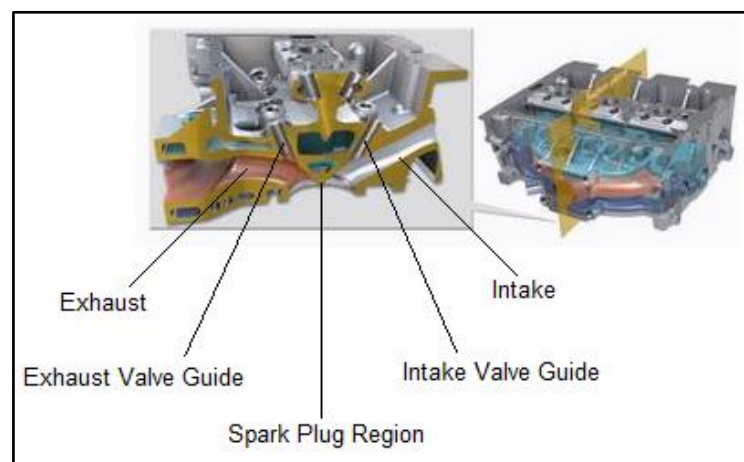


Figure 2.5: Cylinder head with cross-section [Bec11]

Molina et al. (2003) listed the notions which would be taken into account in the future:

- Increased combustion pressures create higher mechanical stresses which are divided into two groups such as static and dynamic stresses on the material,
- When these stresses are combined with very high temperature, the effects of stresses could be increased,
- Higher power density,
- Advanced design concepts of cylinder head lead the complex product to more complex structure [Mol03].

Molina et al. (2003) added some predictions about the next generation engines. The new advanced requirements pushed the casting supplier to improve the quality of casting. The quality of product improve with minimizing casting defects such as porosity and inclusions, improving the microstructure of material to get better mechanical properties [Mol03].

Pavlovic-Krstic (2010) stated that the existing capabilities of present materials must be improved to satisfy the rising demands of the cylinder head. There are two possibilities to improve these capabilities:

- Optimization of the chemical composition of the material,
- Alternative casting method and construction principles.

Optimization of the chemical content can help to improve the quality of microstructure and get finer grain and lower porosity. Alternative constructions such as different part geometries can reduce the mechanical loading [Pav10].

Alternative casting methods or construction principles can cause extremely high investment costs. Therefore, optimization of chemical composition is more preferable than alternative casting method and construction.

As mentioned previously, aluminium cylinder heads are working under high loads. Material has to satisfy sufficient tensile strength, yield strength and elongation requirements which are described by international standards or main manufacturers. In addition to this, high temperature could be transmitted by the material which has high thermal conductivity coefficient.

Pavlovic-Krstic (2010) repeated the importance of lightweight materials with respect to reduction of gasoline consumption and CO₂ emission. Material has to be lightweight by making no concessions to strength and endurance. Lightweight material has an advantage not only on the reduction of consumption and emission but also gives a chance to use additional safety and comfort equipment. For these reasons, weight reduction is defined as one of the most important aims for future automotive applications [Pav10].

Flowing of air and gasoline throughout cylinder heads from intake valves regions to combustion chamber has to be accomplished on a smooth and clean surface. Roughness should be minimized because the notches and micro cracks could initiate and lead to cracks. Thus, the surface quality has to be increased to prevent these threats.

European Aluminium Association (2011) stated that the castability of aluminium could be improved by using Si additive. On the other hand, Cu additive could have negative effects on the feeding behaviour. Beside this, Cu additive is required for higher strength, hardness, machinability and thermal conductivity [NN11]. Because of these, Al-Si-Cu based aluminium alloys are widely used in automotive industry.

Aluminium alloys can satisfy many requirements in automotive industry. So that, aluminium cylinder heads have shown to have advantages over iron cylinder heads in last decades. Aluminium silicon copper alloys such as AlSi6Cu4, AlSi7Cu3 and AlSi7MgCu0.5 are widely used materials in the production of aluminium cylinder heads. In this study, AlSi6Cu4 is used in the experimental study section.

2.3 Foundry technology

European Aluminium Association (2002) listed the ten casting methods which are used in automotive applications. These methods are green sand casting, core package casting, gravity die casting (GDC), low pressure die casting (LPDC), high pressure die casting (HPDC), vacuum die casting, squeeze casting, thixocasting, vacuum riserless casting and lost foam casting [NN02].

Figure 2.6 shows the trends in market share of casting methods for aluminium cylinder heads. As shown, the biggest percentage of market is covered by gravity die casting method.

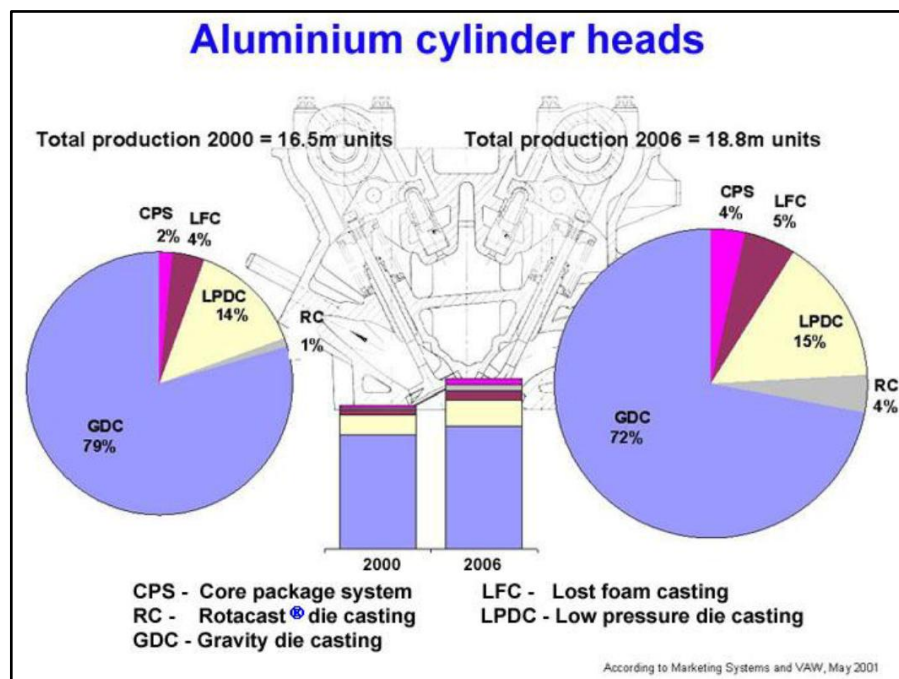


Figure 2.6: Trends in market share of casting methods for aluminium cylinder heads [NN02]

2.3.1 Casting of aluminium cylinder heads

Pavlak (2010) stated that the gating system can affect the casting quality and the design of a gating system is important. Metal flows from ladle to the mould cavity through these gates. The selection of a good gating system is even more important if the gravity casting process is used. Poor gating techniques create turbulent flow which is a negative parameter for casting. There are three types of gating systems which could be used in cylinder head production.

Figure 2.7 compares these three different gating systems. Top casting method (Figure 2.7.a) provides a directional solidification process and it helps to get better mechanical properties. On the other hand, turbulent flow is the biggest disadvantage for top casting. Bottom casting method (Figure 2.7.b) has laminar flow when compared to the top casting method. But this time, cooling conditions get worse and mechanical properties deteriorate. In addition to this, shrinkage and gas pores occur in the bottom gating system. Tilt pouring method (Figure 2.7.c) has all advantages of top casting with lower turbulent flow. Other important factors which affect the quality of products are melt temperature, mould temperature, filling time and alloy composition [Pav10].

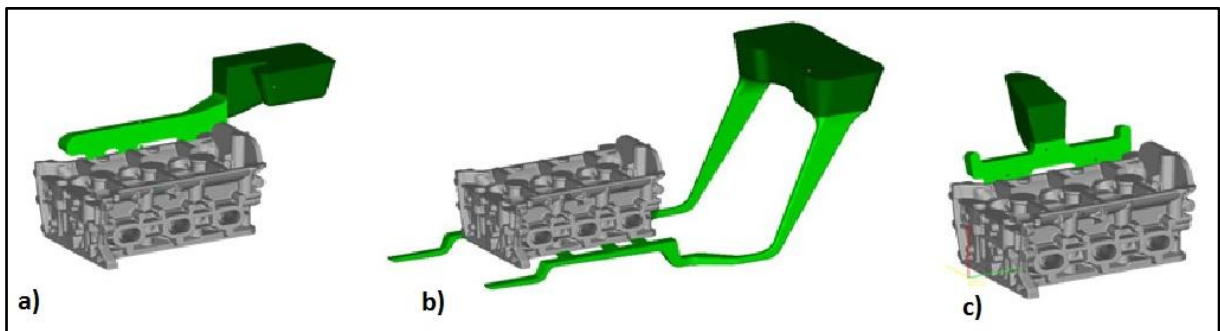


Figure 2.7: a) Top casting method, b) Bottom casting method, c) Tilt casting method [Pav08]

Instead of all casting methods and gating systems, the casting method and gating system used in the experimental method will be detailed in this study. The casting method which is called tilt gravity casting can be listed under the gravity die casting.

Köhler et al. (2010) noted that a variety of casting processes are applied in the production of aluminium cylinder heads. According to the physical principles and the position of the caster, the name of methods shows differences. Tilt gravity casting is described by the caster position which is between 0° and 90° . If the top position angle reaches to 180° , it is called as Rotacast method.

Zero-turbulence flow, low-oxide filling of the mould, directional solidification and fine-grain microstructure with small dendrite arm spacing are demanded for perfect aluminium cylinder heads. The principle of tilt gravity casting is similar to pouring beer into a glass or mug [Koh10].

Smetan et al. (2014) published their study about a new innovative casting process. In last decades, aluminium casting industry is ruled by gravity die casting and low pressure die casting processes. Tilt casting process is relatively new casting process for industry. Figure 2.8 shows this process step by step with respect to time. Pouring process continues around 7 seconds and the solidification of cylinder head finished around 150 seconds.

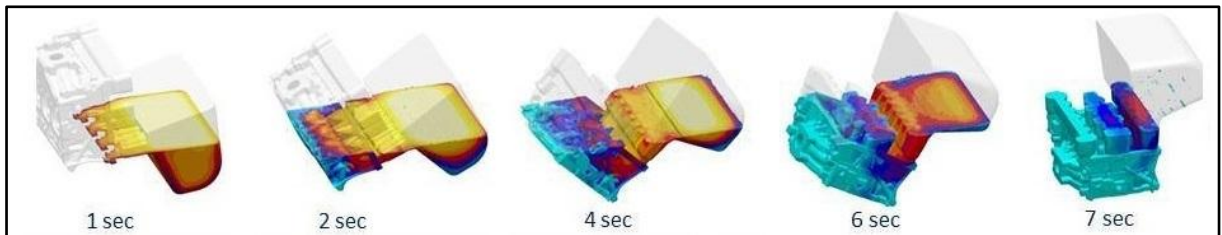


Figure 2.8: Filling of mould cavity in tilt gravity casting [Sme14]

In the experimental methods section of this thesis, similar approach is used as given by Smetan et al. (2014). As the first step in the experimental approach, the basin is filled by a robot arm from the holding crucible with a very low turbulence (Figure 2.9.a). The filled basin is transported to the mould and the mould is positioned to 0° angle simultaneously (Figure 2.9.b). The filled basin is connected to the mould by robot arm and the filled basin is docked to the mould (Figure 2.9.c). Rotational movement of the mould is started from 0° to 90° angle and the cavity is filled by liquid metal (Figure 2.9.d). This filling process takes nearly 7 seconds as mentioned above. When the angle reaches 90° , rotational movement is finished and the solidification starts after pouring (Figure 2.9.e). Finally, discharged casting basin is undocked from mould by robot arm (Figure 2.9.f) and the process is completed. The discharged basin is cleaned by pressurized air and prepared for the next cycle.

The advantages of this experimental approach are:

- Extremely low-turbulence flow,
- Low-oxide filling,
- Rapid and controlled solidification [Sme14].



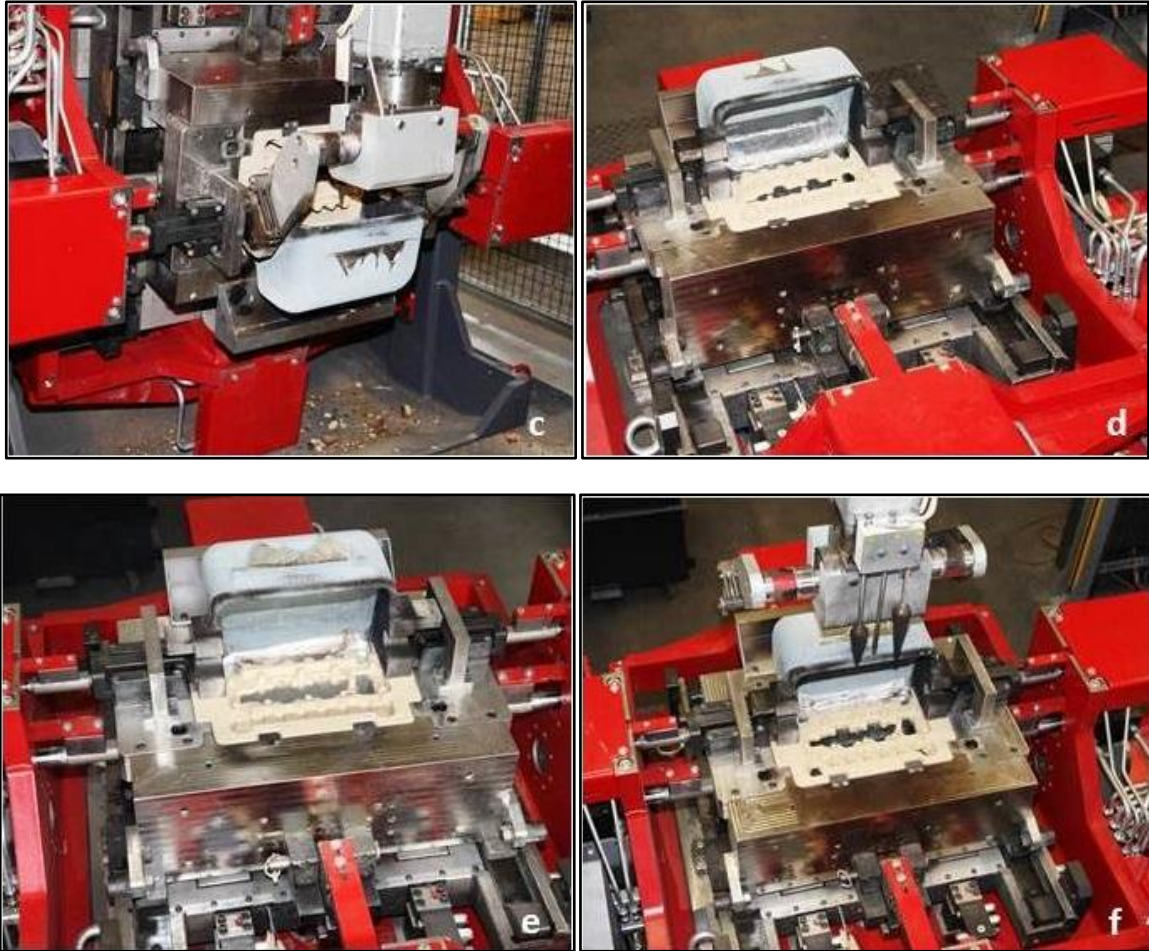


Figure 2.9: a) Lading and dosing, b) Transporting of casting basin, c) Docking of casting basin, d) Starting of casting, e) Ending of casting, f) Undocking of casting basin [Sme14]

The casting process is started with setting of cores. 8 different sand cores are put together into the core holder by the operator. Sand cores will be detailed in the 'Experimental Method' section in this study. Cores are taken from core holder to mould by robot in first section of 'Carousel-Line'. After that, the mould rotates with sand cores as shown in Figure 2.9.b. A second robot arm fills the basin with liquid metal from the holding crucible and attaches it to the mould and so is the pouring process completed in the second section of 'Carousel-Line'. The mould moves from the second section to the third section for solidification. First robot arm takes the new poured part from the third step of 'Carousel-Line' to cooling bands. After cooling down, the part comes to the hammering station. Rosined and pressed sand cores are formed to sand form with hammer pressure. Flashes are sawed before the decoring process for which vibratory mould is used. Sand form cores release easily with vibration after the hammering station. After decoring, runner cutting and feeder cutting processes are done by saw. Finally, the part is taken from the outfeed roller conveyor by an operator. Visual inspection before machining is done by operator. Laser machine marks the part and the casting process is completed.

2.4 Material: Aluminium and aluminium alloys

European Aluminium Association (2011) stated that cast iron cylinder heads have been almost completely replaced by cast aluminium alloys during last 20 years in Europe. Aluminium has the advantages of being light weight, having a high thermal conductivity and being easily machinable as compared to cast iron. The weight reduces around 50% and critical areas such as combustion chamber cool down faster [NN11].

2.4.1 Aluminium and aluminium alloys

Aluminium is preferred for variety of automotive components such as cylinder heads, cylinder blocks, brackets and pistons.

Knirsch et al. (2004) listed the alloys which are used most frequently in manufacturing of cylinder heads. These alloys are G- AlSi6Cu4 , G- AlSi7Mg0.3 , G- AlSi7Mg0.7 , G- AlSi9Cu3 and G- AlSi10Mg(Cu) [Kni04].

In this study, cast cylinder heads made from AlSi6Cu4 are used. The related standard used for the material in this study is DIN EN 1706. The Euro norm is EN AC-45000 and it is chemically in EN AC- AlSi6Cu4 .

Chemical composition and mechanical properties of AlSi6Cu4 are given in Table 2.2 and Table 2.3 from the related standard [EN10]:

Table 2.2: Chemical composition of AlSi6Cu4 [EN10]

	EN AC-45000		EN AC-45000
Si (%)	5.0 – 7.0	Zn (%)	2.0
Fe (%)	1.0 (0.9)	Pb (%)	0.30
Cu (%)	3.0 – 5.0	Sn (%)	0.15
Mn (%)	0.2 – 0.65	Ti (%)	0.25 (0.20)
Mg (%)	0.55	Others (%)	0.35
Cr (%)	0.15	Al (%)	Reminder
Ni (%)	0.45		

Table 2.3: Mechanical properties of AlSi6Cu4 [EN10]

	Temper Designation	Tensile Strength (MPa)	Yield Strength (MPa)	Elongation (%)	Brinell Hardness
EN AC-45000	As Cast	Min. 170	Min. 100	1	75

As an addition to these tables, Brown (1999) noted that the density of aluminium is 2.70 g/cm² which is lower than other metals such as iron and copper. A volumetric shrinkage of between 3.5-6.0% which could vary according to the alloys occurs during solidification of aluminium castings [Bro99]. The volumetric shrinkage percentage should be taken into account before mould design with respect to accuracy and defects such as hot tearing and shrinkage porosity.

The alloy content should be designed to get desired properties. Castability, micro structural phases, mechanical properties could be taken into account during the arrangement of content. Silicon, copper, titanium, boron, strontium, magnesium and other metals can be added to get desired properties.

Pavlovic-Krstic (2010) classified the alloying elements into two groups. Major alloying elements control castability and develop the properties. Minor alloying elements refine the phases, modify the structure, affect the solidification behaviour, reduce the oxidation and sprue [Pav10]. On the other hand, Rana et al. (2012) added two more groups that are called modifier elements and impurity elements. Modifier elements modify the phases, influence castability and improve the properties of the structure [Ran12]. Table 2.4 shows the groups of elements which are used in aluminium alloys.

Table 2.4: Major, minor and modifier elements of aluminium alloys [Ran12]

	Major Elements	Minor Elements	Modifier Elements	Impurity Elements
Examples	Si, Cu, Mg	Ni, Sn	Ti, B, Sr, P, Mn, Cr	Zn, Fe, Be

Actually, Ti and B are known as grain refiners from practical knowledge. Surely, they could be evaluated in the same group with modifiers but it could be more understandable if they are listed under a new group which is called grain refiner elements.

2.4.2 Effect of alloying elements

Silicon (Si): Pure aluminium is not a castable metal and is used in limited applications. Silicon additive improves the fluidity dramatically and is used widely in casting alloys. Because of these, silicon is called a major alloying element. Not only fluidity, but also feeding, hot tear resistances and mechanical properties are improved by silicon addition. Beside all advantages, silicon-rich phases –another expression for hypereutectic alloys- are hard and it causes low ductility and machinability [Bro99].

Kaufmann and Rooy (2004) pointed out another effect of fluidity. Fluidity helps to filling of thin walls and to produce more intricate design and details. It could affect the solidification porosity which is reduced by improved feeding [Kau04].

Copper (Cu): Copper improves the strength, hardness, machinability and heat treatability. Heat treatment is more effective with 4-5.5% Cu in the content and it shows relatively improved casting properties [Kau04]. The addition of copper to Al-Si creates Al- Al₂Cu eutectic and/or Al₂Cu phases and other inter metallic compounds that increase the strength and machinability of the alloys [Pav10]. On the other side, copper reduces the resistance to corrosion and results in hot tear [Kau04].

Titanium (Ti): Titanium is widely used to refine the grain structure of aluminium alloys. In casting, Ti is used with the combination of smaller amounts of B. Al5Ti1B is widely used in the industry as a grain refiner. It contains 5% Ti, 1% B and Al balance. Soluble titanium aluminides (TiAl₃) and insoluble titanium diboride (TiB₂) could be reacted by aluminium, titanium and boron. TiB₂ is more effective in grain refinement. In the production, Ti additive is higher than those required for grain refinement to reduce cracking hazard [Kau04].

From the practical knowledge, Ti ratio is between 0.12% (1200 ppm) and 0.16% (1600 ppm) and it is supplied by Al5Ti1B rods. Al5Ti1B rods do not result in finer grains only but also in bright parts. The time of Ti effect is limited around 30-45 minutes. This means, Ti plays important role on grain refinement in first 30-45 minutes after adding Ti into liquid metal.

Boron (B): As mentioned before, boron combines with Ti to grain refinement in aluminium alloys. Titanium boride forms interact with active grain refining phases such as (TiAl₃) titanium aluminides. Metallic boride reduces tool life in machining and coarse form or agglomerated inclusions show detrimental affect the mechanical properties and ductility [Kau04]. From the practical knowledge, B ratio is between 0.0006% (6 ppm) and 0.003% (30 ppm) and similarly boride is supplied by Al5Ti1B rods.

Strontium (Sr): Strontium uses as a modifier and the effective modification can be done at low levels. This level is around 0.008% (80 ppm) – 0.04% (400 ppm). Higher addition percentage can lead the porosity. Sr could be inactive at low solidification rate [Kau04].

In addition to this, Sr addition improves the Cu distribution in the matrix and Al_2Cu distributes and helps to improve the strength [Gop13]. From the practical knowledge, Sr ratio is between 0.008% (6 ppm) and 0.02% (200 ppm) and it is supplied by AlSr15 rods. It contains 15% Sr and Al balance. Sr modified the structure from coarse plate form to refined fibrous form. This modification provides better mechanical properties and elongation.

2.4.3 Al-Si-Cu (3xx.x) system

Table 2.5: Classification of casting aluminium alloys [Pav10]

	AA	Major Alloying Elements	Heat Treatment
Casting Alloys	1xx.x	Pure Al.	Non-heat treatable alloys
	2xx.x	Al-Cu	Heat treatable alloys
	3xx.x	Al-Si+Cu/Mg	Heat treatable alloys
	4xx.x	Al-Si	Non-heat treatable alloys
	5xx.x	Al-Mg	Non-heat treatable alloys
	6xx.x	Unused Series	Unused Series
	7xx.x	Al-Zn	Heat treatable alloys
	8xx.x	Al-Sn	Heat treatable alloys
	9xx.x	Al-Miscellaneous	Heat treatable alloys

Aluminium alloys are classified into 9 groups with respect to their content. Al + (Si-Cu) or (Si-Cu-Mg) or (Si-Mg) evaluated under 3xx.x system. Al-Si-Cu (3xx.x) system is the most widely used in aluminium casting. The percentages of Si and Cu could affect the properties but Al-Si-Cu (3xx.x) has a big advantage for complex casting in the permanent mould among other systems. Other metals such as titanium, boron, iron, magnesium, manganese and zinc are also important in modifying the basic properties. Al-Si-Cu alloys show good casting characteristics, high strength, high hardness and improved machinability. These properties are obtained in the as-cast condition. However, additional heat treatment could be applied and additive elements could be added to get better results. Heat treatment leads the high strength capabilities. Because of all, Al-Si-Cu alloys are used widely in the production of cylinder heads, blocks, pistons and crankcases [Pav10], [Mey97].

2.5 Solidification

2.5.1 Solidification of Al-Si-Cu systems

The solidification begins with precipitations of primary α aluminium phases in the structure. The primary α aluminium phases grow with temperature reduction and take a dendritic shape. Temperature reduction, in other words cooling rate, could affect the dendritic shape effectively. Similar to dendritic shape, dendritic microstructure is affected by casting parameters such as cooling rate and temperature. In addition to these parameters, chemical composition affects the size of the dendrites. [Pav10].

Djurđević and Grzinčić (2012) wrote four phenomena which control the structure and affect the mechanical properties. These are chemical composition, cooling rate, temperature gradient and liquid metal treatment. Cooling rate plays major role on the mechanical properties [Dju12].

Intricate cast automotive parts have complicated cooling processes. The biggest problem is that the cooling rate is not the same for all regions of parts. According to literature survey, higher cooling rate helps to refine grain size and decrease the SDAS values. Designers have to take into account that the mechanical properties of the part show differences. Critical areas such as combustion chamber area and valve bridges can show different properties from other areas.

Bast and Kotova (2007) noted two different solidification types which are called exogenous and endogenous. There are smooth wall, rough wall, spongy solidification subtypes for the exogenous one and pulpy (or mushy), shell forming solidification subtypes for the endogenous one (Figure 2.10) [Bas07].

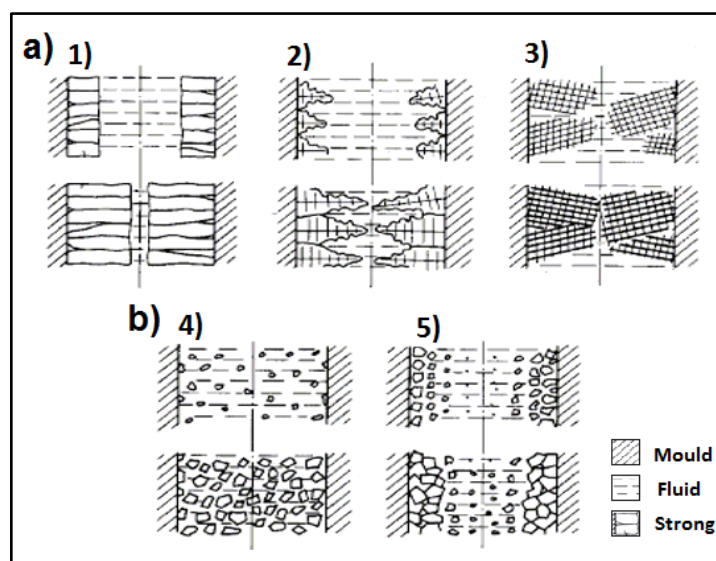


Figure 2.10: a) Exogenous solidification type (1) Smooth wall, (2) Rough wall, (3) Spongy, b) Endogenous solidification type (4) Pulpy or mushy, (5) Shell forming [Bas07]

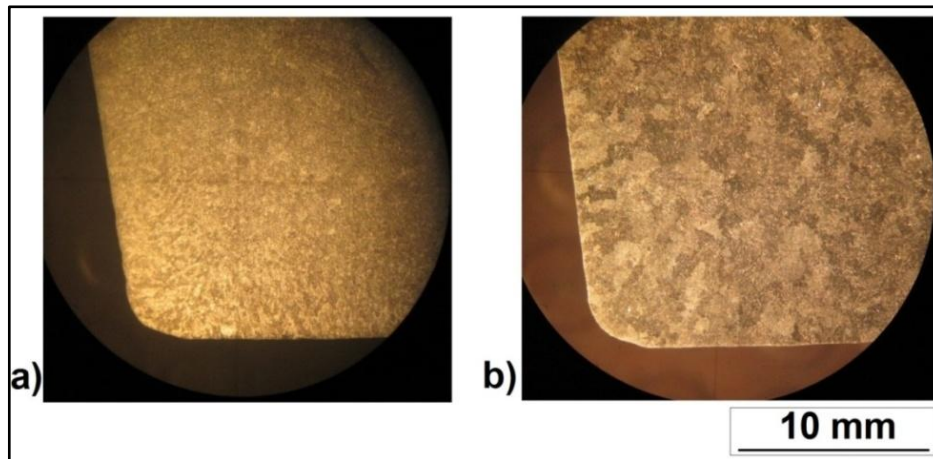


Figure 2.11: a) Higher solidification speed (Rough wall type) (x10 Magnification), b) Lower solidification speed (Spongy) (x10 Magnification)

The macrostructure pictures from Olympus SZ-PT microscope with x10 magnification is shown in Figure 2.11.a and b. The effect of different solidification speeds on the macrostructure is clear. Higher solidification speed which occurs in cold mould gives fine grain size and rough wall type solidification. On the other hand, lower solidification speed which occurs in hot mould gives relatively bigger grain size and spongy type solidification.

2.5.2 Casting defects

The international committee of foundry technical associations standardized the casting defects into the seven basic categories. They are metallic projections, cavities, discontinuities (cracks), defects, incomplete casting, incorrect dimension and inclusions or structural anomalies [Row93]. Theoretically, each category can be divided into the subgroups with examples. In this study, critical defects which occur in aluminium cylinder heads manufacturing process will be discussed in detail. Practical knowledge shows that the casting defects occur during solidification. Campbell and Harding (1994) detailed the casting defects which occur during solidification. Gas porosity, shrinkage defects, oxidation, hot tearing and cracks are the most critical defects. Hydrogen in the liquid metal, air contact and gases in the cores may cause gas porosity. They noted that gas porosities may occur close to the surface which is last solidified region [Cam94]. Gas porosity is reduced by blowing nitrogen into the liquid metal substantially. Nitrogen removes hydrogen which appears in the liquid metal. Reduction of gas content by degassing is experimented in this study and the results are shown in section 'Gas Content'. According to the results, gas reduction can reach up to 98% for the related samples.

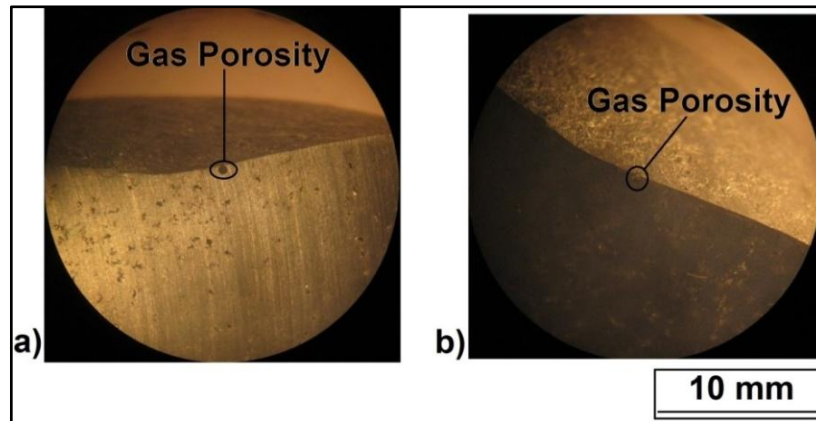


Figure 2.12: Macrostructure pictures of gas porosity. a) x10 Magnification, b) x10 Magnification

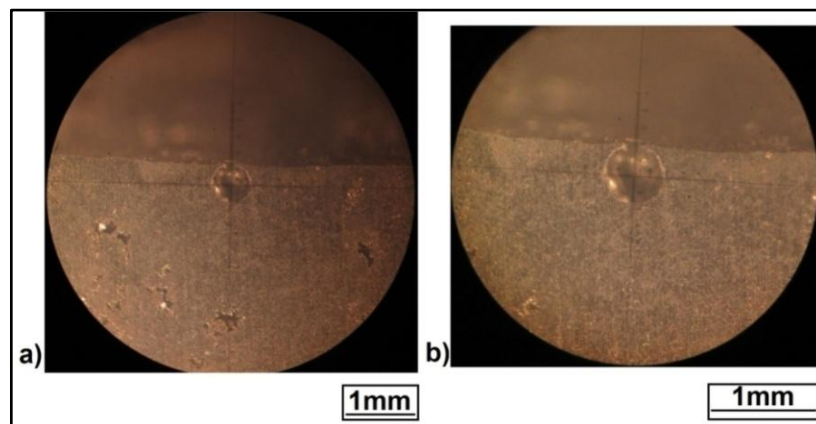


Figure 2.13: Macrostructure pictures of gas porosity. a) x40 Magnification, b) x63 Magnification

Shrinkage porosities are divided into the three groups. These are macroporosity, microporosity and intermediate types. As known, solidification starts along the wall and the solidification rate of the top surface is relatively slow. Thus, primary macroporosity (Figure 2.14) which is called a shrinkage pipe or tail occurs on the top surface. Secondary macroporosity (Figure 2.14) which is called a pore may occur under this pipe or tail [Cam94]. Figure 2.15 shows shrinkage porosities which are located under the tail.

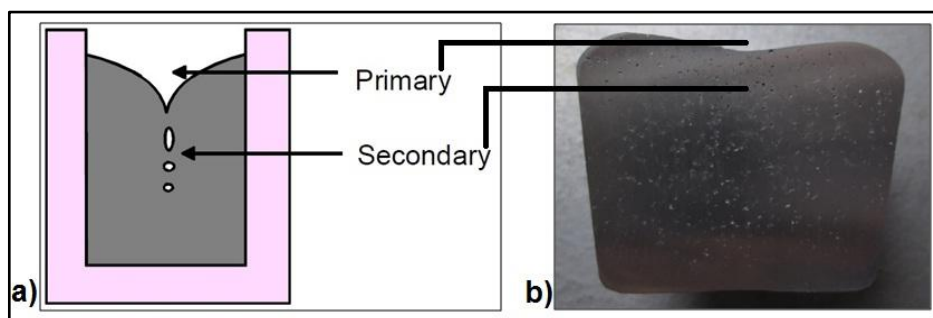


Figure 2.14: a) Primary and secondary macro porosity [Cam94], b) Primary and secondary macro porosity

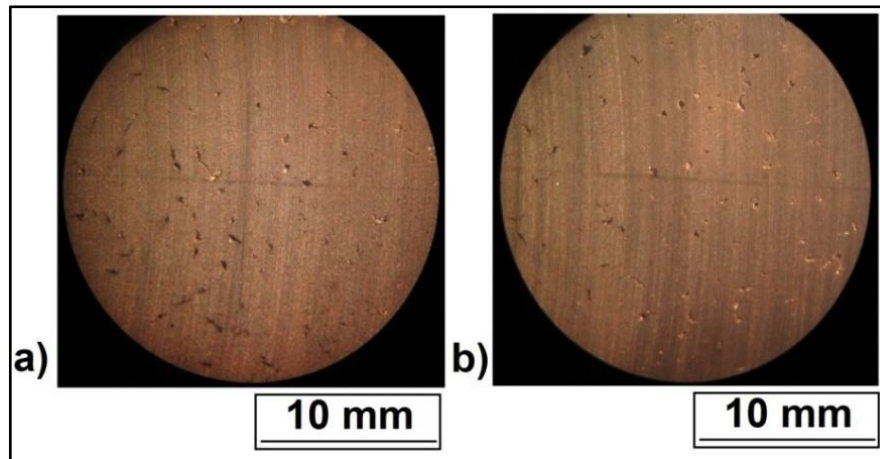


Figure 2.15: Macrostructure pictures of shrinkage. a) x10 Magnification, b) x10 Magnification

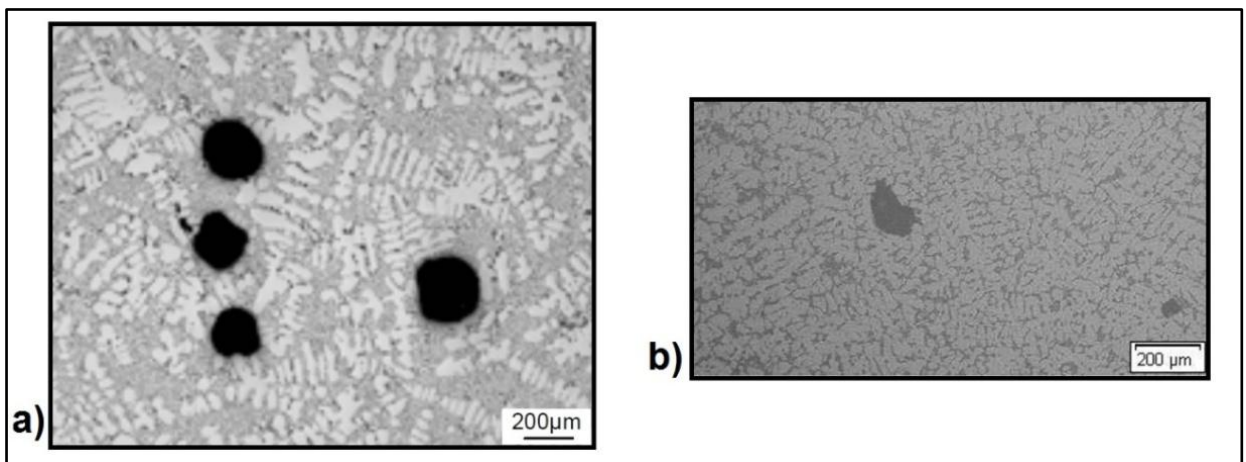


Figure 2.16: a) Optical micrographs of gas porosity in cylinder head casting [Bir08], b) Optical micrographs of gas porosity in cylinder head casting

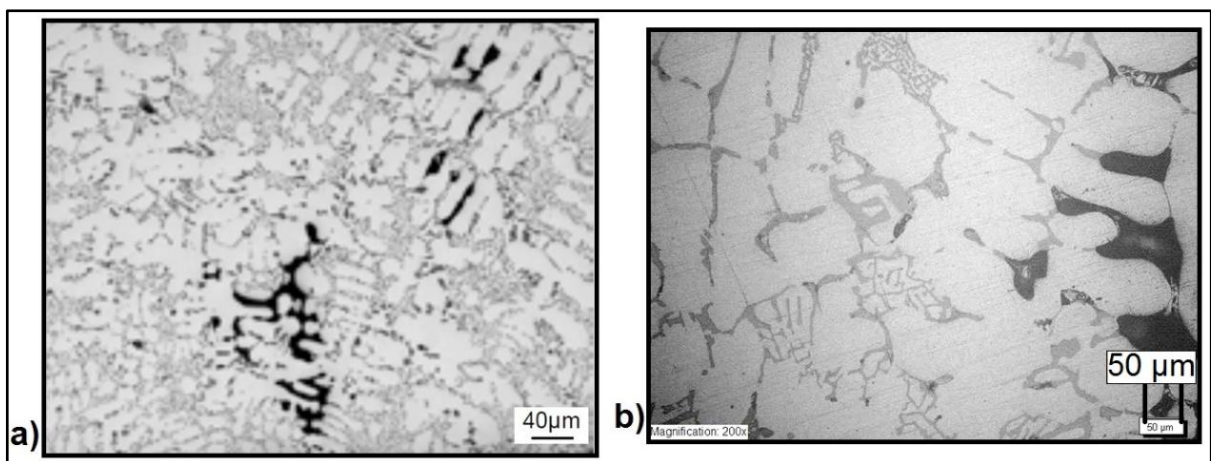


Figure 2.17: a) Optical micrographs of shrinkage in cylinder head casting [Bir08], b) Optical micrographs of shrinkage in cylinder head casting

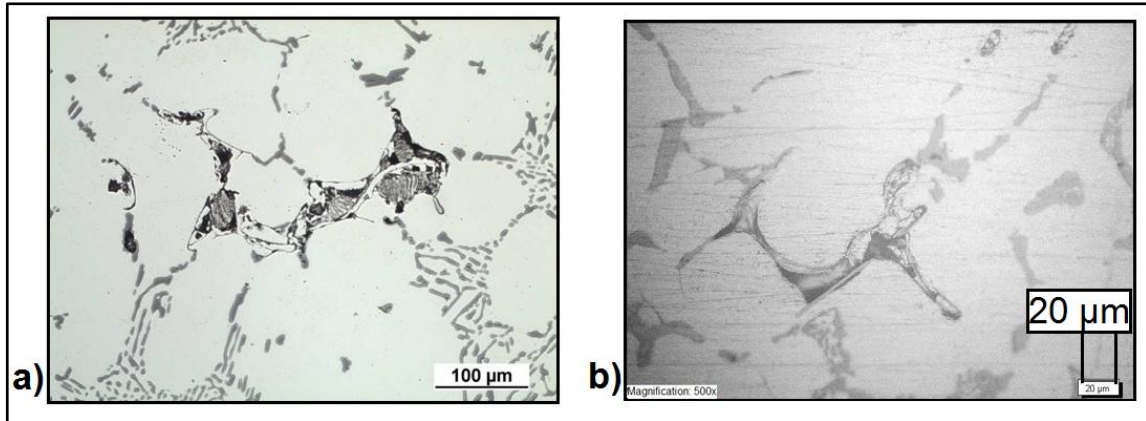


Figure 2.18: a) Optical micrographs of oxide in engine head casting [Kon14], b) Optical micrographs of oxide in cylinder head casting

2.5.3 Dendrite arm spacing (DAS)

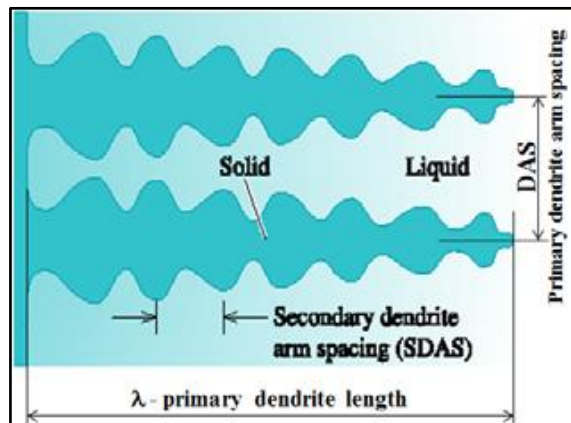


Figure 2.19: Primary and secondary dendrite arm spacing [Dju12]

First, the primary dendrite arms grow and reach the peak point at the liquidus temperature and then secondary and tertiary dendrite arms grow with the temperature decreasing until solidus temperature. Bonollo and Tovo (1999) gave the two important micro structural parameters which are primary dendrite arm spacing (λ_1) and secondary dendrite arm spacing (λ_2).

$$\lambda_1 = A G_L^a R^b \quad (2.1)$$

$$\lambda_2 = C t_s^n \quad (2.2)$$

Where G_L is the thermal gradient in the liquid in front of dendrites, R is solid-liquid interface velocity, t_s is solidification time and A , a , b , C and n are constant values and they depend on the alloys. Secondary dendrite arm spacing (SDAS) parameters is the most commonly used and it increases with decreasing cooling rate [Bon99].

As shown in (2.2), SDAS depends on the solidification time and material content which are varied with different chemical contents.

Serbino et al. (2011) stated that SDAS calculation shows great challenges in theoretical approach regarding the manufacturing methods, geometrical complexity, material content, mould temperature, pouring temperature and feeding. Thus, the intrinsic problems are difficult to solve without computer-assisted tools even for experienced professionals [Ser11].

Pavlovic-Kirstic (2010) described the test specification which is used for the cast sample. The procedure is described to check the secondary dendrite arm spacing in castings. The critical regions which may locate between the intake and the exhaust valves of cylinders are determined to measure secondary dendrite arm spacing values. In the case of cylinder heads with only three combustion chambers, the dendrite arm spacing is measured on the middle combustion chamber [Pav10]. Equations and inequalities for determining the secondary dendrite arm spacing (SDAS) are given as follows [Pav10]:

$$\text{Minimum number of dendrites that must be measured:} \quad n \geq 10 \quad (2.3)$$

$$\text{Index of the measured dendrites:} \quad i = \{1, 2, \dots, n\} \quad (2.4)$$

$$\text{Minimum number of dendrite arms per dendrite:} \quad m_i \geq 5 \quad (2.5)$$

$$\text{Measured length of the } i\text{-th dendrite:} \quad x_i \quad (2.6)$$

$$\text{Mean SDAS of the } i\text{-th dendrite:} \quad \bar{x}_{SDASi} = \frac{x_i}{m_i} \quad (2.7)$$

$$\text{Averaged SDAS:} \quad (2.8)$$

$$\bar{\bar{x}}_{SDAS} = \frac{1}{n} \cdot \sum_{i=1}^n \bar{x}_{SDASi} = \frac{1}{n} \cdot \sum_{i=1}^n \frac{x_i}{m_i}$$

$$\text{Estimated variance of averaged SDAS:} \quad (2.9)$$

$$s_{\bar{\bar{x}}_{SDAS}}^2 = \frac{1}{n-1} \cdot \sum_{i=1}^n (\bar{x}_{SDASi} - \bar{\bar{x}}_{SDAS})^2 \geq 9\mu\text{m}^2$$

$$\text{The mean SDAS ordered by magnitude:} \quad \bar{x}_{SDAS1} \leq \bar{x}_{SDAS2} \leq \dots \leq \bar{x}_{SDASk-1} \leq \bar{x}_{SDASk} \quad (2.10)$$

$$\text{With } k = \{1, 2, \dots, n\}$$

$$\text{Median of mean SDAS:} \quad \tilde{\bar{x}}_{SDAS} = \begin{cases} \bar{x}_{SDAS(\frac{k}{2})} & , \frac{k}{2} \notin IN \\ \frac{\bar{x}_{SDAS(\frac{k}{2})} + \bar{x}_{SDAS(\frac{k}{2}+1)}}{2} & , \frac{k}{2} \in IN \end{cases} \quad (2.11)$$

$$\text{With } |\bar{\bar{x}}_{SDAS} - \tilde{\bar{x}}_{SDAS}| \leq 0,5 \mu\text{m}$$

In addition to the theoretical approach, dendrite arm spacing can be measured by microscopes with special software. The microscope with special software is widely used to save time in the industry. Microscope gives a micro structural view as shown in Figure 2.20.a and the measurement method is clarified in Figure 2.20.b.

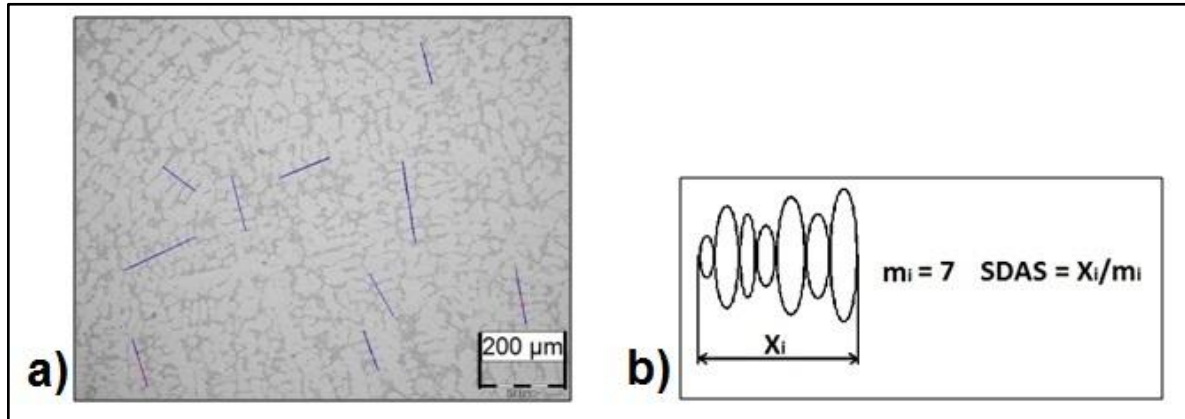


Figure 2.20: a) Microscope view sample (Magnification x100), b) SDAS measurement method (Linear interception method)

This measurement method is called linear interception method. Zhang et al. (2003) defined the linear interception method such as measuring the distance between the adjacent secondary arms of dendrite and dividing it by number of arms. Finer microstructure is related to a lower SDAS values particularly for cast aluminium alloys [Pav10], [Zha03].

Djurdjević and Grzinčić (2012) gave a definition about the SDAS very similar to the one indicated above. They noted that the best properties are associated with the smallest SDAS. A small value of SDAS occurs in the finer microstructure. Smaller grains, finer microstructure, micro homogeneity and distributed porosity which are desired features for the better mechanical properties are associated with small SDAS [Dju12].

Because of the mentioned effects, many automotive companies determined SDAS values limits for cylinder heads. Beside the values, the location of measurement is also important. The critical area of SDAS is determined by the automotive company. The critical areas could be the combustion chamber area, the valve bridge area or the camshaft bearing seats. SDAS value limits depend on the automotive company or the model of cylinder heads. As stated before, Pavlovic-Krstic (2010) wrote that these values range from 20 μm to 40 μm and the samples could be extracted from a distance of 3 mm – 5 mm from the combustion chamber surface [Pav10]. The expectation of limits will be tight in the future application.

In this study, the critical area is shown in Figure 2.21 and the samples for SDAS measurement are extracted from the marked area of combustion chamber surface.

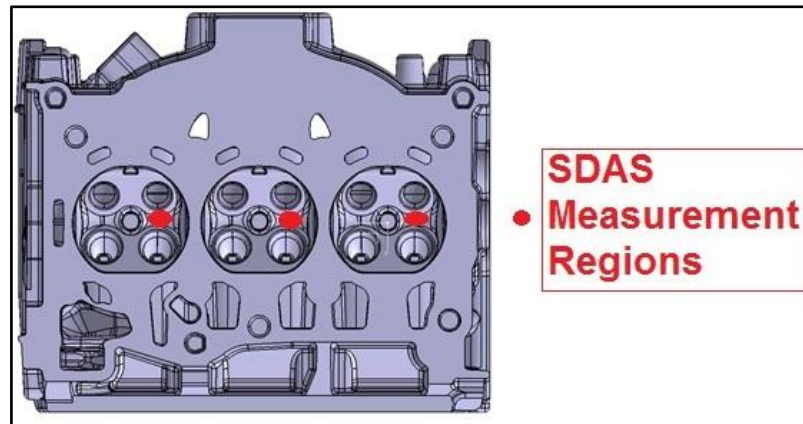


Figure 2.21: The measurement area of SDAS values on the combustion chamber [NN12]

2.6 Grain refinement

According to practical knowledge, grain refiner Al5Ti1B is widely used as master alloy. Beside this, different types such as rod, ingot, waffle plate are on the market. The amount of Al5Ti1B rod depends on the content of other elements.

Sigworth and Kuhn (2007) mentioned that the Ti level has to be 0.10% at least to get the desired benefits about grain refinement. Without this quantity of Ti it is not possible to get a structure with fine grain. In addition, the optimum B percentage must be around 0.0010 – 0.0020% (10 – 20 ppm) to get finer structure [Sig07].

Table 2.6: Ti, B values and grain size of 8 samples

Samples	Ti (%)	B (%)	Grain Size (µm)	Samples	Ti (%)	B (%)	Grain Size (µm)
No.1.1	0.1106	0.0002	500	No.2.1	0.1111	0.0004	500
No.1.2	0.1253	0.001	315	No.2.2	0.1378	0.0012	200
No.1.3	0.1358	0.0017	315	No.2.3	0.1472	0.0018	200
No.1.4	0.133	0.002	315	No.2.4	0.1466	0.0018	200

In this study, 8 different samples are cast to see the effect of grain refiner. From these 8 samples, three different grain size values are found according to 'Atlas Metallographique de l'a-S5 U3'. The pictures are compared to standard pictures with known grain size. Table 2.6 shows the content of all samples which are poured to understand the effect of grain refiner.

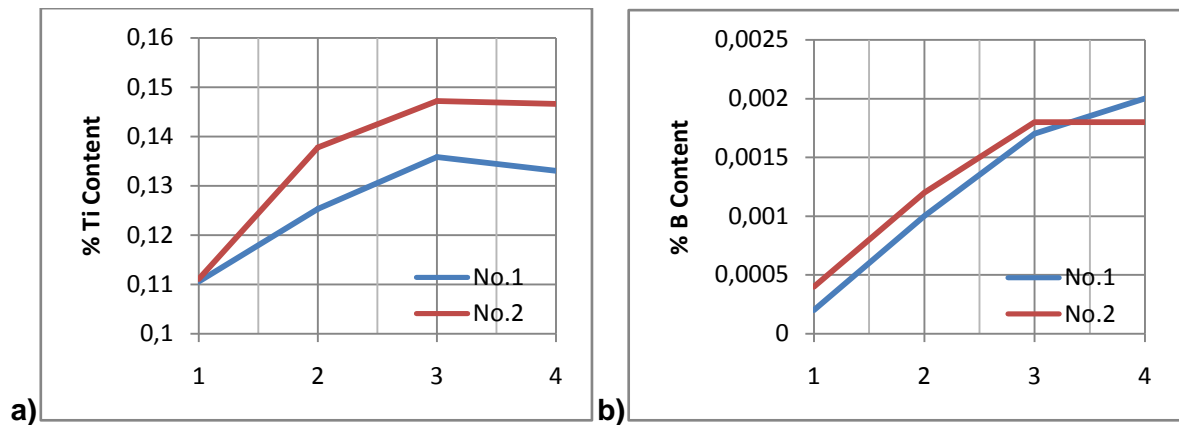


Figure 2.22: a) Ti content of grain refinement samples b) B content of grain refinement samples.

Figure 2.23 shows the pictures of samples. The samples are prepared according to ordinary metallographic preparation procedure as defined and detailed under ‘Specimen Preparation’ in the following chapter. Figure 2.23.a shows ‘No.1.1’ samples and the grain size is 500 μm . Similarly, Figure 2.23.b shows ‘No.1.2’ samples and the grain size is 315 μm and finally Figure 2.23.c shows ‘No.2.2’ samples and the grain size is 200 μm .

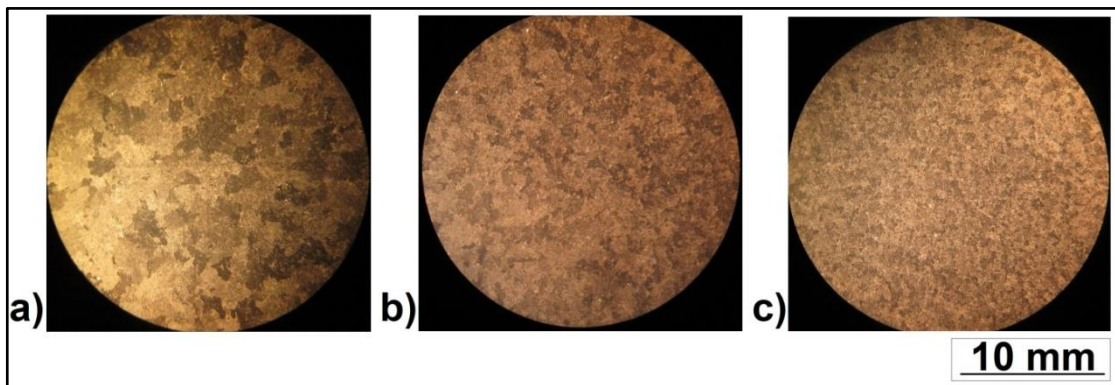


Figure 2.23: a) Macroscope picture of No.1.1 (Grain size: 500 μm), b) Picture of No.1.2 (Grain size: 315 μm), c) Picture of No.2.2 (Grain size: 200 μm)

2.6.1 Mechanism of grain refinement

After adding the master alloys, titanium aluminide (TiAl_3) start to nucleate as shown in Figure 2.24.a. The effect of grain refiner on the cooling curve is given in Figure 2.24.b. The metal is poured into a small metal cup and thermocouple records temperature as explained by Sigworth and Kuhn (2007). The data is transferred to computer and cooling curve can be drawn based on this data. These seven steps in Figure 2.24.a and b are clarified by Sigworth and Kuhn (2007) in detail.

(1) shows the presence of compound. (2) shows that $TiAl_3$ contact with liquid aluminium and the Ti-riched surface occurs. (3) shows the first nucleation of aluminium on the surface of compound. (4 – 5) present the growth of aluminium crystal on the surface. (6) shows the beginning of dendritic growth and continues (7) in the solidification process.

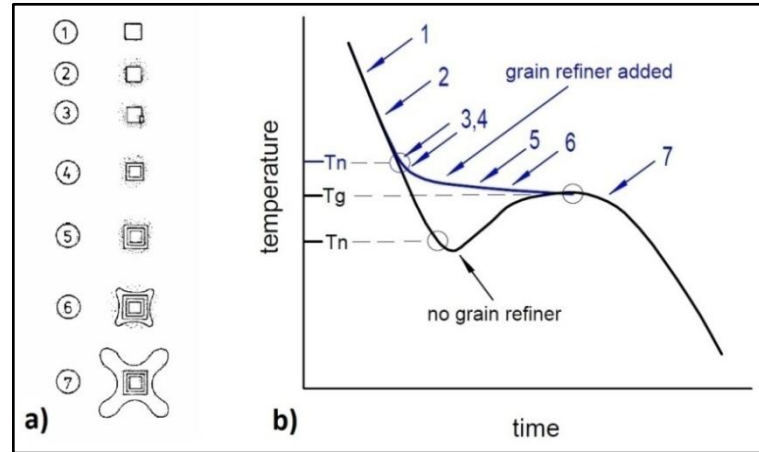


Figure 2.24: a) The nucleation of $TiAl_3$ [Bac83], b) The effect of grain refiner on the cooling curve [Sig07]

The effect of grain refiner on the cooling curve is shown in Figure 2.25.b. Ti is used for grain refinement of Al based alloy. T_n is nucleation temperature and T_g growth temperature. As seen, the nucleation is starting before growth with adding grain refiner. The smaller differences between T_g and T_n means smaller grain size in the structure [Sig07].

Perepezko (1988) explained two different models about the grain refinement. The first model is called carbide-boride model. This model states that carbide-boride compounds such as AlB_2 , TiB_2 and TiC are responsible for nucleation because $TiAl_3$ dissolves suddenly. On the other hand, boride particles located at grain boundaries and it is seen that those borides are insoluble and inactive particles for nucleation during freezing [Per88]. The second model is called peritectic reaction theory. This theory is based on the peritectic reaction. The presence of $TiAl_3$ is more active in the structure and it dominates grain refinement in the structure. The effect of grain refinement is reduced by the reduction of $TiAl_3$. $TiAl_3$ formed below liquidus temperature and promote at the peritectic temperature. In other respect, TiB_2 may act as the substrate for the nucleation of $TiAl_3$ for peritectic reaction at low titanium levels. This process is a transitory, for this reason the effect of $TiAl_3$ on the nucleation decreases with time [Per88].

Granger and Elliott (1988) said despite many studies on the mechanism of grain refinement, the mechanism of grain refinement is not totally clear. The authors added that recent studies show that Al-Ti-B master alloys contain boride (AlB_2 and TiB_2) particles which are effective centers for the Ti concentrations. First, TiB_2 is not effective in nucleation. After the solution of $TiAl_3$ (soluble aluminide) into the melt, AlB_2 and TiB_2 particles become active in nucleation [Gra88].

2.6.2 Methods of grain refinement

The grain refinement methods could be listed as rapid cooling, mechanical agitation and growth-hindering additions. First, rapid cooling gives finer grain structure and reduced grain growth. In addition, high cooling rate helps to get homogeneous distributed nuclei and recrystallization. All these changes affect the mechanical properties positively. Second, mechanical agitations such as stirring, gas purging and vibration could help the grain refinement. Beside the advantages, this method is not used in the industry because of high costs and labor and equipment requirements. Third, growth-hindering additions are using alloying elements which are known as grain refiner to prevent the growth of grain size. The effects of each alloying on the grain refinement are different. Ti and B have greatest effects on the grain refinement and Si, Cu are also effective than other alloying elements [Nef88].

In the following lines, Ti and B values before and after inoculation and the effect on the macrostructure are shown. First, chemical content of the structure before and after inoculation is given in Table 2.7 and macrostructure pictures are shown. As a grain refinement method, Ti - B cut rods are added. Other parameters which can affect the grain refinement such as melting temperature, mould temperature and pouring temperature are constant. Figure 2.25 shows the differences between before inoculation and after inoculation.

Table 2.7: Ti, B values of the structure before and after inoculation

	Ti (%)	B (%)	Grain Size (μm)
Before inoculation	0.1268	0.0003	315
After inoculation	0.1376	0.0011	200

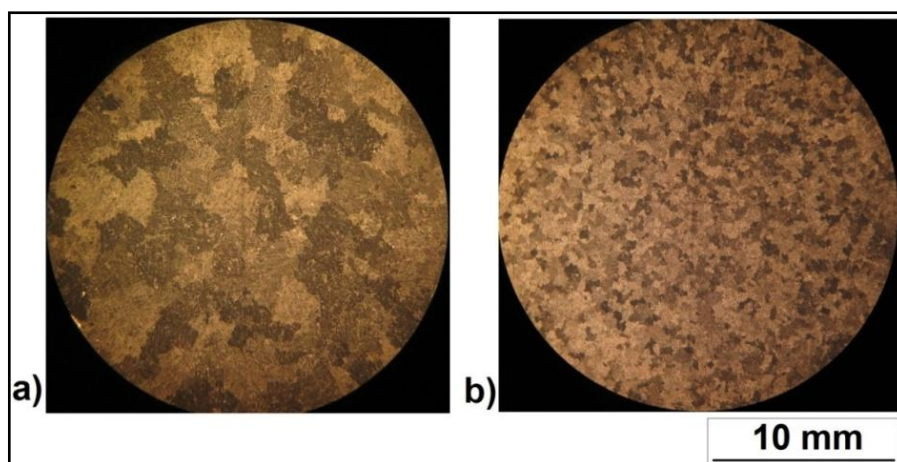


Figure 2.25: a) Macrostructure before inoculation, b) Macrostructure after inoculation

2.6.3 Advantages and disadvantages

Advantages of grain refinement are:

- Finer grain in the structure, it enhances the mechanical properties,
- Increased strength and ductility,
- Increased fluidity, feeding,
- Better castability,
- Reduced tendency of shrinkage,
- Rearranged and redistributed gas porosity and reduced porosity,
- Improved fatigue life [Suh07], [Sig07].

Disadvantages of grain refinement are:

- Agglomeration,
- Blockage of filters,
- Poisoning [Yu05].

The limitation of grain refinement depends on the amount of TiAl_3 and TiB_2 which are nucleate the $\alpha\text{-Al}$ phases. Basically, Ti is required to get finer structure. However, very high Ti content causes TiAl_3 growth instead of new nuclei and these phases hinder the Ti [Hu97], [Hu98], [Yu05].

2.6.4 Gas content

As mentioned before, the main precautions such as grain refinement, structure modification and degassing are applied during casting. In practice, degassing is applied to remove the gas from the structure. Degassing takes nearly 10-15 minutes while nitrogen is blown into the crucible. Nitrogen helps to remove hydrogen from the liquid metal.

Gas content reduction is calculated by using the density of sample which is solidified in air (d_{air}), density of sample which is solidified in vacuum (d_{vacuum}), and density index (DI) [Mad11].

$$DI = \left(1 - \frac{d_{\text{vacuum}}}{d_{\text{air}}}\right) * 100 \quad (2.12)$$

To determine the gas content of cast aluminium sample, weighing machine MK 2200 (Figure 2.26.a) and vacuum machine (Figure 2.26.b) are used for the determination of d_{air} , d_{vacuum} and DI. First group of samples are solidified in the air and second group samples are solidified in vacuum for 3 minutes and at a pressure of 640 mmHg (0.85326 bar) (Figure 2.26.c). To see the effect of the modifier and the degassing process on the gas content, two groups are arranged before modification / degassing (Group A) and after modification /

degassing (Group B) for the same material which is used in serial production of aluminium cylinder heads.

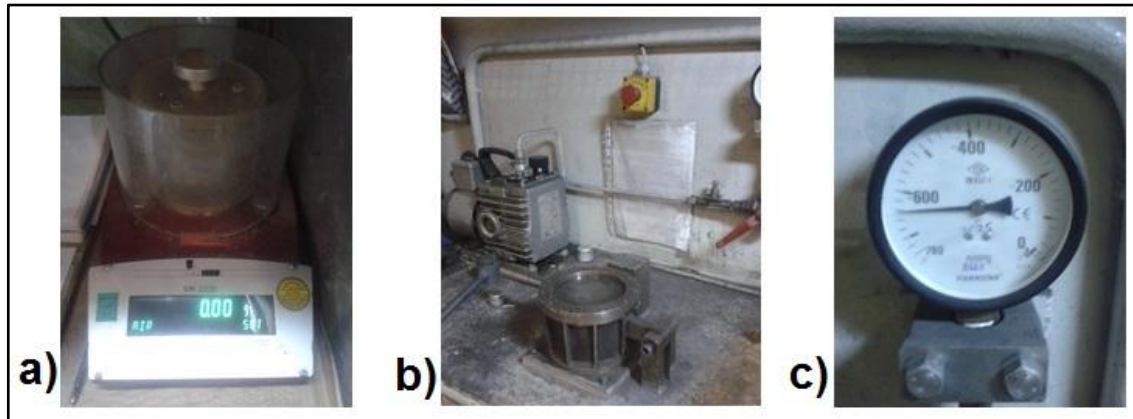


Figure 2.26: a) Weighing machine MK2200, b) Vacuum machine, c) Pressure gauge (640 mmHg)

Table 2.8: Density in air, density in vacuum and density index

		Density in air (d_{air}) (g/cm^3)	Density in vacuum (d_{vacuum}) (g/cm^3)	Density index (DI) (%)
Group A (Before Degassing)	No.1	2,7601	2,6026	5,7063
	No.2	2,7568	2,559	7,1750
	No.3	2,7627	2,5593	7,3624
Group B (After Degassing)	No.1	2,7477	2,7456	0,0764
	No.2	2,7487	2,7437	0,1819
	No.3	2,7494	2,7339	0,5638

Sample No.1 shows 98.66%; Sample No.2 shows 97.46%; and sample No.3 shows 92.34% gas reduction in group B when compared with group A. These results show that the modification and degassing process remove most of the gases in the structure and modification and degassing are essential processes for casting. Figure 2.27 shows samples before and after degassing process. These samples are solidified in the vacuum. Figure 2.27.a shows a sample before degassing (Group A) and Figure 2.27.b shows a sample after degassing (Group B). Other samples which are solidified in the air gave similar pictures with Figure 2.27.b. As seen in Table 2.8, they have similar density values with group B which is solidified in vacuum.

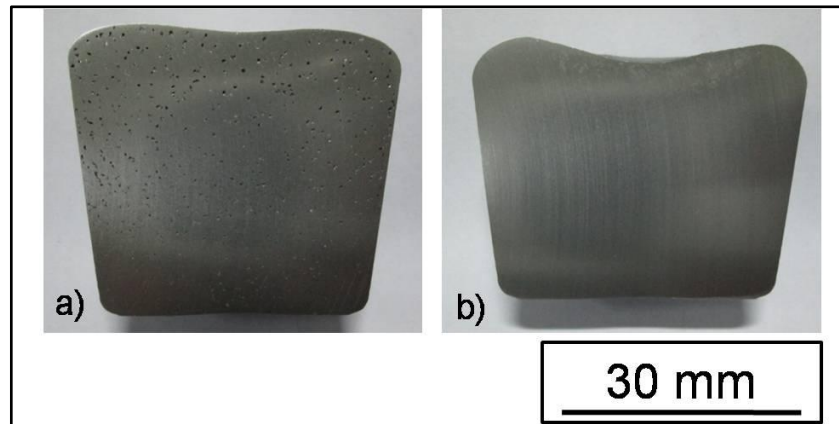


Figure 2.27: a) Before degassing in the vacuum (Group A), b) After degassing in the vacuum (Group B)

2.7 Stress relieving

2.7.1 Stress relieving and annealing (TS condition)

Controlled cooling condition for complex shaped parts such as cylinder heads is extremely hard. Therefore the internal stresses which can affect the mechanical properties negatively occur in the structure during manufacturing. The additional heat treatment after production can help to remove these internal stresses.

In this thesis, aluminium cylinder heads are heat treated at $225^{\circ}\text{C}\pm 10^{\circ}\text{C}$ for 4 hours and the cylinder heads are cooled down in air as proposed in '02-40-110/--H' standard.

Table 2.9: Mechanical properties of AlSi7Cu3Mg0.35Fe with and without stress relief process [Ren14]

	UTS (MPa)	YS (MPa)	Elongation (%)	Brinell Hardness (HB)
Without Stress Relief (F)	190	130	1 – Fire Face 0.5 – Camshaft Bearing Seat	75 – Fire Face
With Stress Relief (T5)	210	175	1 – Fire Face 0.5 – Camshaft Bearing Seat	90 – Fire Face 80 – Camshaft Bearing Seat

As seen in the Table 2.9., UTS increases by 10%, YS increases almost 35% and hardness increases by 20% by the stress relief process. The stress relief process has no significant effect on the elongation. Fire face where the combustion chamber is located on it is harder than camshaft bearing seat.

3 Experimental Methods

The experimental part of this study can be divided into two main parts. First, the manufacturing process is described beginning from the tilt casting process to stress relief process. And next, the measurements and tests are explained in detail. The measurements section can be also divided into the subsections which are chemical composition, grain size and SDAS measurements. As tests, Brinell hardness, tensile and fatigue tests are explained.

3.1 Casting

3.1.1 Casting the cylinder head

In the experimental approach, the tilt gravity casting method is used. As mentioned before, tilt gravity casting method has all advantages of top casting such as directional solidification. At the same time, tilt casting method reduces the turbulence which is the greatest disadvantage of top casting. In addition to this, the cooling condition of tilt casting is better than bottom casting method. The production line which is used in experimental approach is shown in Figure 3.1.



Figure 3.1: The production line [NN15]

The first step of the experimental work starts with the melting furnace. Aluminium ingot and aluminium scrap are melted down in the melting furnace. The percentage of reused aluminium depends on the manufacturing approach. In this study, 60% aluminium ingot and 40% aluminium scrap are used. In other application examples, aluminium scrap ratio may reach 50%.

The liquid metal is transferred from melting furnace to holding crucible by transfer ladle (Figure 3.2). The electrically heated holding crucible furnace (Hindenlang Giessereitechnik GmbH, Germany) holds the aluminium based liquid metal at $680\pm 10^{\circ}\text{C}$. This melting temperature is controlled by a thermocouple and displayed on a computer screen. The capacity of the holding furnace is 1600 kg and these silicon-carbide based holding crucibles have abrasion resistance at temperature higher than the melting temperature of aluminium based alloys.



Figure 3.2: Transferring the liquid metal from melting furnace to transfer ladle [NN15]

After transferring the liquid metal to the holding crucible, a modifier element such as Sr and grain refiner elements such as Ti and B are added into the liquid metal. In addition, (HMC 37) flux additions for cleaning and getting dry dross are added. The quantities of these elements depend on the related material type and the capacity of the holding crucible. After all, nitrogen gases blow into the liquid metal for degassing. The pressure of nitrogen gas is 1.5 ± 0.5 bar and gas flow rate is 10 ± 2 lt/min. Degassing process takes 15 ± 2 min. During the degassing process, hydrogen gases are released from the liquid metal.

This process decreases the gas content of the liquid metal dramatically. Finally, the liquid metal is ready to cast. The effects of this step are investigated in the 'Gas Content' section of this study.

Cores are used to create spaces and cavities in the parts. As mentioned before, cylinder heads which have structural cavities are very complex components. After the pouring, cores create the spaces which are called oil channels, water jackets channel, intake valve guide and exhaust valve guide in the cylinder heads (Figure 2.4). Figure 3.3.a shows the positions of sand cores in the mould. Figure 3.3.b shows all sand cores which are called water jackets, side oil channels, inlet sand core, outlet sand core, top sand core and oil gallery.

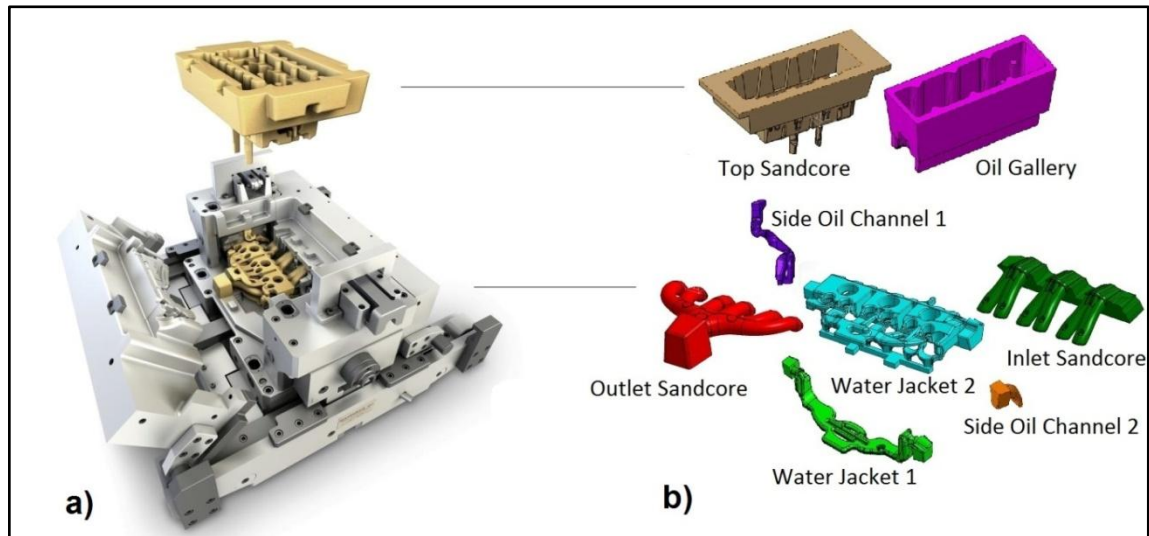


Figure 3.3: a) Positions of sand cores in the mould [Sme14], b) Named sand cores [NN12]

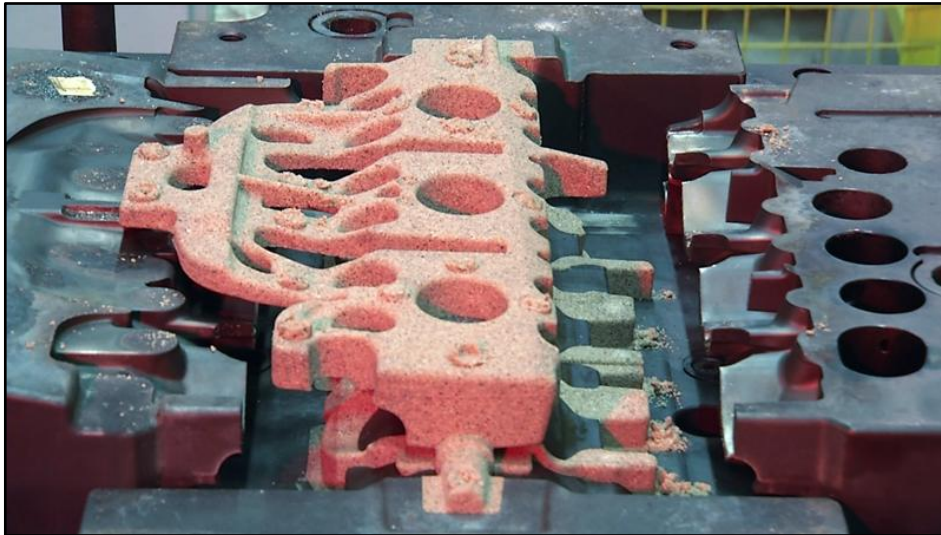


Figure 3.4: Gathered sand cores in the mould [NN15]

The mould and sand cores are prepared simultaneously. As mentioned before, 8 sand cores are used for related cylinder heads (Figure 3.3). These sand cores are divided into two groups according to the manufacturing methods. The first group is ‘no-bake cores’ which are called cold cores in practice and the second group is ‘bake cores’ which are called hot cores in practice. In no-bake cores manufacturing process, the sand is blown into the cold sand box and hardened with blowing amine gases. On the other hand, bake cores is prepared similarly but the cores are baked instead of using amine gas. Sand for no-bake core is 78 AFS grain fineness number which is obtained with a mixture of 11 kg very fine sand (110 – 120 AFS grain fineness number) and 39 kg fine sand (60 – 65 AFS grain fineness number). Similarly, sand for bake core is 36 AFS grain fineness number which is obtained with a mixture of 9 kg fine sand (60 – 70 AFS grain fineness number) and 41 kg coarse sand (25 – 27 AFS grain fineness number). All details of sand cores are given in Table 3.1.

Table 3.1: Sand cores properties

	AFS	Resin	Catalyzer	Protector	Hardening	Mix. Time
Cold Core	78	0.85%	0.85%	-	Amine Gas	25 sec.
Hot Core	36	1.9%	0.475%	0.1%	Baking	30 sec.

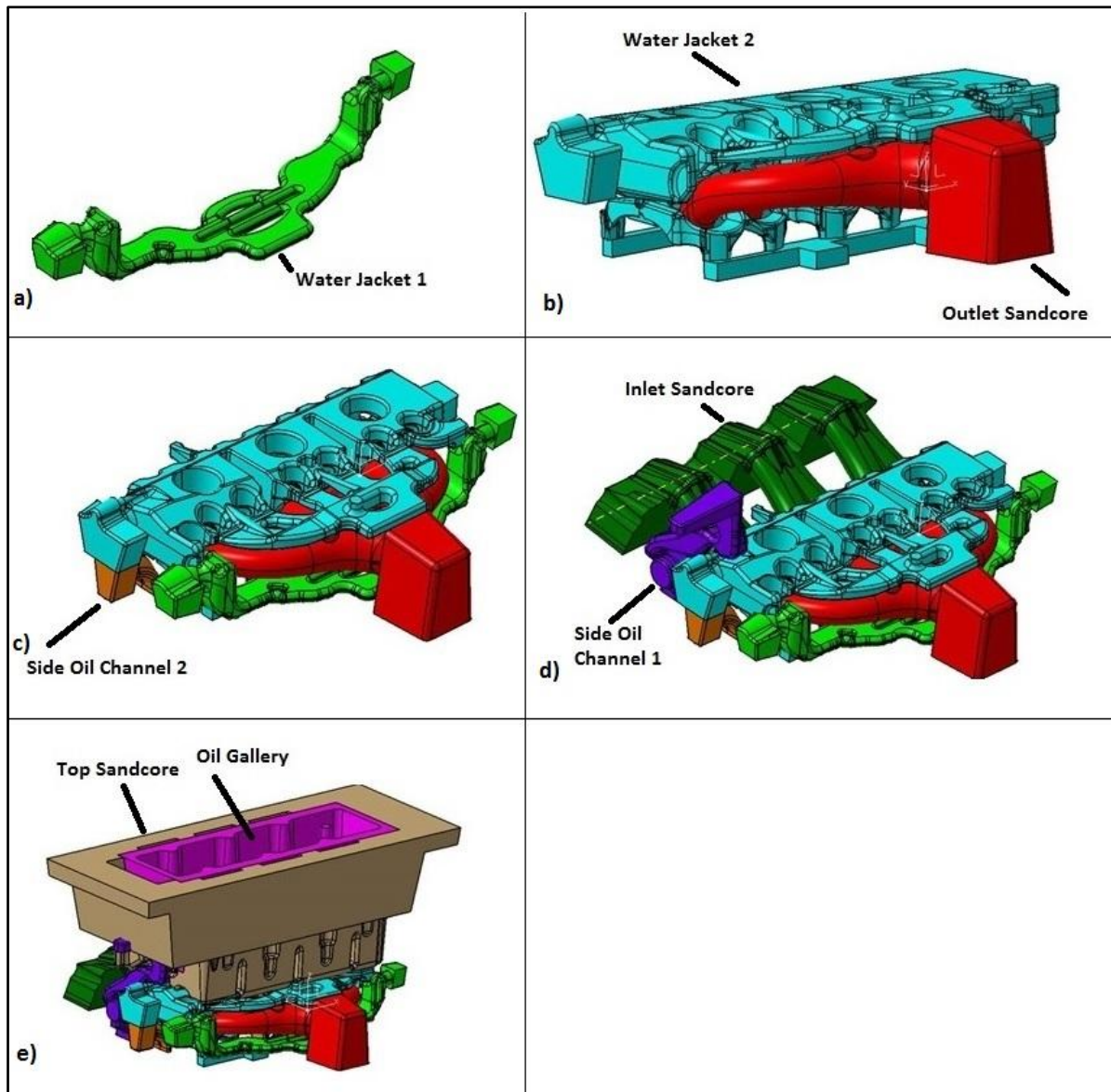


Figure 3.5: a) Water jacket 1, b) Water jacket 2 and outlet sand core, c) Side oil channel 2, d) Side oil channel 1 and inlet sand core, e) Top sand core and oil gallery [NN12]

Top sand cores, oil gallery, inlet – outlet sand cores are produced as no-bake cores. Water jacket 1 – 2 and side oil channel 1 – 2 are produced as bake cores. All sand cores are gathered in the core holder (Figure 3.4 and 3.5).

All sand cores are gathered into the core holder by an operator. Next, all sand cores are transferred from core holder to mould by a robot arm. The preparing of mould plays a vital role on the quality of the product. Cleaning and cooling of the mould directly affects the product's quality. The mould is cleaned by pressurized air before the placement of sand cores. Simultaneously, the mould has to be cooled down. The critical regions such as combustion chamber areas and the regions between the combustion chambers are cooled down with cooling water channels which are located in the mould. According to practical knowledge, the temperature of the mould is $350\pm 100^{\circ}\text{C}$ and the maximum temperature of the combustion chamber is 180°C . Temperature of cooling water that flows in the cooling water channels which is located in the mould is $40^{\circ}\text{C} - 60^{\circ}$. If the recirculation time of cooling water in the mould increases, the temperature of combustion chamber can decrease from 180°C to around $110^{\circ}\text{C} - 120^{\circ}\text{C}$.

Another vital parameter in casting is the pouring temperature. The liquid metal is transferred from the holding furnace with ladle. During the transfer, the liquid metal partially cools down. This temperature difference between melting and pouring temperature is estimated to be around $8^{\circ}\text{C} - 10^{\circ}\text{C}$ from the practical knowledge. Surely, this estimate must be corrected and the pouring temperature has to be measured during the casting. After pouring, the solidification takes 150 ± 20 seconds in air before going the cooling line. Figure 3.6 shows all steps of cooling.

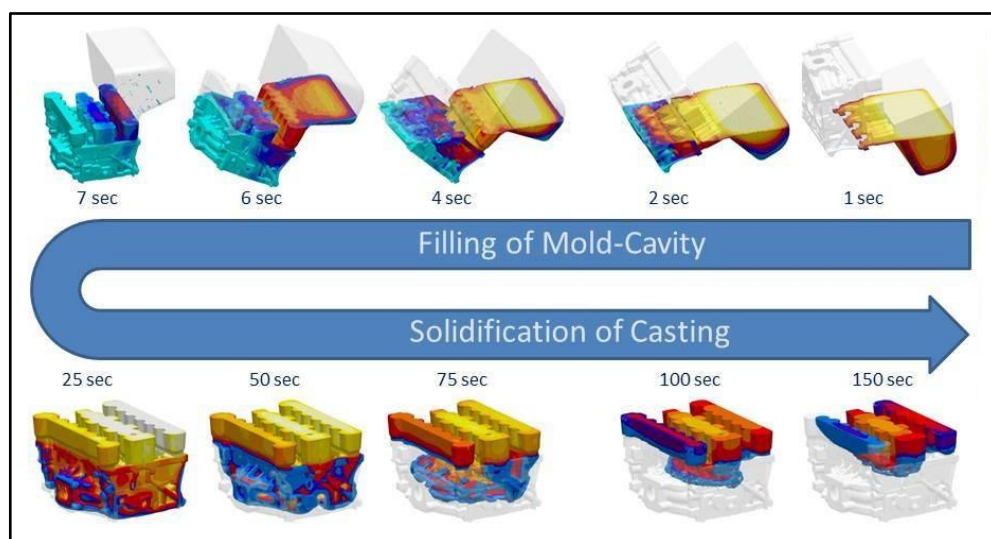


Figure 3.6: Solidification of cast in tilt casting process [Sme14]

After solidification, the cast part is cooled down on the cooling bands. Cooled part is taken into the hammering station and cores are released easily in a vibratory mould after hammering. Flashes are sawn and finished cast parts are taken from outfeed roller by an operator.

3.1.2 Design of all tests

The main aim of this study is to determine the effect of grain refinement on the mechanical properties. Grain refinement is mostly achieved by the addition of different elements in the foundry industry. These additive elements such as Ti and B cause different chemical compositions in the structure. In other words, different chemical compositions result different grain refinements. Similarly, different mould temperature affects the solidification condition and cooling rate of the parts. High cooling rate results in fine grains. Basically, grain refinement improves the mechanical properties which are of great concern in the automotive industry. In addition, stress relief process is applied to cylinder heads along with the grain refinement to improve mechanical properties of the samples in this study. As an output, SDAS values of critical regions which are located on the combustion chamber are determined and compared with limits which are strictly determined by automotive industry. Beside this, Brinell hardness test is applied to determine the effect of stress relief process on the hardness. Similarly to SDAS values, the limits of hardness are predetermined by the industry. Cast cylinder heads have to ensure these limits. Finally, tensile and fatigue tests are designed to determine the mechanical properties of critical regions of cylinder heads. Test conditions may be predetermined by customer and cylinder heads have to ensure the predetermined mechanical value limits.

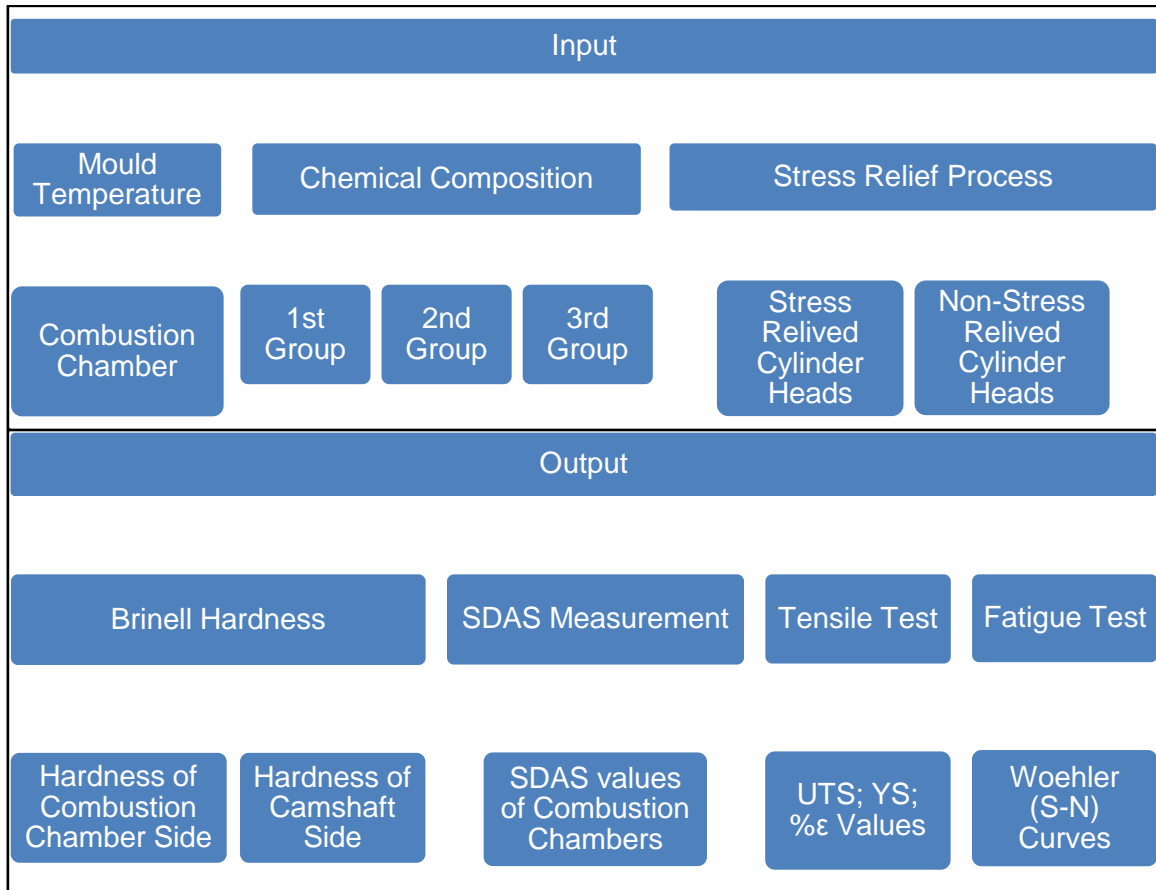


Figure 3.7: Design of all measurements and tests

3.1.3 Casting cylinder head with different additions

In this study, three different groups of aluminium cylinder head are poured. In this section, manufacturing approach of first group will be given in detail only. Other groups are cast using the same experimental approach. Different manufacturing parameters such as mould temperature, chemical composition and different element additions are given in tables.

All manufacturing parameters which can directly affect the mechanical properties will be given in this section. Aluminium based material which is prepared in same melting furnace is used. As mentioned previously, this material is prepared with 60% aluminium ingots and 40% recycled aluminium which came from same production line.

After transferring the material from the melting furnace to the holding crucible, 5 pieces (500 gr.) Al5Ti1B cut rod, 6 pieces (900 gr.) Al15Sr cut rod and 400 gr. HMC37 flux are added into the holding crucible for the first group of aluminium cylinder heads. Then, the degassing process is started which continues for 15 minutes. During the degassing, nitrogen gas is blown into the aluminium based material through the rotor which is rotating around its own axis. The reason for this is to help release hydrogen from the crucible. After the degassing process, slag which occurs at the top of crucible are taken away and cleaned by an operator. This cleaning process is important since slag may lead to defects and negative effect the mechanical properties. After cleaning, the holding crucible holds the material for another 15 minutes which is called the holding time. There are some experimental studies about the optimization of the holding temperature in the literature. Hu and Li noted that holding times between 10 and 20 minutes resulted in the lowest grain size for their own Al-Si-Cu based material [Hu98]. From practical knowledge, the holding time can vary between 10 and 30 minutes. As mentioned above, the holding time temperature is 15 minutes for this study. After the holding time, the material which is held in the crucible is ready for casting.

Before casting, the melting temperature, pouring temperature, and the temperatures of combustion chambers have to be determined. These parameters are very important and directly affect the mechanical properties. The melting temperature is measured as $677\pm 3^{\circ}\text{C}$ by a thermocouple and it can be observed on a computer screen. The melting temperature is determined as 680°C in the booklets of the casting line. Thus, the melting temperature is available for casting.

Another parameter which plays a vital role is the pouring temperature. As mentioned before, the material is transferred from the holding crucible to the mould by a ladle for casting. This ladle is always heated to minimize the difference between the melting temperature and the pouring temperature. However, a temperature difference is not completely unavoidable. The pouring temperature is measured on the transfer ladle by a portable contact pyrometer

before pouring. The pouring temperature is measured as 668°C. The temperature difference is determined to be around 10°C.

The critical areas of a cylinder head are the combustion chamber regions and the regions between the combustion chambers. Thus, the temperatures of the combustion chamber regions on the mould have to be measured. Therefore, the temperatures of combustion chambers may have different values in time. The important point is to determinate the exact time at which pouring begins. First, the time gap has to be determined between the start of cooling of the mould and the start of pouring. This mentioned time gap is determined as 82 seconds. Next, the operator waits for 82 seconds after the start of the cooling of the mould. At that moment, the temperature of the combustion chamber is measured so that the temperature of the combustion chamber exactly at start of the pouring can be measured. Temperatures of three combustion chambers are measured and they are T1=110°C, T2=118°C and T3=116°C, respectively (Figure 3.8).

These temperatures are measured by a contactless (infrared) pyrometer. Simultaneously, the temperature of combustion chamber is measured by a system and shown on the screen. The temperatures measured by the infrared pyrometer are corrected by the computer with a $\pm 5^\circ\text{C}$ tolerance.

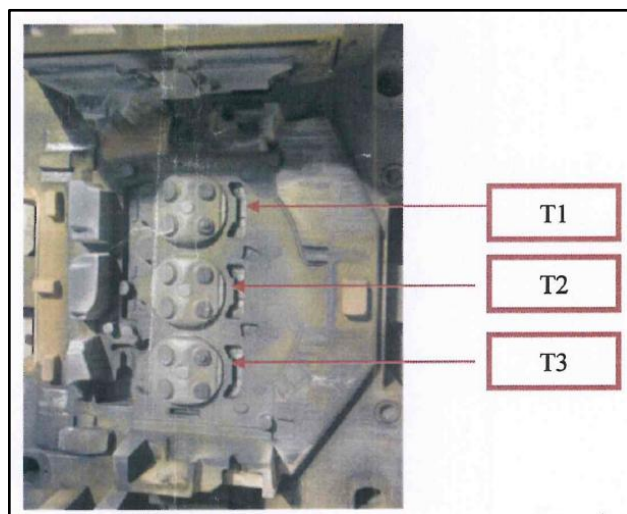


Figure 3.8: Temperature measurement points on the combustion chambers

After all, the following cycle is started and the first group cylinder heads are cast. After gathering all of the sand cores in the core hold mould, there is no more interference by any operator. All process steps which are stated before are carried out by robots. Finally, the cast aluminium cylinder heads are taken from the outfeed roller for visual inspection. After visual inspection, X-Ray inspection is done to detect the porosities, shrinkages and other casting defects. The minimum value of a defect which can be detected by X-Ray inspection is around 300 μm in a 20 cm thickness. Lower defect values can be achieved in thinner parts.

Table 3.2 shows all manufacturing parameters for all groups. As seen, melting temperature values are measured between the limits of $677\pm 3^{\circ}\text{C}$ as given in the booklet of the production line. As mentioned earlier, although the transfer ladle is heated the pouring temperature may decrease slightly. This value is estimated around $8^{\circ}\text{C} - 10^{\circ}\text{C}$ from the practical knowledge. The measurement corrected the estimation. The cooling water channels located in the mould and they are cooling the combustion chambers. So, the temperatures of the combustion chambers do not show different values. The biggest temperature difference measured is 8°C which can be tolerated well.

Table 3.2: Manufacturing parameters of all groups

	Melting Temperature	Pouring Temperature	Combustion Chamber Temperature			Degassing Time	Holding Time
	($^{\circ}\text{C}$)	($^{\circ}\text{C}$)	T1 ($^{\circ}\text{C}$)	T2 ($^{\circ}\text{C}$)	T3 ($^{\circ}\text{C}$)	(Min.)	(Min.)
Group1	676	668	110	118	116	15	15
Group2	679	669	115	121	119	15	15
Group3	675	666	110	114	117	15	15
	Al5Ti1B (gr.)	Al15Sr (gr.)	HMC 37 (gr.)				
Group1	500	900	400				
Group2	1500	900	400				
Group3	3000	900	400				

3.1.4 Specimen preparation

Tensile specimens, SDAS measurement specimens and fatigue specimens are taken directly from the cylinder heads in this study. The specimens that are extracted from the cylinder head which has higher cooling rate can give more close results to actual values. Some studies from the literature work with the specimens which are poured into a tensile test bar mould which has lower cooling rate produced for tensile test specimens.

Tensile specimens are prepared according to DIN 50125 standard [DIN91] which gives the specimen geometry as shown in Figure 3.9.

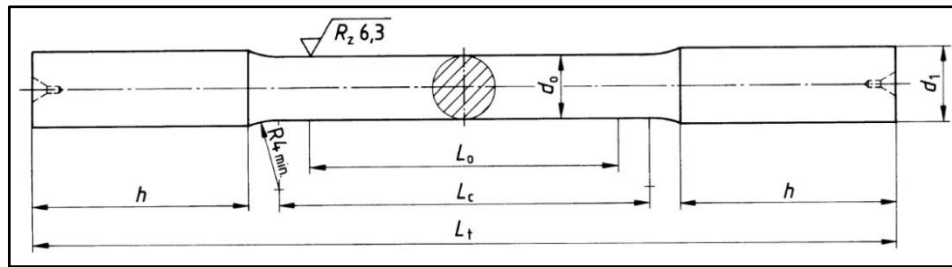


Figure 3.9: Drawing of tensile test bar in DIN 50125 [DIN91]

First, specimens are poured to tensile test bar mould directly as shown in Figure 3.21. All specimens are machined with horizontal CNC turning machine after casting to obtain desired dimensions. 'LER TC 150 b' model CNC turning machine with 5000 rpm rotating speed is used in these operations. Based on prior experience and knowledge the milling machine limitations of the following parameters are applied: Spindle speed shows differences depending on the work piece's regions and the machining operations. Spindle speed is 1600 rpm for rough machining, 2500 rpm for fine machining and 3000 rpm for finishing operation. Similarly, feed rate is 150 m/min for rough machining of large diameter and 50 m/min for finishing operation of small diameter. Depth of cut is 0.5 mm and it could be reduced by half for finishing operation. High speed steel (HSS) is used as a cutting tool. Diameter of specimen is machined to $d_0=12$ mm, $d_0=5$ mm and other dimensions are machined according to DIN 50125 standard [DIN91].

The different solidification condition between the test sample poured into a tensile test specimen mould and extracted from cylinder head is clear. To see the effect of different solidification conditions on the tensile properties, tensile specimens are poured into the tensile test bar mould beside the samples which are extracted from the cylinder heads in this study. Figure 3.10 shows the process step by step from pouring to a tensile test bar mould to machining to $d_0=12$ mm. On the other hand, Figure 3.11 and 3.12 show the process step by step from the cylinder head to tensile test bar machined to $d_0=5$ mm.

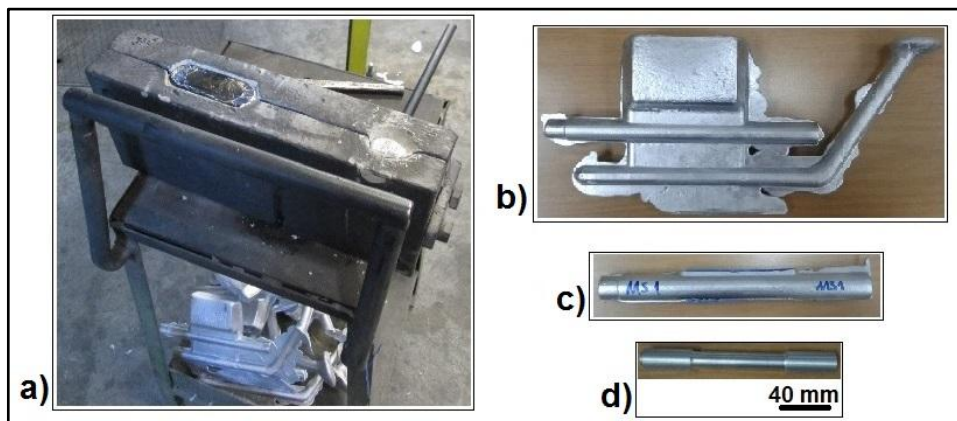


Figure 3.10: a) Tensile test bar mould, b) Uncut specimen, c) Sawed specimen, d) Machined to $d_0=12$ mm tensile test bar

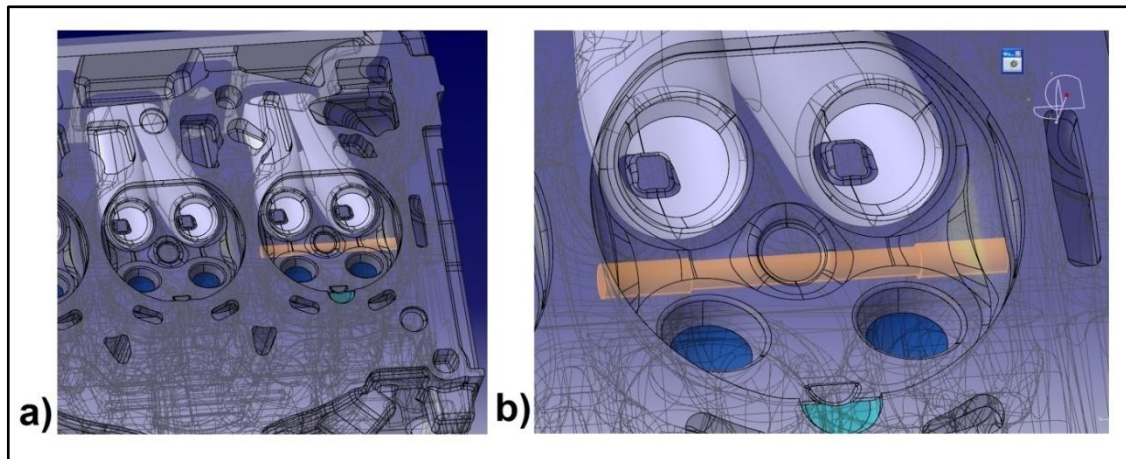


Figure 3.11: a) CAD picture of $d_0=5$ mm tensile test bar under the combustion chamber, b) CAD picture of $d_0=5$ mm tensile test bar under the combustion chamber with zoom.

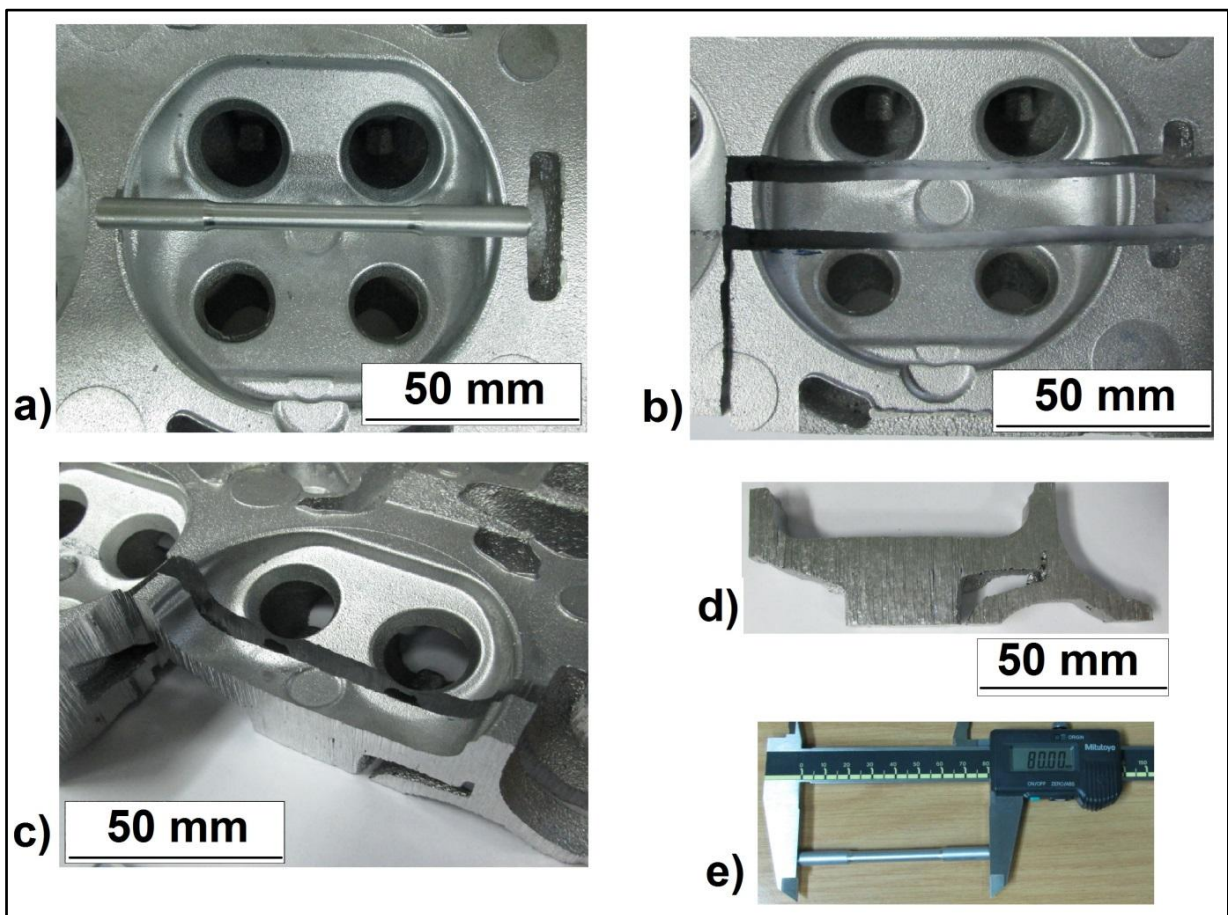


Figure 3.12: a) Combustion chamber and tensile test bar, b) Sawed cylinder head, c) Perspective view of critical region, d) Separated critical region, e) Machined $d_0=5$ mm tensile test bar

After machining, the roughness of the specimen is measured. As shown in Figure 3.13, Hommel Wave roughness test machine and Hommel – Etamic Tester T8000 is used for determining the R_z value. Roughness test is carried out according to ISO 11562 (M1) and ISO 4287 standards.

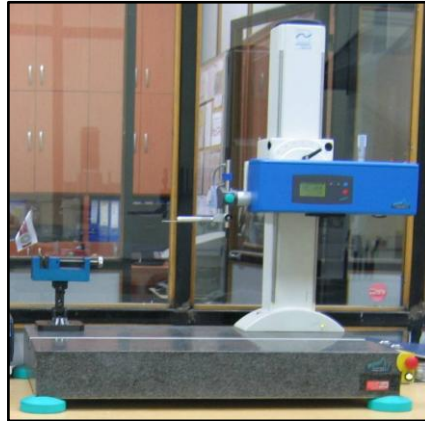


Figure 3.13: Roughness test machine [NN12]

The average R_z value is $5.04 \mu\text{m}$ and standard deviation is 1.21 for $d_0=12 \text{ mm}$ tensile test samples. The average R_z value is $5.53 \mu\text{m}$ and standard deviation is 0.73 for $d_0=5 \text{ mm}$ tensile test samples.

First visual inspection is done to detect the pores, cavity and shrinkage on the surface by an operator. After visual inspection, X-Ray inspection (Figure 3.14.a) is conducted on the samples to catch casting defects which are located in the structure. Figure 3.14.b shows the X-Ray photograph of two tensile test specimens. X-Ray results are evaluated according to ASTM E 155: Standard reference radiographs for inspection of aluminium and magnesium castings.

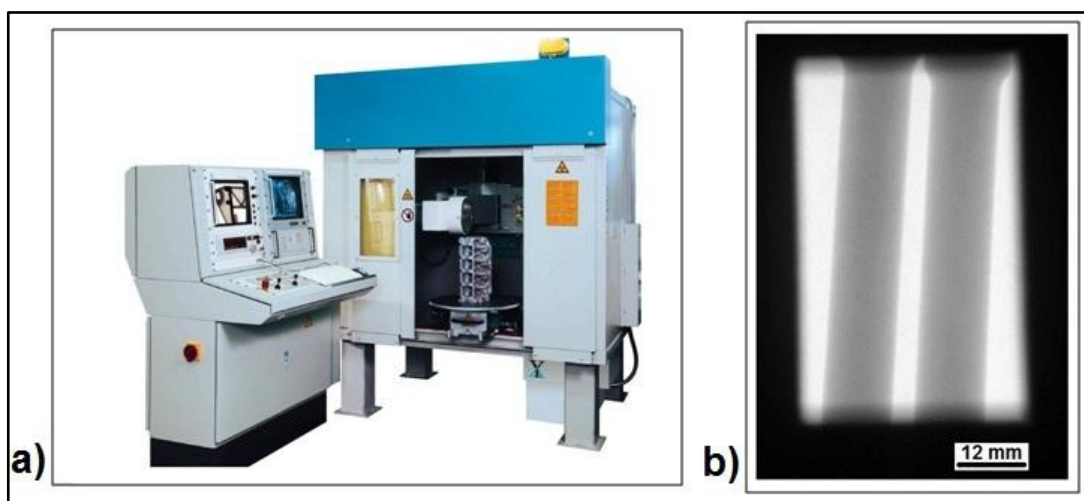


Figure 3.14: a) X-Ray inspection [NN12], b) X-Ray photograph of two $d_0=12 \text{ mm}$ tensile test specimens.

SDAS measurement specimens are extracted from the combustion chambers. All preparations and measurement are done according to 'PV 1112: Aluminum cast alloy; testing of dendrite arm spacing' standard. From the practical knowledge, first or third combustion chamber is used to measure the SDAS values (Figure 3.15.a). The SDAS is measured on the region between the intake valve and the exhaust valve of cylinder head. After cutting off the samples, they are prepared as stated in 'microstructure in metallurgical approach' section. Microscopic analysis is carried out to measure the SDAS values. The surface area of the specimen has to be at least 10 mm x 10 mm (Figure 3.15.b).

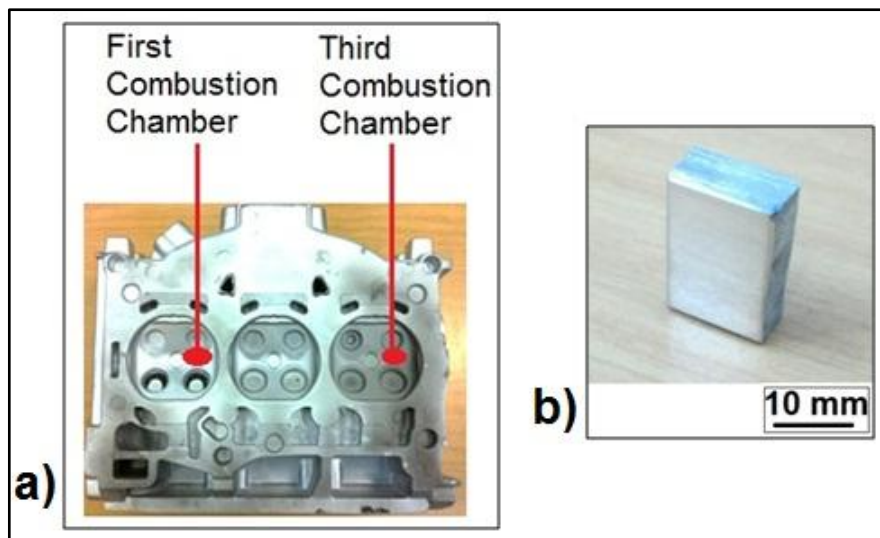


Figure 3.15: a) Measured area on the first and third combustion chamber region, b) Sample for microstructure and SDAS measurement.

The dimension of used fatigue specimens are given by instruction manual of Hi-Tech Scientific Model HSM 19 rotating bending fatigue test machine [Rob01]. This specimen geometry is given in Figure 3.16.

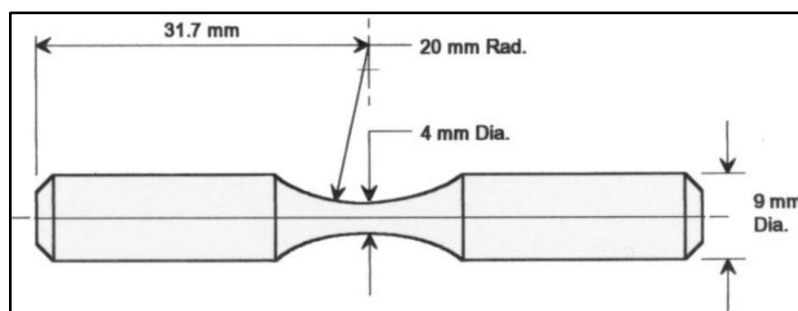


Figure 3.16: Used fatigue specimen [Rob01]

As mentioned before, fatigue specimens are extracted from the region between the combustion chambers. Similar to other specimen preparation steps, the specimens are shown on the cylinder head and photographed step by step (Figure 3.17).

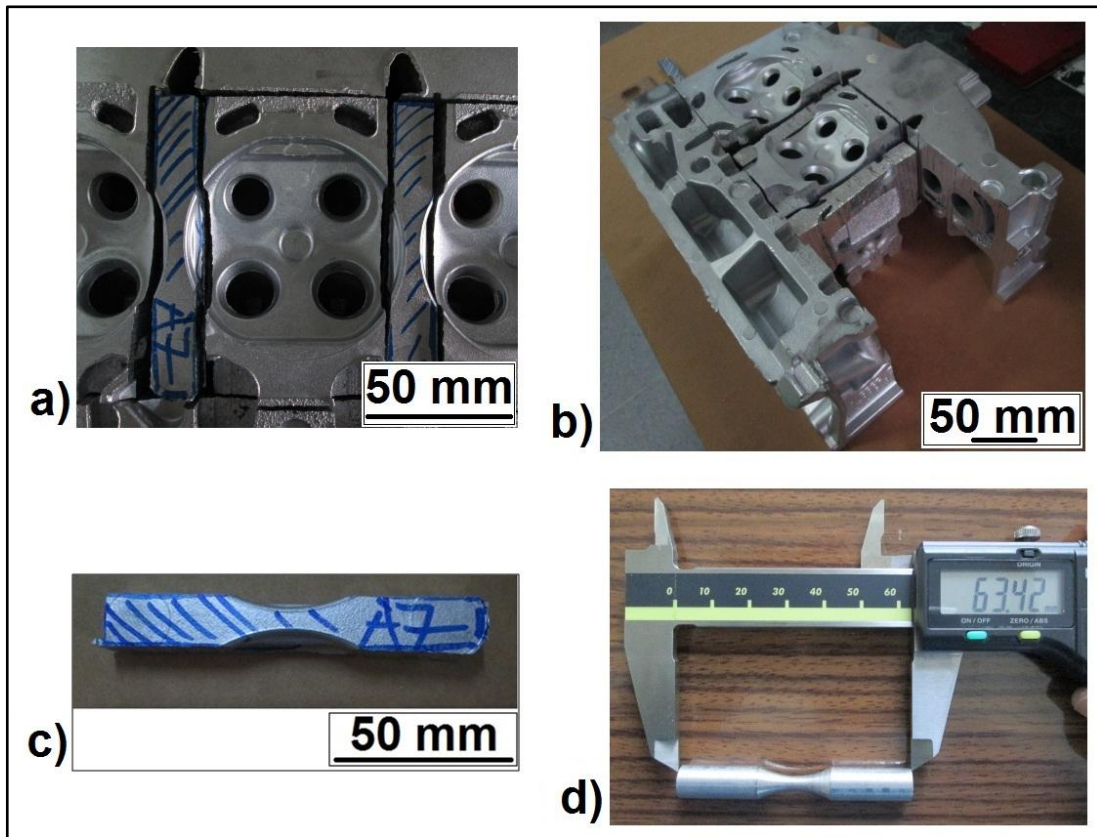


Figure 3.17: a) Combustion chamber and specimen region, b) Perspective view of cylinder head, c) Sawed specimen, d) Machined fatigue specimen.

The surface condition directly affects the fatigue results. Although the instruction manual does not give any specific limit for surface condition, the preparation process is detailed as machining, grinding and polishing steps. In addition, they noted that 'If the equipment is available, measure and record the surface roughness in the direction of the stress' [Rob01]. The roughness measurement equipment which is used for tensile test bar is used for fatigue test samples. The average R_z value is $1.13 \mu\text{m}$ and standard deviation is 0.47 for $d_0=4 \text{ mm}$ fatigue test samples. The surface roughness of necked region is minimized with fine emery paper. In addition to this, the critical surface is polished with polishing cloth using $1 \mu\text{m}$ diamond paste and finally cleaned with cotton. After all, the roughness values of any 3 specimens are measured. The average value is around $1 \mu\text{m}$.

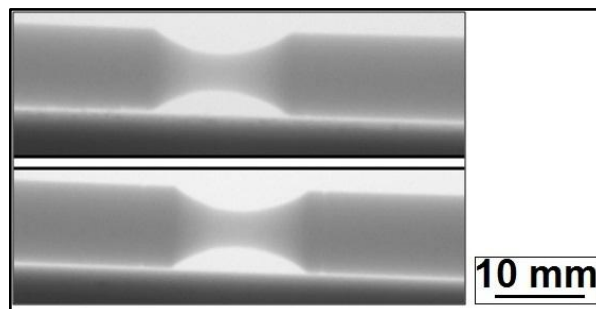


Figure 3.18: X-Ray pictures of two fatigue specimens

3.1.5 Stress relieved cylinder heads

As known, different solidification conditions cause residual stress in the structure. This residual stress could be tensile and compressive. The critical regions of cylinder head work under tensile stress. So that, relieved residual stress may lead to better mechanical properties. Stress relief process for related material is determined in 'Renault 02-40-110/--H' standards. The standard which is named 'aluminium alloys for automobile moulded casting in house bought out' is based on ASTM E155 and E505. The parts are hold at $225\pm 6^{\circ}\text{C}$ for 4 hours. After the stress relief process, the parts are taken out from the furnace and left to cool down naturally. The temperature is monitored on the furnace main control screens. In addition to that, a time counter starts when the temperature reaches 225°C and counts for 4 hours (Figure 3.19.a and b).

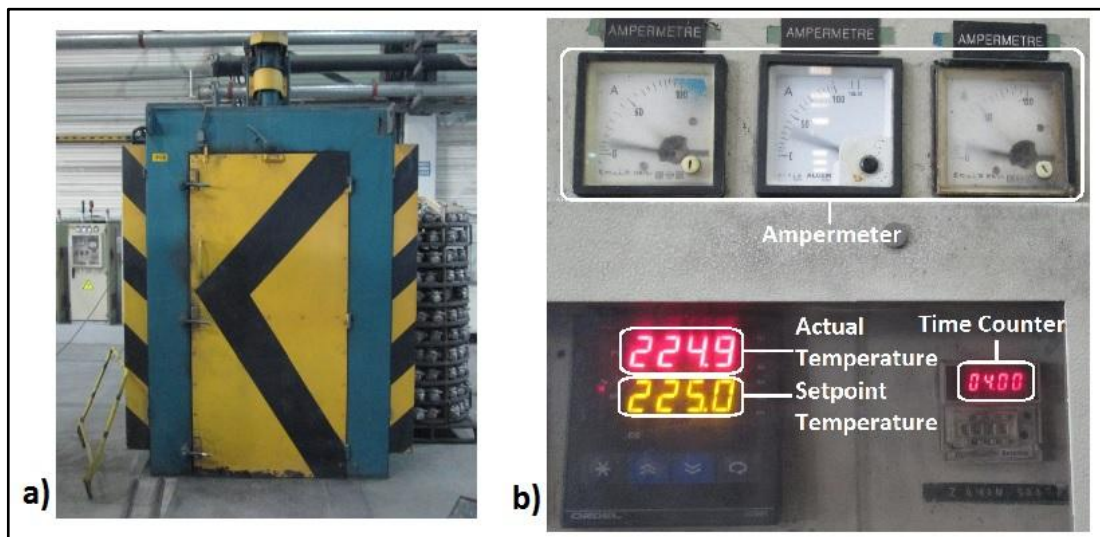


Figure 3.19: a) Furnace, b) Screen of furnace.

As planned before, stress relief process applied to half of cylinder heads in each group and to half of the tensile specimens which are poured directly to the tensile specimen mould.

3.2 Metallurgical approach

3.2.1 Chemical composition

The chemical composition is determined by optical emission spectrometer (Figure 3.20). The samples are poured to a metal base mould. The diameter of the sample is 35 mm. The height which is not important for chemical determination is around 40 mm. The spectrometer determines the composition on the surface machined with milling machine. Clear and machined surfaces give the best results. The optical emission spectrometer can determine more than 20 different materials in the aluminium based alloys. The resolution of optical emission spectrometer is 0.00001 (wt %).



Figure 3.20: Optical emission spectrometer [NN15]

For each group, the chemical composition of the sample which is taken from the holding crucible after adding grain refinement and modifier and degassing process are given in Table 3.3. This chemical composition shows the materials which are originated from the melting furnace and used for each group. The chemical composition is determined from three different points of the surface to minimize the measurement errors. (Figure 3.21)

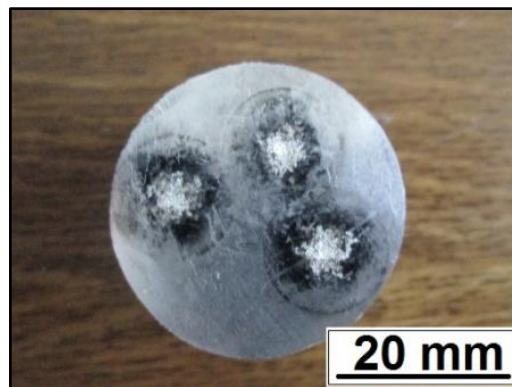


Figure 3.21: Chemical composition is determined from three different points

The abbreviation 'AVG' is used for the average values of these three points and 'SD%' is used for the % standard deviation of measurements. As mentioned previously, more than 20 different materials are determined but the amount of some of them is extremely low and they do not play important role so that, those materials are ignored in the Table 3.3. As seen in the table, chemical content of melting furnace material and following group materials are conformed with the composition of AlSi6Cu4 in DIN EN 1706 which is detailed before (Table 2.2). After addition of grain refiner (Al5Ti1B) and modifier (Al15Sr) the chemical composition changes and it affects the grain size directly.

Table 3.3: Chemical content of melting furnace material and material of the three groups

	Melting Furnace		1 st Group		2 nd Group		3 rd Group	
	AVG	SD%	AVG	SD%	AVG	SD%	AVG	SD%
Si (%)	6.7948	0.47	6.7931	1.27	6.9162	2.01	6.6381	0.97
Fe (%)	0.54	2.24	0.5496	1.00	0.5748	4.47	0.5436	2.48
Cu (%)	3.734	0.75	3.8201	0.83	3.7197	1.48	3.6062	3
Mn (%)	0.4305	1.41	0.4337	1.35	0.4129	2.37	0.3990	2.15
Mg (%)	0.2834	0.64	0.2820	0.53	0.2977	2.86	0.2653	2.16
Zn (%)	0.335	2.86	0.3447	2.14	0.6697	0.39	0.6279	0.47
Ti (%)	0.1268	0.79	0.1316	2.27	0.1375	5	0.1460	2.88
Ni (%)	0.0425	1.66	0.0458	1.72	0.0295	2.36	0.0296	3.99
Pb (%)	0.0435	0.96	0.0451	1.42	0.0351	3.86	0.0397	8.55
Sn (%)	0.0197	1.58	0.0213	1.14	0.0155	1.32	0.0138	3.14
Cd (%)	0.0019	1.1	0.0019	3.54	0.0012	4.24	0.0009	8.13
V (%)	0.0057	2.07	0.0057	9.52	0.0091	1.83	0.0074	7.21
Cr (%)	0.0142	0.92	0.0142	1.31	0.0186	3.64	0.0163	7.53
B (%)	0.0003	8.68	0.0003	9.48	0.0009	6.72	0.0019	5.83
Sr (%)	0.0036	4.58	0.0036	5.82	0.0167	5.50	0.0133	2.79
Al (%)	87.6239	0.05	87.6239	0.11	87.1450	0.27	87.6499	0.09

3.2.2 Macrostructure

First, the samples are poured into sand cores to observe the macrostructure of material. The bottom diameter of sample is 30 mm, the top diameter is 40 mm and the height is 90 mm. After casting, samples for macrostructure inspection are prepared in two consecutive steps. In first step, the samples are cut with using 'Struers Unitom - 2' (Figure 3.22.a). In the next step, the samples are ground and polished using 'Ostas' sample preparation equipment (Figure 3.22.b) while the parts are cooled down with water during grinding and polishing.

Determining the grain size of aluminium alloys which contain copper is more difficult than other alloys.

‘One procedure that works reasonably well is to etch the sample at room temperature in a solution of 10% HF. This results in a black smudge on the sample produced by the copper in the alloy. This smudge can be cleaned by rubbing the surface under running water or by rinsing it in a dilute solution of nitric acid’ [Sig07].

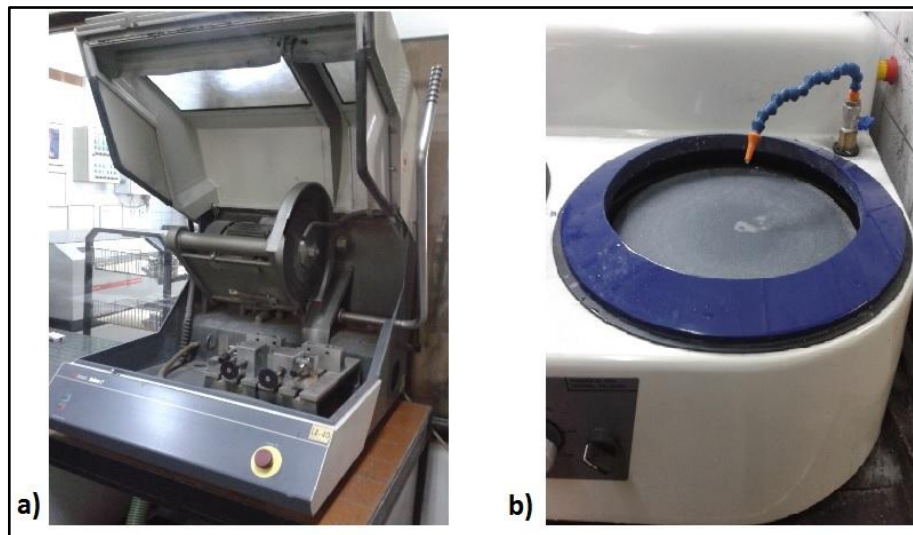


Figure 3.22: a) Streuers Unitom – 2 Cutting machine, b) Ostas grinding machine

Relatively; 120, 400-800, 600-1200, 1000, 1200 and 2500 grit emery papers (silicon carbide papers) are used for grinding and polishing. After each step, the parts are dried and examined visually by an experienced operator. At the end of these processes, the samples are etched in the etching solution for 35-40 seconds. The etching solution contains 10% H_2SO_4 , 5% HF, 85% H_2O .

After etching, the samples are cleaned under water and dried. Finally, the grain size can be seen and determined according to ‘Atlas Metallographique de l’a-S5 U3’ [Cen80].

3.2.3 Grain size

Grain size was measured by as comparing method is used for commercial purposes widely. ‘Atlas Metallographique de l’a-S5 U3’ which can be translated as ‘Metallographic atlas of S5 U3’ gives the reference pictures of grain size with classification (Figure 3.23). The reference pictures are taken under x10 magnification. Grain size classes are coded as SG – 1 (125 μm), SG – 2 (200 μm), SG – 3 (315 μm), SG – 4 (500 μm), SG – 5 (800 μm), SG – 6 (1250 μm) and SG – 7 (2000 μm) [Cen80].

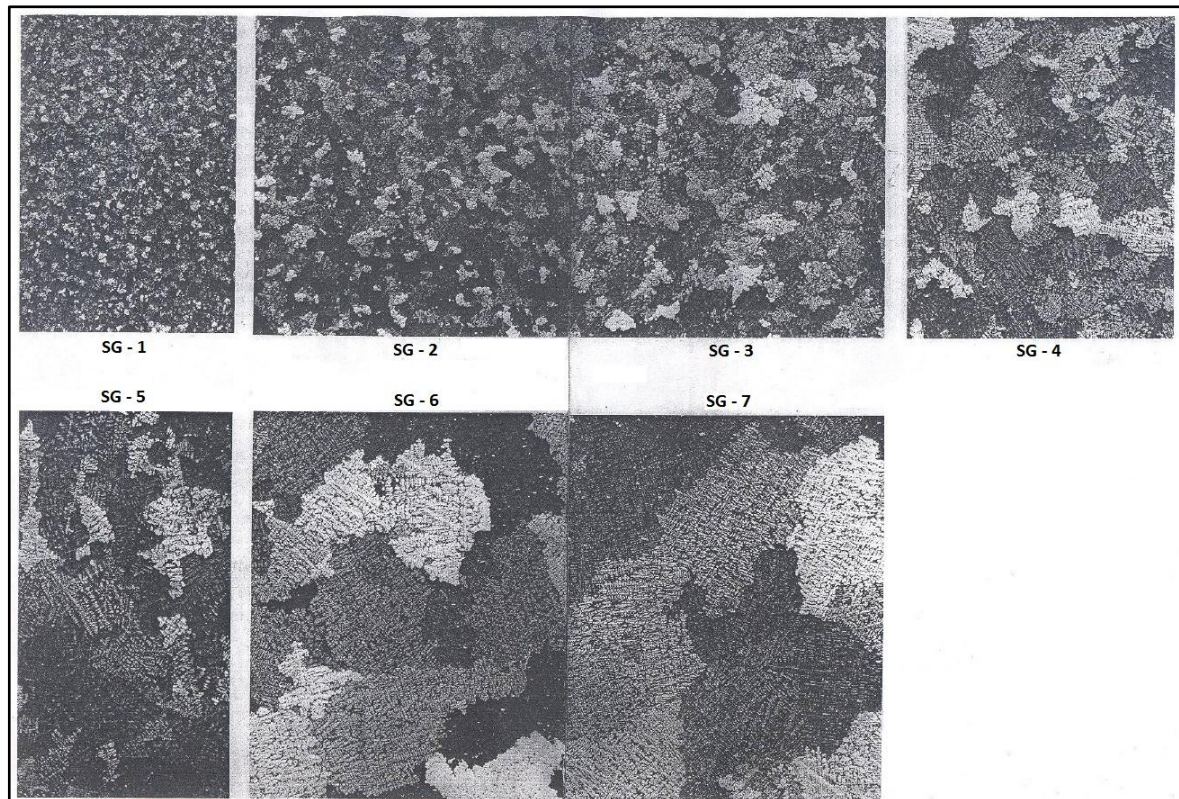


Figure 3.23: Reference pictures of grain size under x10 Magnification [Cen80].

Figure 3.24 shows pictures which are taken by digital camera to see the differences of grain size classes of sample. Similarly, Figure 3.25 shows macrostructure pictures of same samples. The macro pictures are taken under x10 magnification. All samples are AlSi6Cu4. First step, Figure 3.24.a shows the sample which is taken from holding furnace before pouring of first group cylinder heads.

Second step, Figure 3.24.b shows the sample which is taken from melting furnace. As mentioned before, 60% aluminium ingot and 40% aluminium scrap are used in melting furnace.

Third step, the sample is taken from holding crucible and 5 pieces (500 gr.) Al5Ti1B cut rod, 6 pieces (900 gr.) Al15Sr cut rod and 400 gr. HMC37 flux are added into the holding crucible before degassing (Named as Group 1 in this study). The differences between third step and fourth step are degassing process.

Fourth step, sample is taken from holding crucible after degassing.

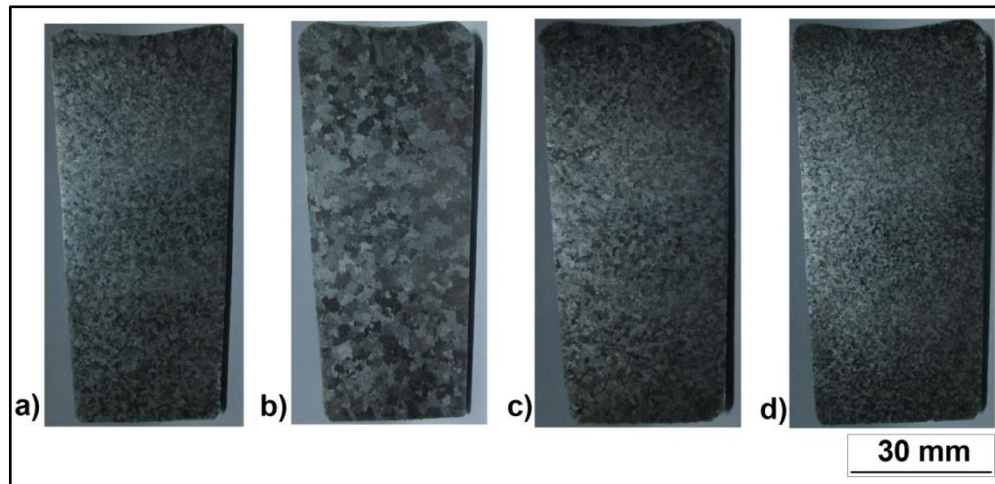


Figure 3.24: a) 1st Step of sample in group 1, b) 2nd Step of sample in group 1, c) 3rd Step of sample in group 1, d) 4th Step of sample in group 1.

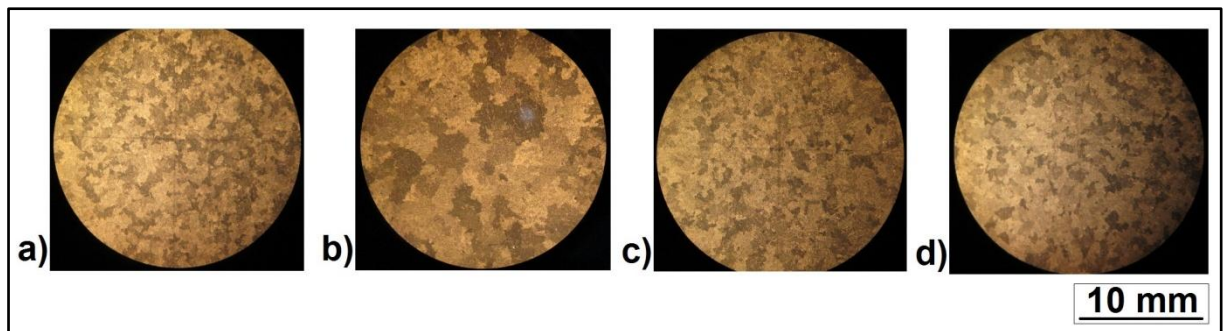


Figure 3.25: a) 1st Step of sample in group 1 (x10 Magnification) (Grain size: 315 μm), b) 2nd Step of sample in group 1 (x10 Magnification) (Grain size: 500 μm), c) 3rd Step of sample in group 1 (x10 Magnification) (Grain size: 315 μm), d) 4th Step of sample in group 1 (x10 Magnification) (Grain size: 315 μm)

As seen in Figure 3.24, the grain size classes of samples can be evaluated in same class before and after degassing process (Figure 3.24.c and Figure 3.24.d). On the other hand the effect of Ti and B on the grain size is appreciable (Figure 3.24.b and Figure 3.24.c)

Figure 3.25 shows exactly the same pictures with a higher magnification. These pictures help to understand the differences of different manufacturing stepson the grain size.

In addition to this, the samples which are extracted from cylinder heads are examined and shown in Figures 3.27-29 which visualize the differences of the macrostructure in the different regions of the same part. Since the mould is cooled down before casting the combustion chamber side of cylinder heads is cooled down first. That is the reason why the combustion chamber side has finer grains than the riser neck side (Figure 3.26).

For all samples, the finer structure on the combustion chamber side can be recognized. The reason of this observation is that the combustion chamber side is cooled down first. Structure and this result in better mechanical properties. The differences of stress relieve process can be observed easily in Figure 3.27 and 3.28. Besides this, the differences of Ti-B level are shown in Figure 3.27 and 3.29.

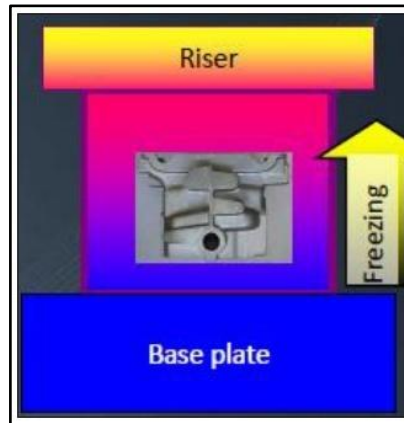


Figure 3.26: Freezing direction of cylinder heads [NN12]

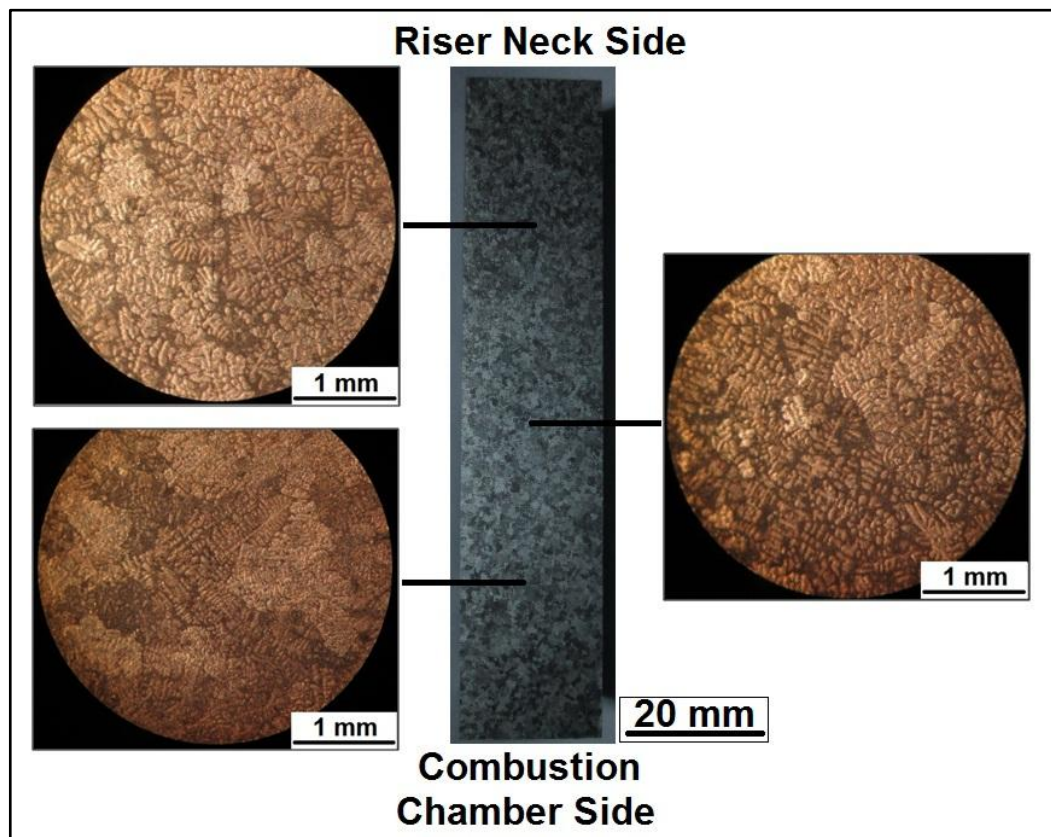


Figure 3.27: Macrostructure of different regions on group 2 sample (Non-stress relieved)

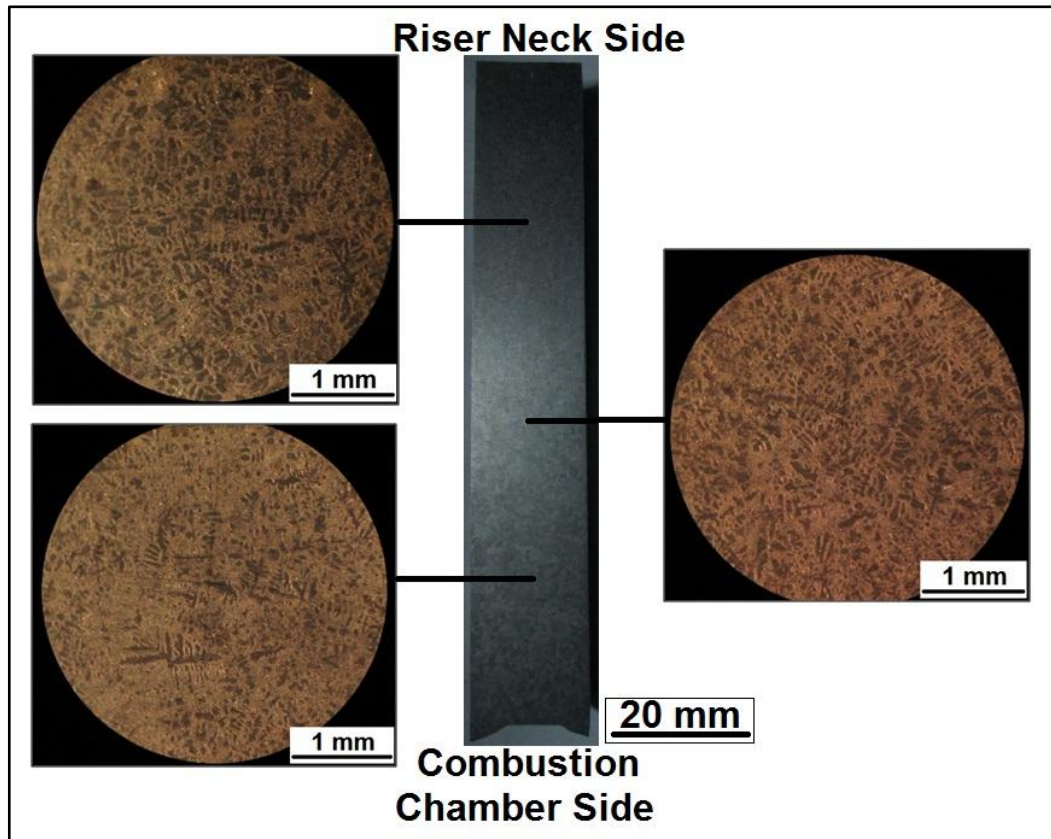


Figure 3.28: Macrostructure of different regions on group 2 sample (Stress relieved)

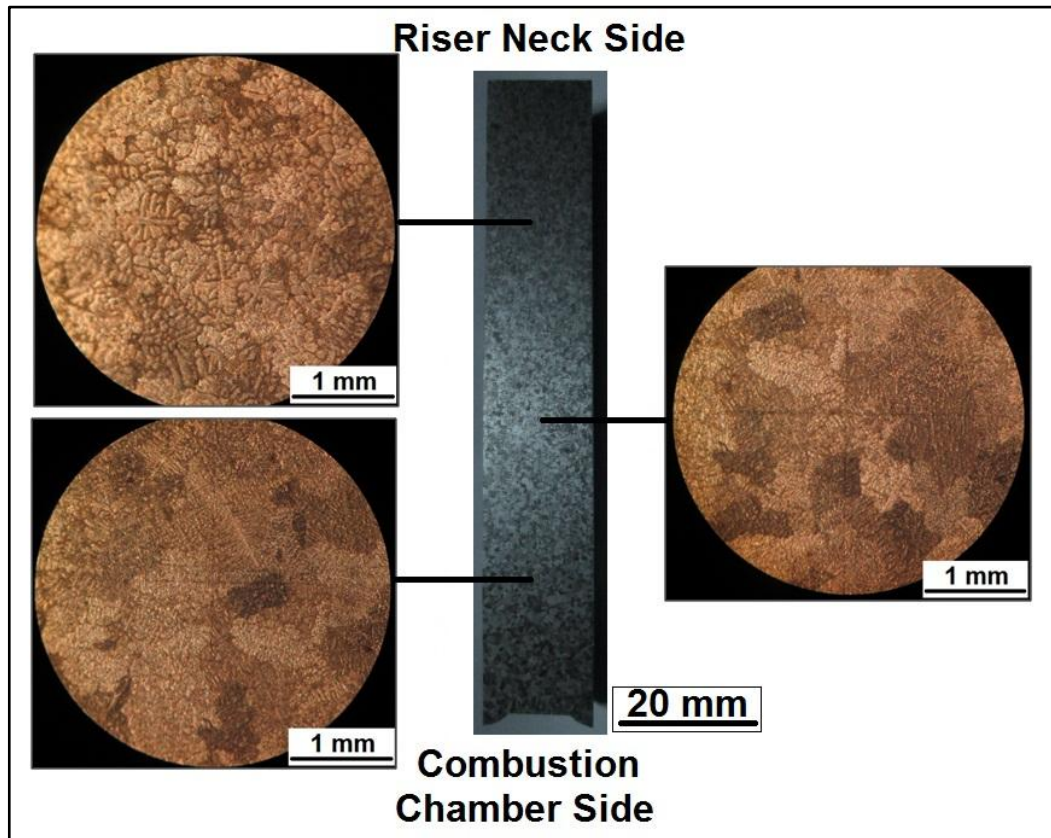


Figure 3.29: Macrostructure of different regions on group 3 sample (Non-stress relieved)

3.2.4 Microstructure

Basically, the sample preparation procedure for microscope is similar to that for macroscope. The grinding and polishing procedures are the same as explained previously in the 'macrostructure' section. Based on practical knowledge, three types of polishing cloths namely, nyloncloth, microcloth or texmet are used in the polishing steps of microstructure preparation. Aluminium oxide solution or diamond paste which is used in the industry widely is preferred for aluminium based samples. Diamond pastes are classified according to the size of contained particles given in μm values. For instance, $0.25\ \mu\text{m}$, $1\ \mu\text{m}$, $3\ \mu\text{m}$, $6\ \mu\text{m}$, $9\ \mu\text{m}$ and $15\ \mu\text{m}$ diamond pastes are used on the polishing cloth. In this study, Metadi® II diamond polishing compound ($1\ \mu\text{m}$) is used. The diamond paste has water content less than 0.1% therefore it is suitable for water-free preparation. In addition to paste, alcohol is applied on the sample surface for cleaning purposes and to obtain a better surface quality. Finally, an etching solution similar to the etching solution for macrostructure is prepared. This time, sulfuric acid is replaced completely by water. The etching solution contains 85% H_2O , 15% HF. Etching solution is applied on the polished surface for nearly 10-15 seconds. After that, samples are cleaned with alcohol and dried. The surface has a mirror-like appearance after all preparation process.

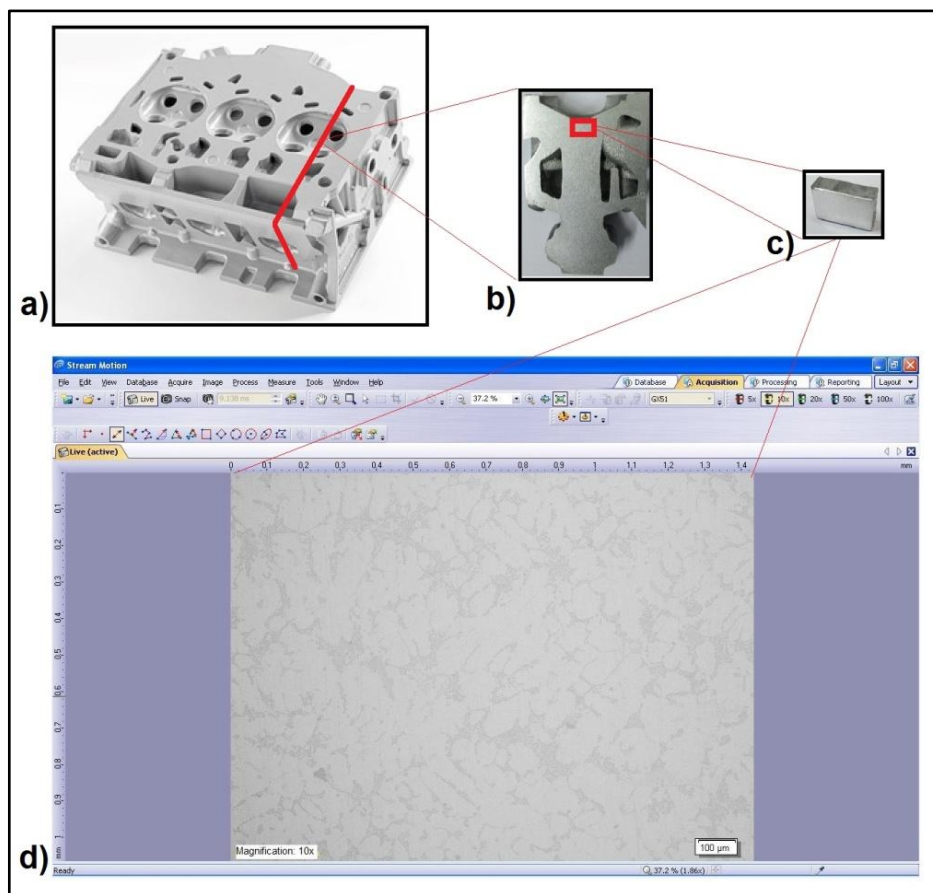


Figure 3.30: a) Aluminium cylinder head, b) Cross-section of related area, c) Sample for microstructure and SDAS measurement, d) Software interface

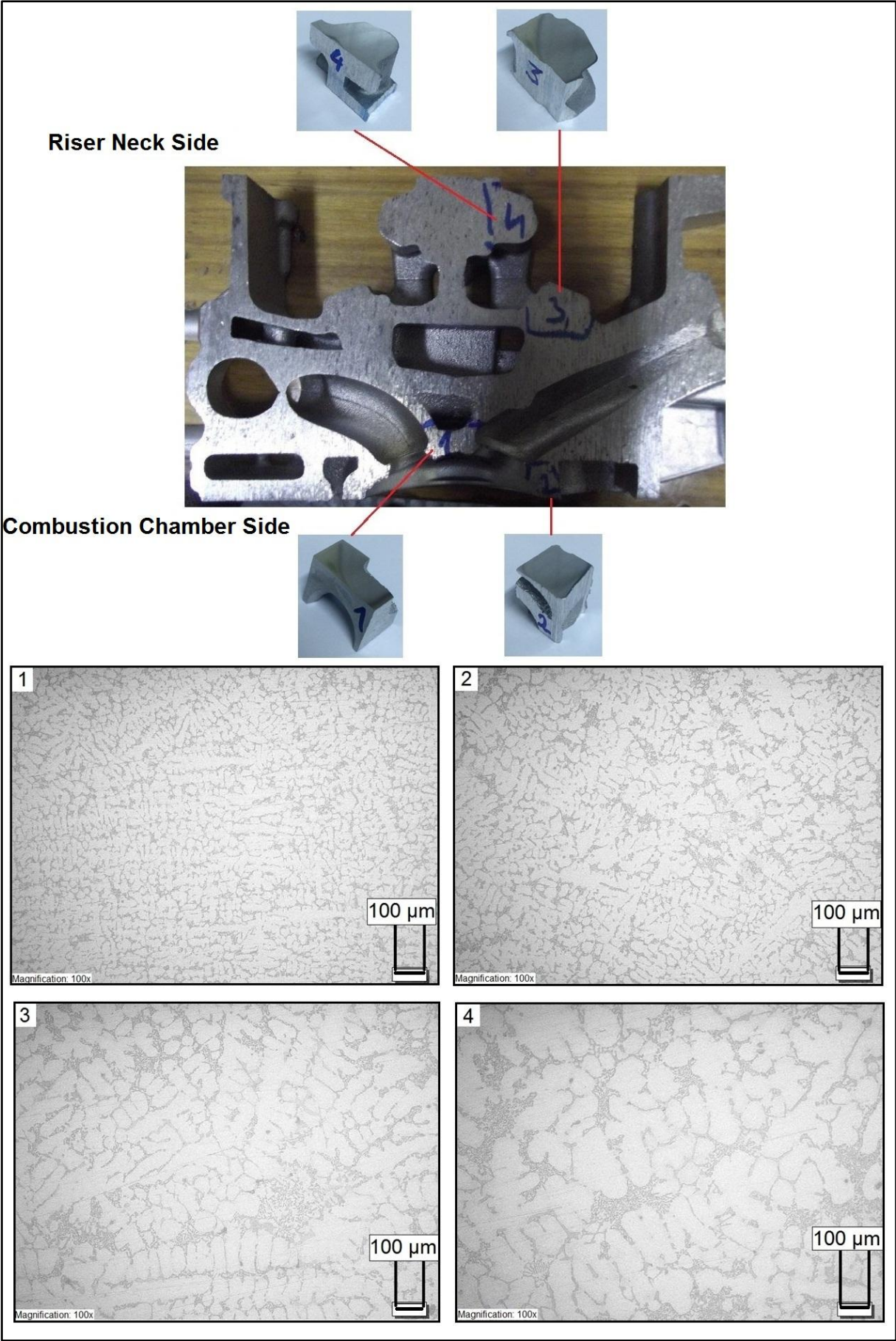


Figure 3.31: Four different areas of cross section and microscopic photos

The microstructure of AlSi6Cu4 is shown in Figure.3.32. Surely, properties of the optical microscope used, etching conditions and other variables may affect the contrast and quality of the pictures. As seen in the picture, dark grey areas show Si phase and light grey areas show Al phase. Al phases are mainly globular, whereas Si phases are mainly granular.

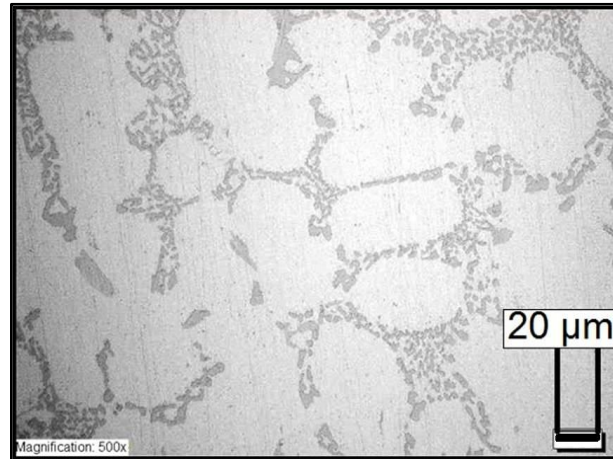


Figure 3.32: Micrographs of AlSi6Cu4

Al-Si-Cu cast alloys contain many different phases. Primary Al phase (α phase), Si, Al_2Cu and Al-Si-(FeMn) phases which are observed in two different form as 'Chinese script' or 'fish bone' and 'monoclinic' phase. Figure 3.33.a shows the typical microstructure of Al-Si-Cu alloy. Al-Si-(FeMn) phases can be observed as 'Chinese script'. Nevertheless, Al-Si-(FeMn) phases are observed as 'fish bone' is in Figure 3.33.b. Although having different appearances, these phases can be evaluated as being the same. On the other hand, 'monoclinic' Al-Si-(FeMn) phases is observed in Figure 3.35. 'Monoclinic' phase is critical for the structure playing a role as stress raiser.

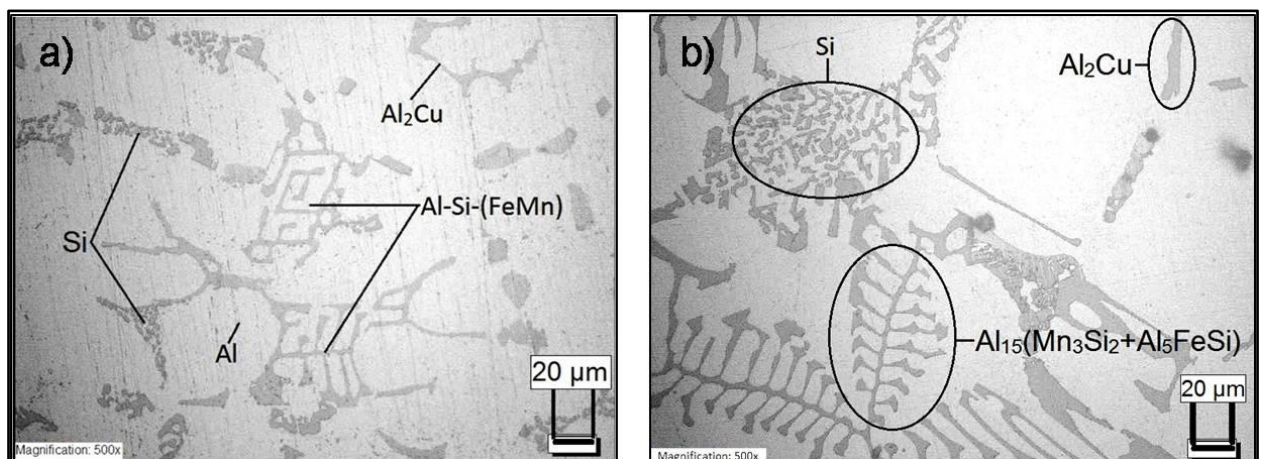
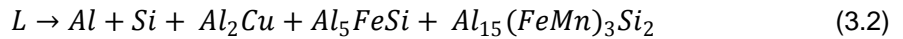
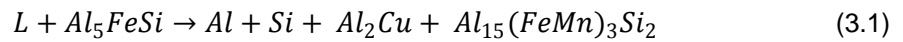


Figure 3.33: a) Micrographs of the structure, b) Typical phases in a cast AlSi6Cu4

Belov et al. (2005) said 'According to the quaternary diagram Al-Fe-Mn-Si, Al-Cu-Fe-Si, and Al-Cu-Mn-Si, only three phases - Al_2Cu , Al_5FeSi , $Al_{15}(Mn_3Si_2)$ – can be equilibrium with Al and Si. This conforms to one of the following invariant reactions:' [Bel05]



Belov et al. (2005) tabulated these reactions with reaction temperature.

Table 3.4: Chemical reactions in the structure and temperature [Bel05]

Reactions	Temperatures (°C)
$L \rightarrow Al + Al_2Cu$	548 – 517
$L \rightarrow Al + Si$	577 – 517
$L \rightarrow Al + Al_{15}Mn_3Si_2$	649 – 517

Cast AlSi6Cu4 material contains Si, Al_2Cu and Al-Si-(FeMn) phases in addition to the Al primary phase in the structure.

The Si phase in the refined Al-Si eutectic structure is almost entirely in compact and fine grained form. Primary duty of Si phase is improving fluidity and feeding. In the microstructure, Si phase can be recognized easily because of fine grained form. The under refined Al-Si eutectic structure gives grained form and fine grained form in the structure. Over refined Al-Si structure gives coarse grained or lamellar Si form in the structure.

The addition of copper to Al-Si creates Al_2Cu phase which helps to increase the strength and machinability of the alloys. Al_2Cu phase can be recognized by its shape and tint (light greyscale).

Iron (Fe) and manganese (Mn) creates compound with Al-Si. This compound is $Al_{15}(Mn_3Si_2+Al_5FeSi)$ for related AlSi6Cu4 material. Al-Si-(FeMn) can be recognized in the structure easily. Two types of shapes can occur in the structure. These shapes are called 'Chinese script' or 'fish bone' and 'monoclinic'. Needle shaped Al-Fe-Si before modification changes to 'Chinese script' or 'fish bone' with Mn after modification. This structure is evaluated as acceptable in the related customer standards.

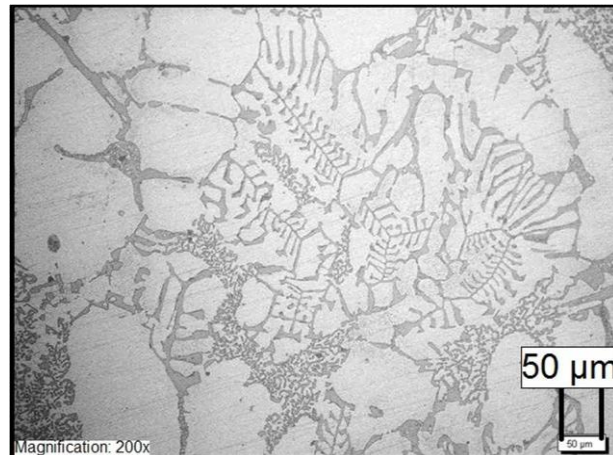


Figure 3.34: Chinese script samples in the structure

Beside this, 'monoclinic' phase which is β (Al-Fe-Si) causes brittle fracture which is very dangerous for the structure. 'Monoclinic' phase is evaluated as unacceptable in the industry.

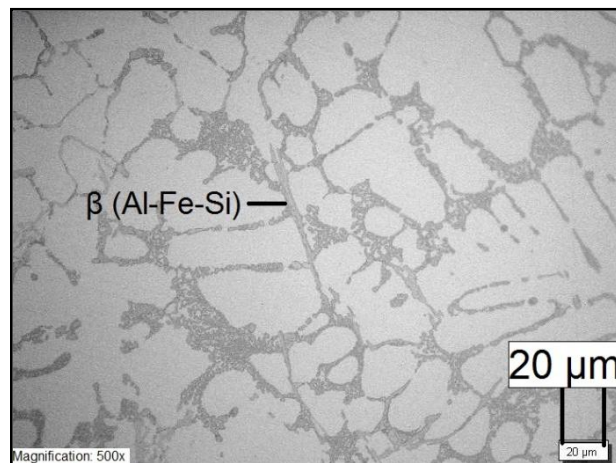


Figure 3.35: β (Al-Fe-Si) samples in the structure

As shown in the following figure, coarse silicon structures changes to fine round shaped silicon.

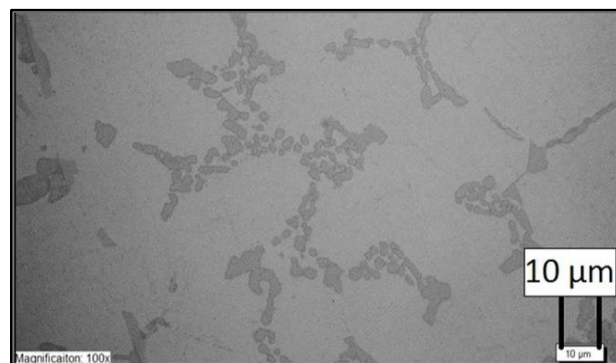


Figure 3.36: Fine round shaped silicon in the structure

3.3 Brinell hardness test

Brinell hardness tests are carried out according to EN ISO 6506 – ASTM E 10. The Brinell hardness (HB) value is shown directly on the screen by test machine. Beside this, the theoretical calculations are shown below:

$$HB = Constant \frac{\text{Test Load}}{\text{Surface of the impression}} \quad (3.3)$$

Similarly,

$$HB = 0.102 \frac{2F}{\pi D (D - \sqrt{D^2 - d^2})} \quad \text{and} \quad d = \frac{d_1 - d_2}{2} \quad (3.4)$$

Stress relief process does not only release the residual stress but also improves mechanical properties and hardness value. In this section, hardness values of three cylinder heads with stress relief and three cylinder heads without stress relief were measured. These three cylinder heads which were stress relieved were located differently in the furnace. Thus, the effect of different locations in the same furnace on the Brinell hardness value will be determined.

Before hardness test, the surfaces of critical regions for test have to be grinded and polished. After polishing, the cylinder heads were ready for Brinell hardness test. Totally, six different cylinder heads with and without stress relief were tested.

Emco-Test test machine is used for Brinell hardness measurement (Figure 3.37). Test method is called as 'HBW 5/250' code. 5 in this code shows 5 mm ball holder as penetrator and 250 shows 250 kgf -in the other word- around 2452 N. Brinell hardness is measured according to EN ISO 6506 – ASTM E-10. Brinell hardness tests were carried out at room temperature.

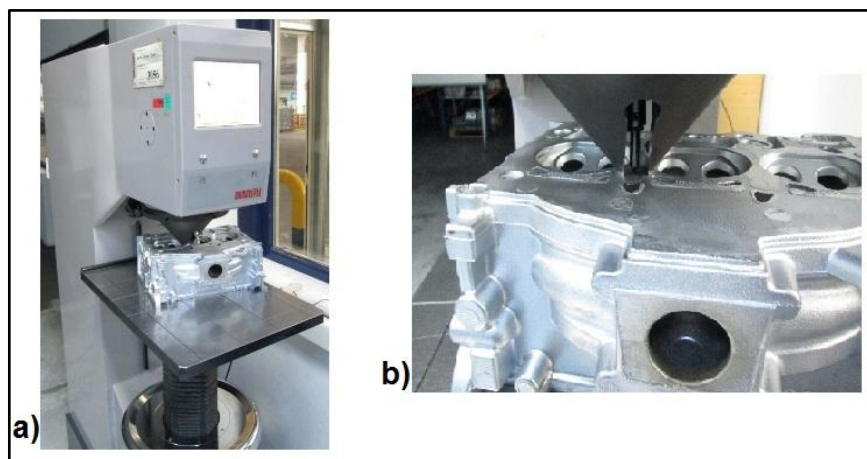


Figure 3.37: a) Emco-Test test machine, b) Hardness measurement of cylinder head

Related 'Cevher Aluminium Foundry' document which is named as 'hardness measurement regions' and is defined 'TGT-KA-05' code and the critical regions were determined in this document for Brinell hardness test for related cylinder heads (Figure 3.38.a) [NN14]. According to related documents, the Brinell hardness value has to be 95 ± 10 HB on the combustion chamber and 85 ± 10 HB on the back side of combustion chamber (Riser neck side) [NN14]. Three regions were marked for test. Two of them which are located between combustion chambers are designated as 1 and 2. Third one which is located on the back side of combustion chamber called 3. (Figure 3.38.b, c and d)

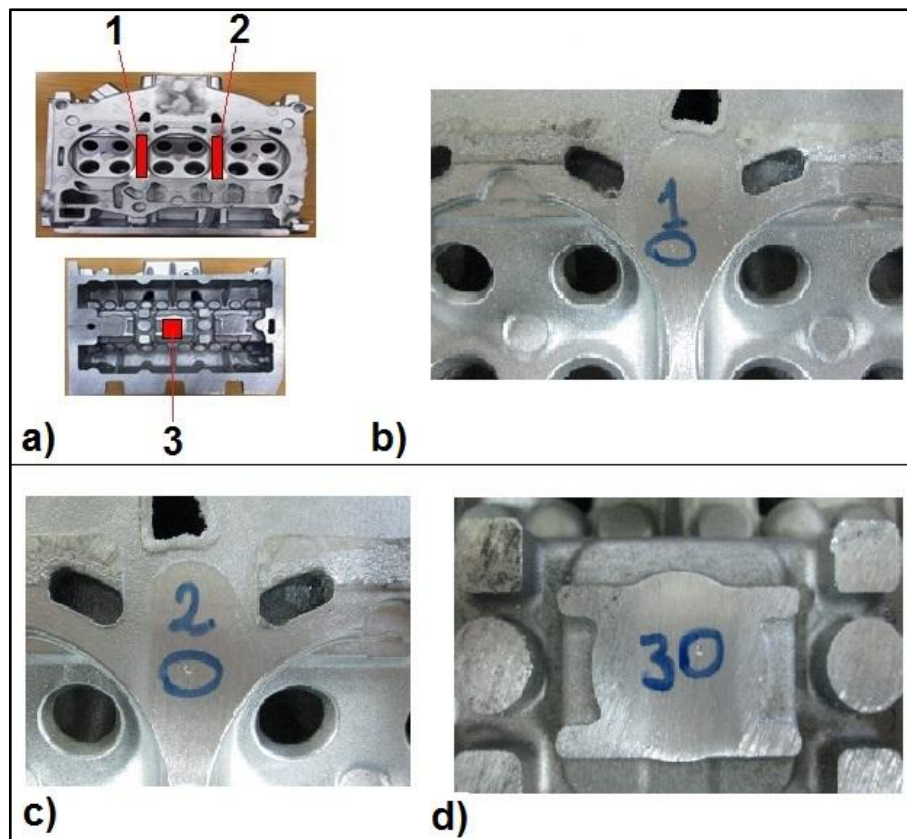


Figure 3.38: a) Hardness measurement regions [NN14], b) 1st Region, c) 2nd Region, d) 3rd Region

3.4 SDAS measurement

Microstructures and SDAS measurement were examined using Olympus GX 51 (light optical microscope) with Stream Motion software. This software shows the microstructure with x50, x100, x200, x500 and x1000 magnification and it is capable of doing SDAS measurements. The linear interception method which is detailed before is applied to measure the SDAS. Based on the linear interception method, SDAS is measured as a ratio of length of dendrite arm to the number of arms.

The critical regions on the cylinder head were determined and shown before in Figure 2.21. SDAS measurements were done on the critical areas. The SDAS is measured at the specified measurement locations 0,5 mm and 1,5 mm below the surface of the part.

Pavlovic-Kirstic (2010) detailed the procedure of SDAS measurement. The author noted these 'SDAS measurement has been performed using only dendrites which possess minimal 5 dendrite arms.' and 'In order to determine the average value of SDAS in one sample, it was necessary to carry out minimal 10 measurements or in other words to chose 10 different primary dendrites containing more than 5 secondary arms.' [Pav10]

Equations and inequalities for determining the secondary dendrite arm spacing (SDAS) were given before (Equations from 2.3 to 2.11). All measurements from the critical regions have to satisfy these equations and inequalities. In the following figure, sample for the SDAS measurement with x100 magnification is given in Figure 3.39.

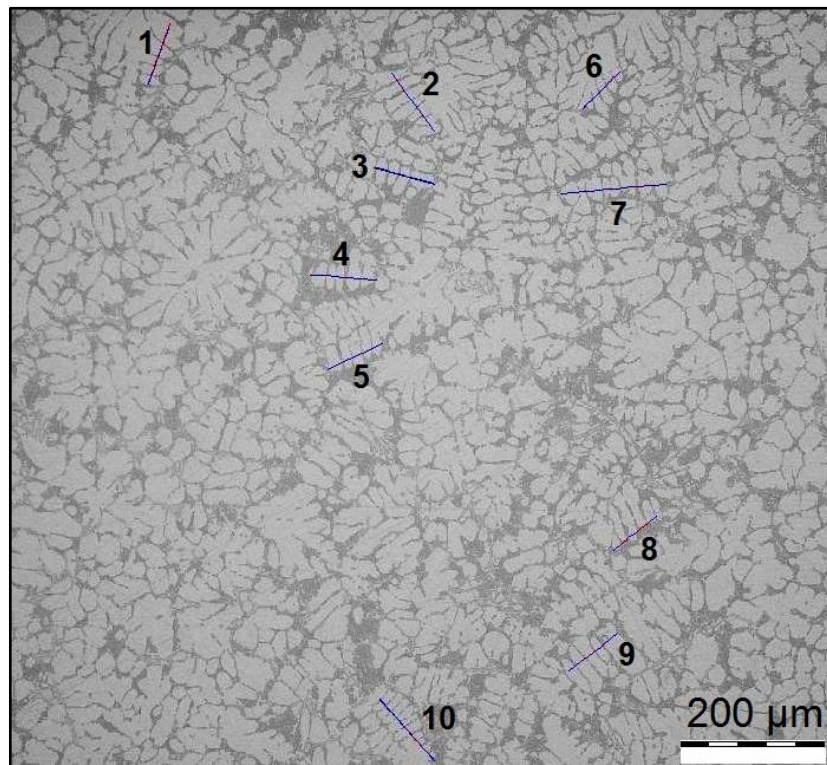


Figure 3.39: SDAS measurement sample

3.5 Tensile test

Tensile tests were carried out by 'Zwick ZS 100' tensile-compression test machine in Cevher Aluminium Foundry mechanical test laboratory. The test machine can carry out the tensile tests with 100 kN. The test machine is shown in Figure 3.40. The test machine is connected to a computer and the results of tensile test were recorded by 'testXpert V8.1' test software.



Figure 3.40: Zwick ZS 100 tensile test machine

Table 3.5: Inputs of tensile tests

Input	Explanation	Value
Grip to grip separation	Gap between jaws at the starting of tests	111.8 mm
Pre-Load	Pre-Load before starting of tests	10 N/mm ²
Specimen data	Dimension (d ₀), Shape of specimen	12mm, Round specimen
E-Modulus	Starting - ending points to determine E-Modulus	30 N/mm ² - 80 N/mm ²
Test velocity	Velocity of crosshead during tests	10 mm/min

3.6 Fatigue test

In this study, stress controlled rotating bending fatigue tests are carried out. Different loads are applied and different stress levels are obtained on the surface. To carry out comparative tests on the chosen material, three different sets of aluminium cylinder heads were cast and fatigue test samples were taken from between combustion chambers which is known as critical region and machined for rotating bending fatigue test machine. All tests were carried out at room temperature and under atmospheric conditions. The rotating bending fatigue test machine which is called 'Hi-Tech Scientific - Model HSM 19 mk3' is used to perform the tests. The frequency is 50 Hz and 2890 rpm. The picture of test machines is given in Figure 3.41.



Figure 3.41: Rotating bending fatigue test machines



Figure 3.42: Dial indicator

Specimen has to be fixed on same axial direction of rotating bending test machine. The position of specimens can be controlled by using dial indicator. As seen in Figure 3.42, dial indicator attached to magnetic base indicator holders. Pointer of dial indicator touches the face of specimen and differences can be transformed to mechanism with plunger. Pointer shows the differences directly on the bigger indicator which is scaled from 0 to 100. Each unit shows 0.01mm. Small indicator which is called as turn counter changes from 0 to 1 with one full turn of pointer. Instruction manual of machine gives recommended standard specimen with a throat diameter of 4 mm for fatigue test. The bending stress on the specimen with a minimum diameter (d_{min}) for a load P (N) is: [Rob01]

$$\sigma = \frac{114.6P * 32}{\pi * d^3} = \frac{114.6P * 32}{\pi * 4^3} = 18.24 P [N/mm^2] \quad (3.5)$$

Before fatigue test, at least one tensile test specimen must be carried out in order to obtain ultimate tensile strength (UTS), yield stress (YS) and elongation ($\epsilon\%$). From the tensile test results the minimum bending stress that can be applied must not be greater than the yield stress and could be taken as 0.9 of that test value. A set of bending tests from 0.9 of the yield stress to 0.4 of the ultimate strength should be selected to match the specimens with each other. The surface condition of specimen affects the fatigue results directly thus after machining, grinding and polishing have a vital importance for the samples [Rob01]. Surely, neck part which is machined to $\text{Ø}4$ mm is critical for test and this region has to be polished and the roughness should be minimized. After polishing, the roughness of all samples will be controlled as tensile test specimens.

The shaft and loading arm chucks have a collet to grip the fatigue test sample. After assembling of sample, tighten the collets with the spanners. Set up of test machine is given in Figure 3.43. Elements of test machine are detailed on the figure [Rob01].

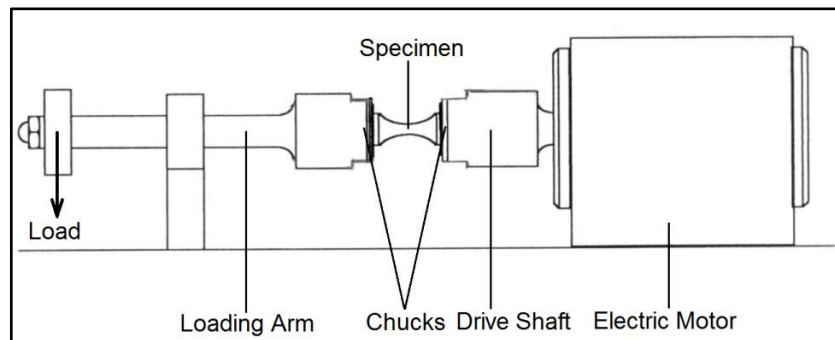


Figure 3.43: Fatigue machine setting up [Rob01]

In order to eliminate the effect of weight of system on the cantilever, the counterbalance weight is designed and located in the structure as shown in Figure 3.44 [Rob01].

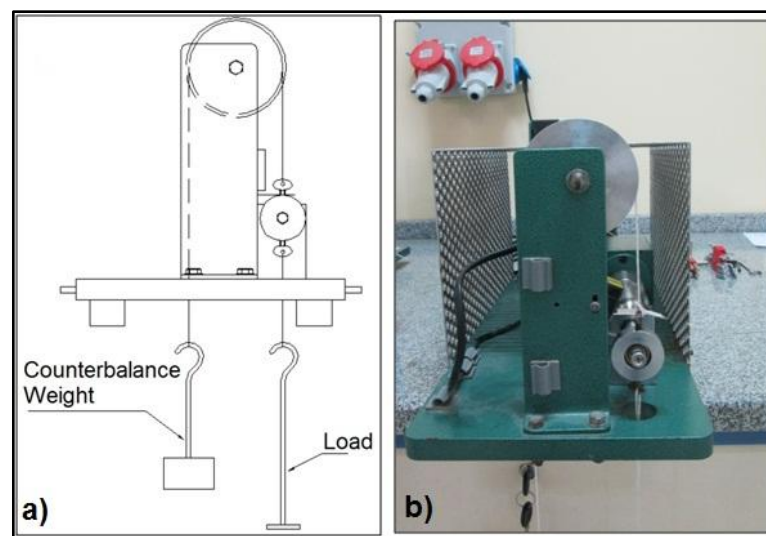


Figure 3.44: a) Counterbalance weight and load on the fatigue testing machine [Rob01], b) Counterbalance weight and load on the fatigue testing machine

4 Results

4.1 Results of Brinell hardness test

The screen of Emco-test (DuraVision200, Austria) machine shows the results. In addition to this, the surfaces of samples and the marks of the indenter are seen from the screen with magnification. Figure 4.1.a and b show the results of cylinder heads with and without stress relief process respectively. As seen, the values for non-stress relieved samples are close to desired values which are shown in related 'Cevher' document which is based on DIN 1706. In addition, the effect of stress relief process on Brinell hardness is determined and shown in Table 4.1. Measuring points were previously shown in Figure 3.50.

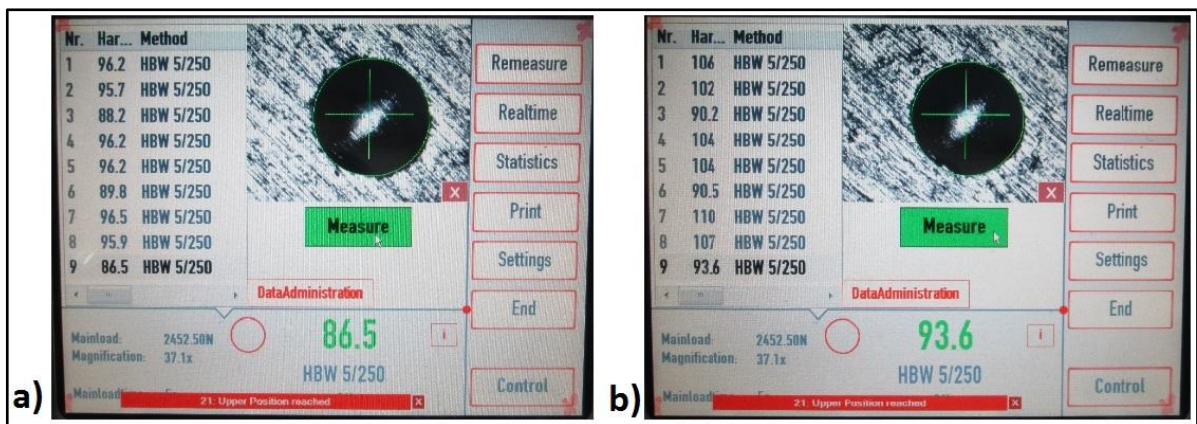


Figure 4.1: a) Brinell hardness results of non-stress relieved cylinder heads, b) Brinell hardness results of stress relieved cylinder heads

Table 4.1: Arranged results of Brinell hardness test

		Measuring Point 1 (HB)	Measuring Point 2 (HB)	Desired Value (HB)	Measuring Point 3 (HB)	Desired Value (HB)
Non Stress Relief	Group 1	96.2	95.7	95±10	88.2	85±10
	Group 2	96.2	96.2	95±10	89.8	85±10
	Group 3	96.5	95.9	95±10	86.5	85±10
Stress Relief	Group 1	106	102	100±10	90.2	105±15
	Group 2	104	104	100±10	90.5	105±15
	Group 3	110	107	100±10	93.6	105±15

The hardness values are average of three measured points. All Brinell hardness values are acceptable according to the values of AlSi6Cu4 in DIN EN 1706. In addition to this, the results show that the Brinell hardness is improved with the stress relief process. The effect of improvement depends on the measuring points regions. The hardness value between combustion chambers improves around 10%. There are no significant differences between the 1st and 2nd measuring points on the same part. On the other hand, the improvement of the hardness on the riser neck side of cylinder heads is relatively low. The improvement is around 4% (Figure 4.2). In conclusion, the HB values of non stress relieved cylinder heads can reach to desired values. Beside this, the increasing of HB values is distinguishable difference after stress relief. The ratio of increasing shows differences according to region.

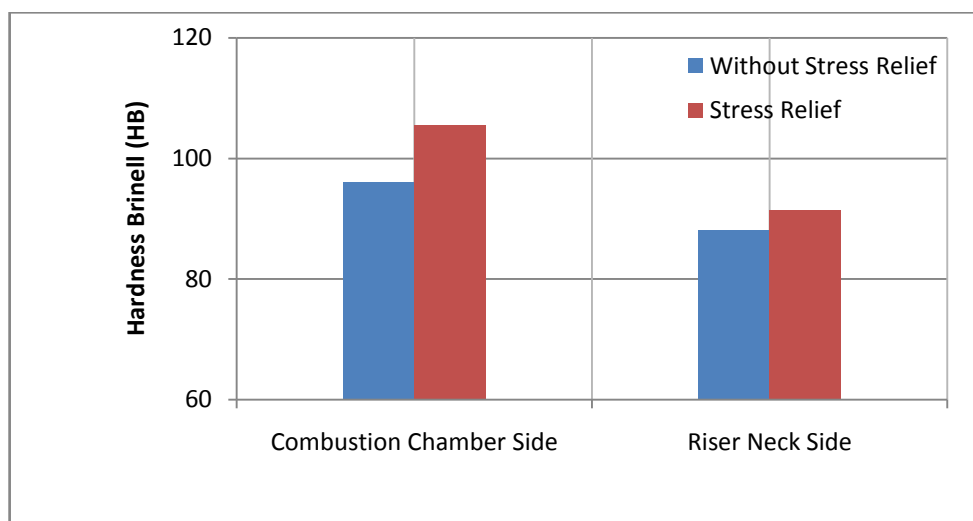


Figure 4.2: Comparing the Brinell Hardness (HB) values of different regions

4.2 Results of SDAS measurement

Used formulas and equations were given in the 'Dendrite Arm Spacing' section in this study but they should be revisited again before the evaluation the results (Table 4.4). First, measurements were taken at different locations (Figure 4.3.b) of the cross-section of cylinder heads to understand the effect of measuring point location.

It should be noted that SDAS values can be affected by and therefore vary with the experimental approach, material content, location of measuring points, the distance from the combustion chamber surface to measuring points, cooling conditions and labor. Therefore, comparisons of the SDAS values with other studies are relatively difficult. Beside this, other parameters except material content have to be same to evaluate the results. Therefore, the differences in SDAS results may be evaluated based on the differences in material contents.

Table 4.2: Measured distance, dendrite count and mean SDAS values of measuring point 1 and 2

Measuring Point 1				Measuring Point 2			
No	Measured distance (μm)	Dendrite count	Mean SDAS (\bar{x}_{SDASi})	No	Measured distance (μm)	Dendrite count	Mean SDAS (\bar{x}_{SDASi})
1	100.61	10	10.06	1	200.38	6	33.40
2	149.77	10	14.98	2	136.07	6	22.68
3	109.02	7	15.57	3	167.14	8	20.89
4	205.51	12	17.13	4	129.05	8	16.13
5	128.72	7	18.39	5	130.77	5	26.15
6	132.92	7	18.99	6	168.30	10	16.83
7	125.40	6	20.90	7	126.71	8	15.84
8	159.03	7	22.72	8	169.37	6	28.23
9	169.47	7	24.21	9	186.08	7	26.58
10	135.11	5	27.02	10	85.59	6	14,26

Table 4.3: Measured distance, dendrite count and mean SDAS values of measuring point 3 and 4

Measuring Point 3				Measuring Point 4			
No	Measured distance (μm)	Dendrite count	Mean SDAS (\bar{x}_{SDASi})	No	Measured distance (μm)	Dendrite count	Mean SDAS (\bar{x}_{SDASi})
1	238.60	6	39.77	1	326.11	8	40.76
2	235.31	5	47.06	2	408.69	9	45.41
3	266.58	6	44.43	3	332.88	10	33.29
4	725.91	13	55.84	4	355.89	6	59.32

5	292.90	7	41.84	5	325.69	7	46.53
6	261.67	6	43.61	6	400.70	8	50.09
7	177.17	5	35.43	7	265.84	5	53.17
8	174.28	5	34.86	8	363.13	8	45.39
9	262.29	6	43.72	9	258.39	6	43.07
10	199.43	5	39.89	10	328.05	8	41.01

Mean SDAS (\bar{x}_{SDASi}), averaged SDAS ($\bar{\bar{x}}_{SDAS}$) and median of mean SDAS ($\tilde{\tilde{x}}_{SDAS}$) can be calculated as shown in Table 4.4. The results are shown in Table 4.5.

Table 4.4: Equations of SDAS calculations [Pav10]

Mean SDAS	$\bar{x}_{SDASi} = \frac{x_i}{m_i}$
Averaged SDAS	$\bar{\bar{x}}_{SDAS} = \frac{1}{n} \cdot \sum_{i=1}^n \bar{x}_{SDASi} = \frac{1}{n} \cdot \sum_{i=1}^n \frac{x_i}{m_i}$
Median of mean SDAS	$\tilde{\tilde{x}}_{SDAS} = \begin{cases} \bar{x}_{SDAS(\frac{k}{2})} & , \frac{k}{2} \notin IN \\ \frac{\bar{x}_{SDAS(\frac{k}{2})} + \bar{x}_{SDAS(\frac{k}{2}+1)}}{2} & , \frac{k}{2} \in IN \end{cases}$ <p>With $\bar{\bar{x}}_{SDAS} - \tilde{\tilde{x}}_{SDAS} \leq 0,5 \mu m$</p>

Table 4.5: Averaged SDAS, median of mean SDAS and standard deviation

	Point 1	Point 2	Point 3	Point 4
$\bar{\bar{x}}_{SDAS} (\mu m)$	19.00	22.10	42.64	45.80
$\tilde{\tilde{x}}_{SDAS} (\mu m)$	18.69	21.79	42.73	45.40
$ \bar{\bar{x}}_{SDAS} - \tilde{\tilde{x}}_{SDAS} (\mu m)$	0.31	0.31	0.08	0.40
Standard Deviation	4.95	6.39	6.04	7.22

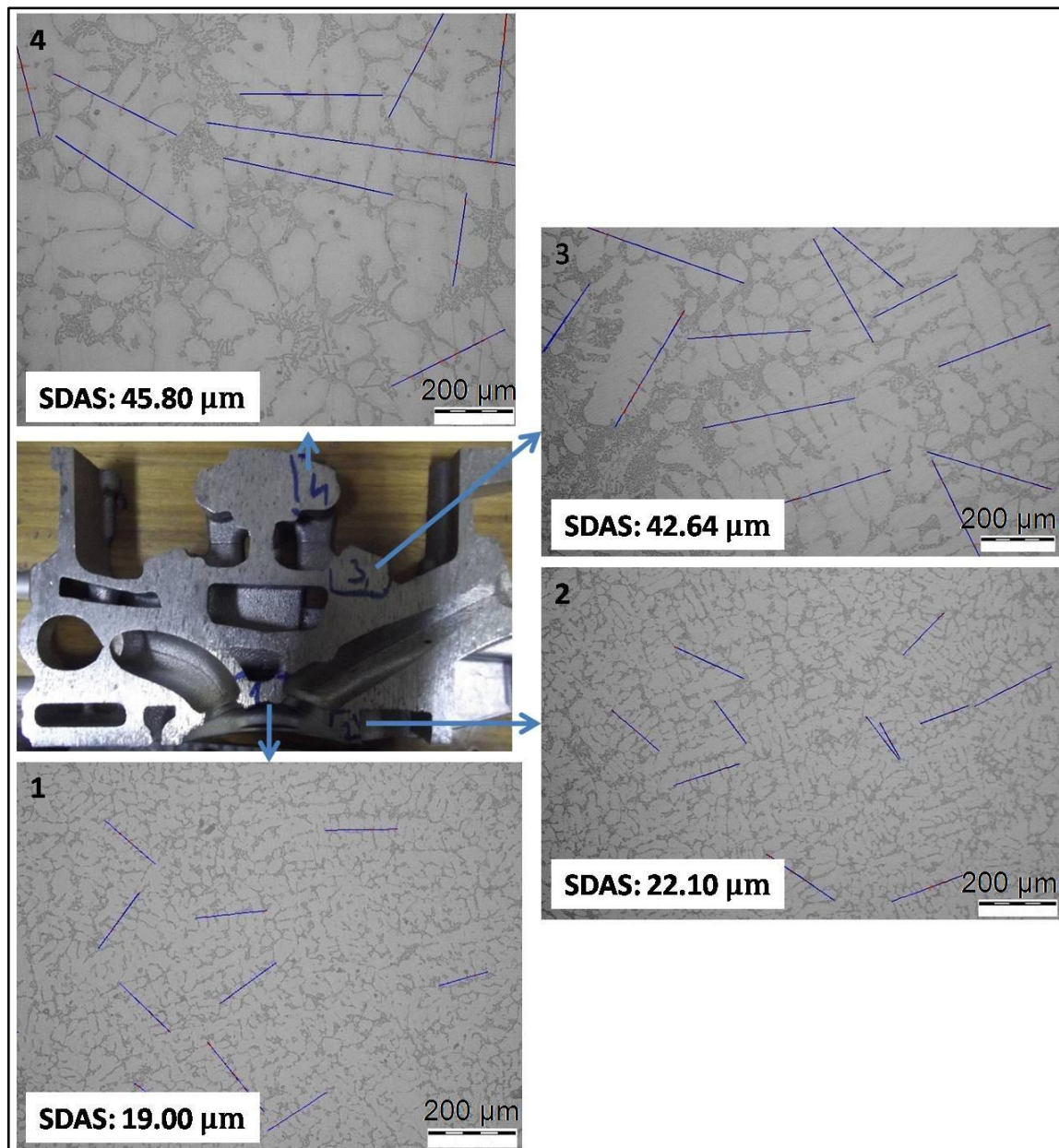


Figure 4.3: Secondary dendrite arm spacing values of AlSi6Cu4 aluminium cylinder head in different regions

When higher measuring points were selected, the SDAS values increased. Middle and high-middle regions gave greater SDAS values by almost a factor of two. As mentioned previously, the critical area is the combustion chamber side so that preset limits are determined according to combustion chamber side.

Regions 1 and 2 can be called combustion chamber side in Figure 4.3. The difference between region 1 and 2 is the cooling condition. Region 1 is cooled down by water channel in the mould whereas region 2 is cooled down naturally. There is not any extra precaution about the cooling in the mould for region 2. This difference results in the difference in the measured SDAS values. The values of SDAS measurement and the measuring points are given in detail in Table.4.6.

Table 4.6: SDAS values of different measuring points in cross-section of aluminium cylinder head

Measuring Point	Explanation	Distance from Combustion Chamber (cm)	SDAS Values (μm)
1	Combustion chamber region with water cooling	~1	19.00
2	Combustion chamber region without water cooling	~1	22.10
3	Middle Region	~7,5	42.64
4	Top Region	~11	45.80

Next, the SDAS values of standardized points (Figure 2.21) were measured and calculated.

Table 4.7: Measured distance, dendrite count and mean SDAS values of 1st group

1 st Group without stress relief				1 st Group with stress relief			
No	Measured distance (μm)	Dendrite count	Mean SDAS (\bar{x}_{SDASi})	No	Measured distance (μm)	Dendrite count	Mean SDAS (\bar{x}_{SDASi})
1	99.54	5	19.91	1	134.37	5	26.87
2	157.25	7	22.46	2	89.87	6	14.98
3	148.47	7	21.21	3	85.99	5	17.20
4	230.22	10	23.02	4	64.14	5	12.83
5	189.63	7	27.09	5	154.37	6	25.73
6	105.62	6	17.60	6	126.78	6	21.13
7	120.16	5	24.03	7	129.87	5	25.97
8	151.12	5	30.22	8	117.30	6	19.55
9	114.86	5	22.97	9	116.05	5	23.21
10	135.32	6	22.55	10	78.35	5	15.67

Table 4.8: Measured distance, dendrite count and mean SDAS values of 2nd group

2 nd Group without stress relief				2 nd Group with stress relief			
No	Measured distance (μm)	Dendrite count	Mean SDAS (\bar{x}_{SDASi})	No	Measured distance (μm)	Dendrite count	Mean SDAS (\bar{x}_{SDASi})
1	152.48	9	16.94	1	176.84	8	22.10
2	99.94	5	19.99	2	132.58	7	18.94
3	158.59	9	17.62	3	86.25	5	17.25
4	97.40	5	19.48	4	78.32	5	15.66
5	71.72	5	14.34	5	104.14	5	20.83
6	123.78	5	24.76	6	133.64	5	26.73
7	132.54	5	26.51	7	141.25	6	23.54
8	101.13	5	20.23	8	135.72	8	16.97
9	97.84	5	19.57	9	117.10	5	23.42
10	89.84	5	17.97	10	78.22	5	15.64

Table 4.9: Measured distance, dendrite count and mean SDAS values of 3rd group

3 rd Group without stress relief				3 rd Group with stress relief			
No	Measured distance (μm)	Dendrite count	Mean SDAS (\bar{x}_{SDASi})	No	Measured distance (μm)	Dendrite count	Mean SDAS (\bar{x}_{SDASi})
1	80.50	5	16.10	1	135.19	6	22.53
2	105.26	5	21.05	2	87.64	5	17.53
3	76.74	6	12.79	3	56.31	5	11.26
4	56.92	5	11.38	4	114.82	7	16.40
5	69.77	6	11.63	5	95.13	6	15.86

6	66.38	5	13.28	6	113.51	5	22.70
7	114.20	7	16.31	7	192.62	7	27.52
8	104.76	7	14.97	8	124.29	6	20.72
9	96.11	5	19.22	9	112.22	5	22.44
10	163.03	8	20.38	10	85.72	5	17.14

Mean SDAS (\bar{x}_{SDASi}), averaged SDAS ($\bar{\bar{x}}_{SDAS}$) and median of mean SDAS ($\tilde{\tilde{x}}_{SDAS}$) can be calculated and the results are shown in Table 4.10.

Table 4.10: Averaged SDAS ($\bar{\bar{x}}_{SDAS}$), median of mean SDAS ($\tilde{\tilde{x}}_{SDAS}$) and standard deviation

	1 st Group		2 nd Group		3 rd Group	
	Non-Stress Relief	Stress Relief	Non-Stress Relief	Stress Relief	Non-Stress Relief	Stress Relief
$\bar{\bar{x}}_{SDAS}$ (μm)	23.11	20.31	19.74	20.11	15.71	19.41
$\tilde{\tilde{x}}_{SDAS}$ (μm)	22.76	20.34	19.52	19.88	15.54	19.12
$ \bar{\bar{x}}_{SDAS} - \tilde{\tilde{x}}_{SDAS} $ (μm)	0.35	0.03	0.22	0.22	0.18	0.29
Standard Deviation	3.53	5.05	3.59	3.80	3.56	4.64

Adherence to prescribed secondary dendrite arm spacing is required to improve the resistance to thermal shock and the fatigue strength of cylinder heads. Not only SDAS calculation but also other equations which are detailed in 'Dendrite arm spacing' section in this study have to be conducted.

Table 4.7, Table 4.8 and Table 4.9 show the measured distances and dendrite counts. Measured distance is divided by the dendrite count to obtain the mean SDAS. This calculation method is named the linear interception method in the literature [Pav10], [Zha03].

Beside the formulas in Table 4.4, there is a limit determined median of mean SDAS. The limit is checked after calculations. The values provide the appropriate conditions. This situation shows that the calculations are suitable. Results show that, grain refiners (Ti and B) help to decrease the SDAS values. When the grains are refined, SDAS values may decrease.

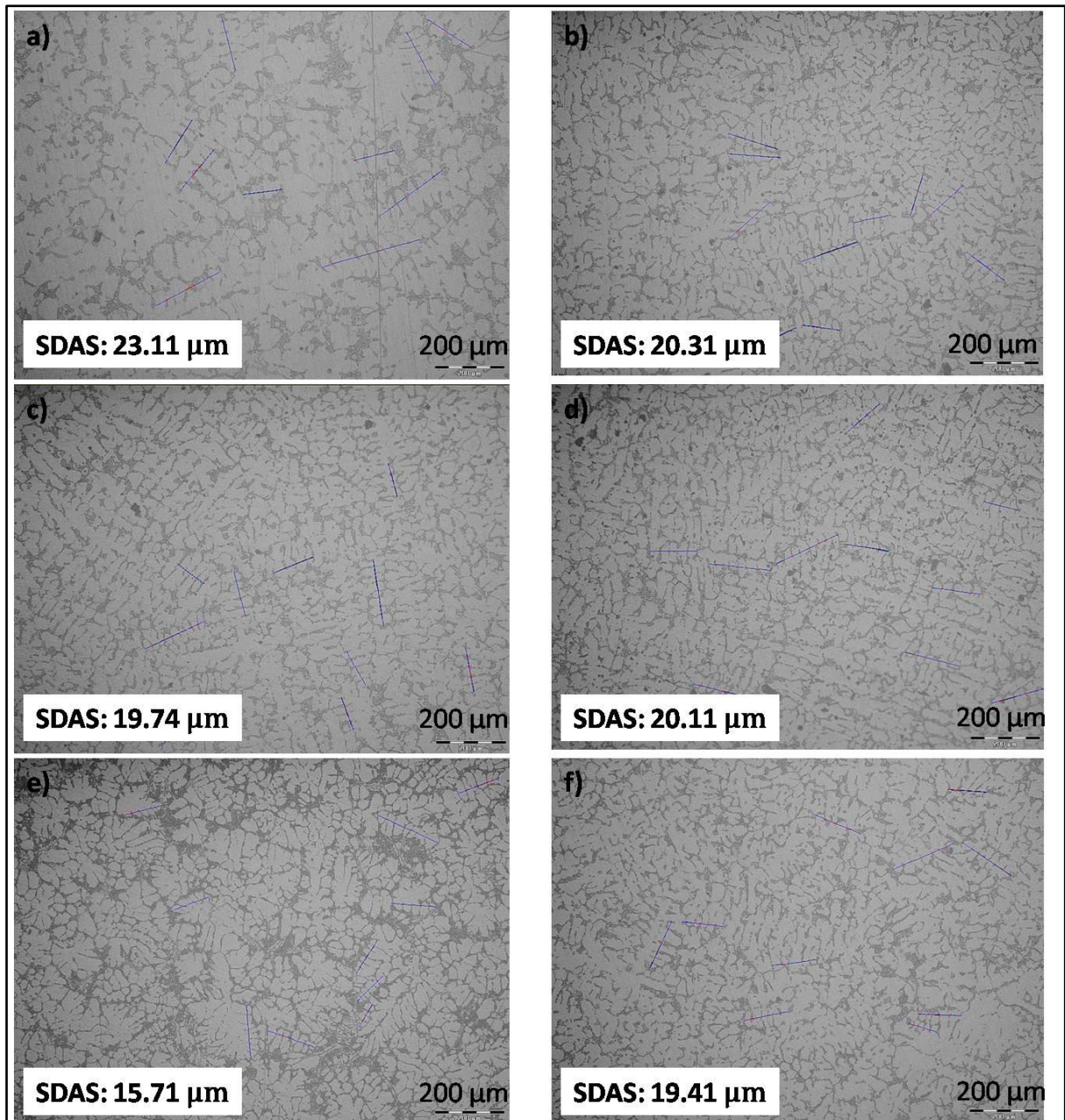


Figure 4.4: a) 1st group cylinder head without stress relief, b) 1st group cylinder head with stress relief, c) 2nd group cylinder head without stress relief, d) 2nd group cylinder head with stress relief, e) 3rd group cylinder head without stress relief, f) 3rd group cylinder head with stress relief.

The analysis of the results of averaged SDAS (\bar{x}_{SDAS}) shows that 1st group without stress relief can be evaluated as insufficient because SDAS values reach 23.11 μm. This type of aluminium cylinder head demands 19-20 μm or lower SDAS values. After stress relief, SDAS values can be decreased to SDAS limit but as seen in the following group, it cannot be guaranteed for all the time. Since the 1st group cannot satisfy the SDAS limits, lower grain refiner additions were not tested. It is to be expected that lower additive levels give worse results in SDAS.

As seen, the 2nd group gives appropriate values and there is not a distinguishing difference before and after stress relief process. Finally, the 3rd group gives the best result in SDAS. As known from the literature [Hu97], more than 0.15 wt % Ti cannot make important differences so that, higher percentage grain refiner addition is not necessary for this type of aluminium cylinder heads.

4.3 Results of tensile test

In this study, two types of tensile specimens are prepared. The first type was the specimens which were extracted from the combustion chamber region of cylinder heads. Because of the dimensional restrictions, this type of specimens were machined to $d_0=5$ mm. The second type was the specimens which were directly poured into the tensile test bar mould. The second type of specimens are machined to $d_0=12$ mm. Obviously, the tensile test bar mould and cylinder head mould have different cooling rates. These differences result in different mechanical properties. Zhang et al. noted that different cooling rates may give different mechanical properties [Zha05]. It is predicted that cylinder head mould has a higher cooling rate than tensile test bar mould so that, the extracted specimens from combustion chamber would have better mechanical properties than poured specimens into the tensile test bar mould.

Before the tests, the conditions of fracture surface were cleared. The fracture surface can be named 'clean fracture surface' if there are no casting defects (Figure 4.5.a and b). Beside this, inclusions can affect the mechanical properties dramatically. The most common inclusions are oxide flakes which are described in the 'Casting defects' section in this study. The oxide can be discriminated into the three groups which are called as small (Figure 4.6.a and b), medium (Figure 4.7.a and b) and large (Figure 4.8.a and b) oxide flakes. All macrostructure pictures are compared with the study of DasGupta et al. [Das04]. They noted that when the size of oxide flake increases, the mechanical properties should be decreased. The mechanical values of the tested samples are given in Table 4.11.

Table 4.11: The effects of oxide flakes on the mechanical properties

	UTS (MPa)	YS (MPa)	ϵ (%)
Clean Fracture Surface	203.12	144.15	1.05
Small Oxide Flakes	205.82	159.28	0.91
Medium Oxide Flakes	197.35	159.91	0.70
Large Oxide Flakes	193.35	150.74	0.83

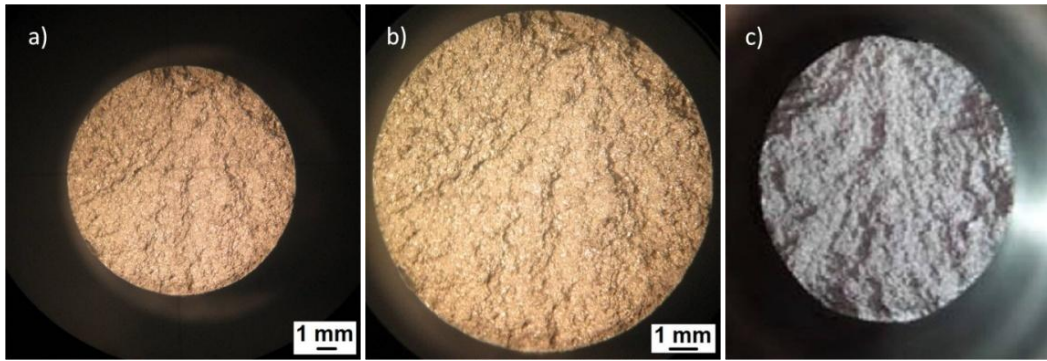


Figure 4.5: Clean fracture surface. a) x10 Magnification, b) x15 Magnification, c) [Das04]

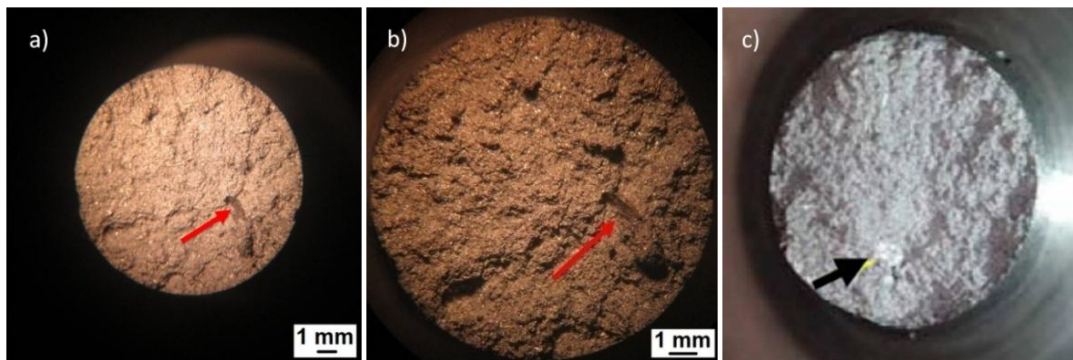


Figure 4.6: Small oxide flakes. a) x10 Magnification, b) x15 Magnification, c) [Das04]

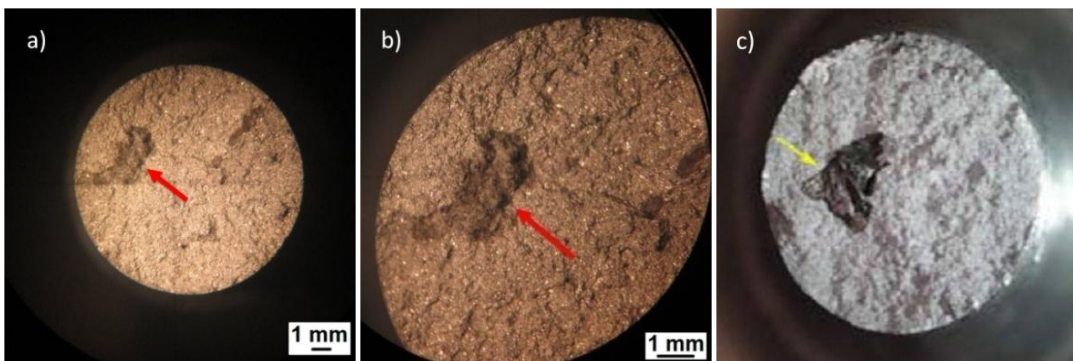


Figure 4.7: Medium oxide flakes. a) x10 Magnification, b) x20 Magnification, c) [Das04]

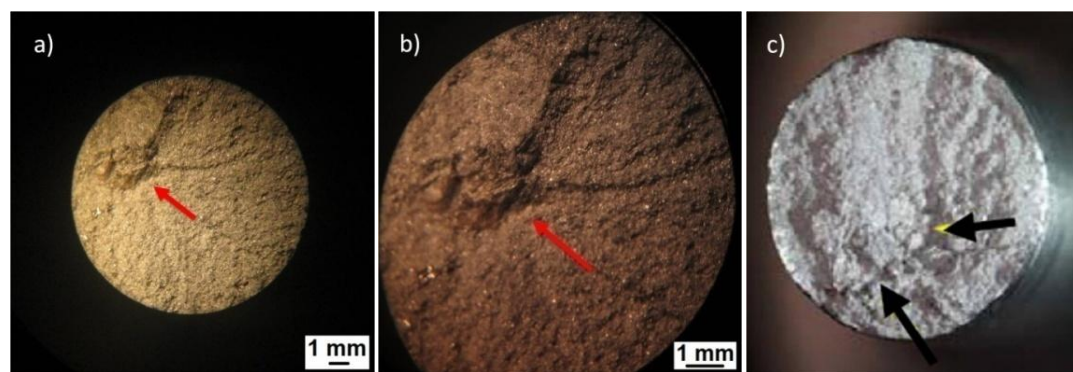


Figure 4.8: Large oxide flakes. a) x10 Magnification, b) x20 Magnification, c) [Das04]

The results of tensile test of $d_0=5$ mm specimens are investigated and shown in Table 4.12. The mechanical values such as UTS, YS and $\epsilon\%$ are in conformance with the AISi6Cu4 in DIN EN 1706. On the other hand, the elongation values of specimens which include small, medium and high oxide flakes are below the standard limits (in DIN EN 1706) as seen in Table 4.11. These oxides cause a lower elongation and result in a brittle structure. According to DIN EN 1706 limits, these types of oxides are unacceptable for the related material.

The grain refinement is increasing from 1st group to 3rd group. The effects of them on the SDAS values are shown in Figure 4.4. The first expectation would be that ultimate tensile strength, yield strength and elongation may increase with lower SDAS values. It is noted and proven in the literature by Zhang et al. (2005) who have studied the effect of dendrite arm spacing on mechanical properties of aluminum alloy cylinder heads and engine blocks [Zha05].

The second expectation would be that the stress relief releases the residual tensile stress in the structure and helps to improve the mechanical properties. The ratio can be calculated in related standard for similar materials. UTS values increase around 10% and YS values increase around 35% [Ren14]. It shows the stress relief gives better UTS and YS values. Besides this, there is no significant difference noted for elongation.

Table 4.12: Tensile test results of $d_0=5$ mm specimens which are extracted from combustion chamber region

$\text{Ø}5$ specimens		UTS (MPa)	YS (MPa)	ϵ (%)
1 st Group	Non Stress Relief	236.39	178.19	1.30
	Stress Relief	231.86	181.56	1.09
2 nd Group	Non Stress Relief	248.74	182.35	1.43
	Stress Relief	276.09	225.80	1.22
3 rd Group	Non Stress Relief	258.12	183.25	1.81
	Stress Relief	279.98	230.36	1.18

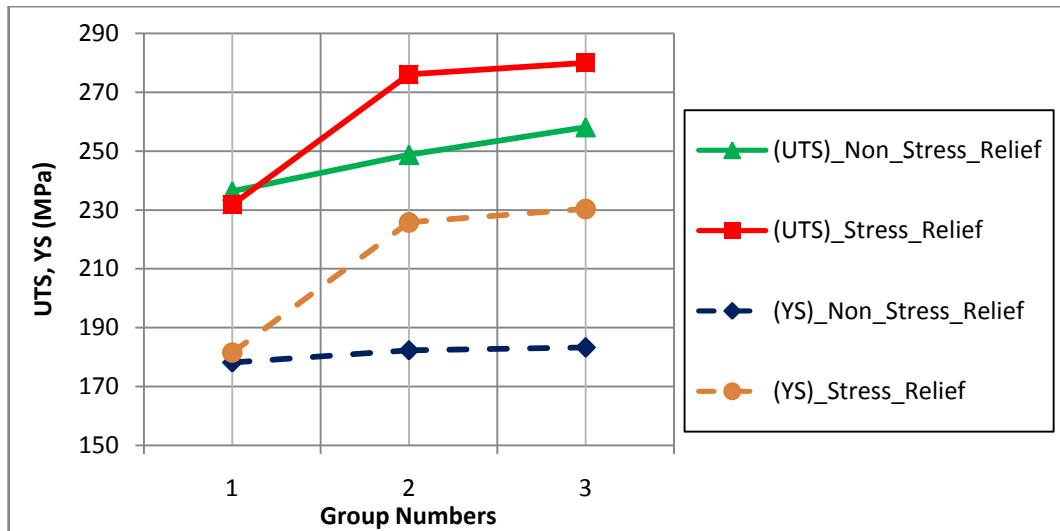


Figure 4.9: Comparing UTS and YS of $d_0=5$ mm specimens

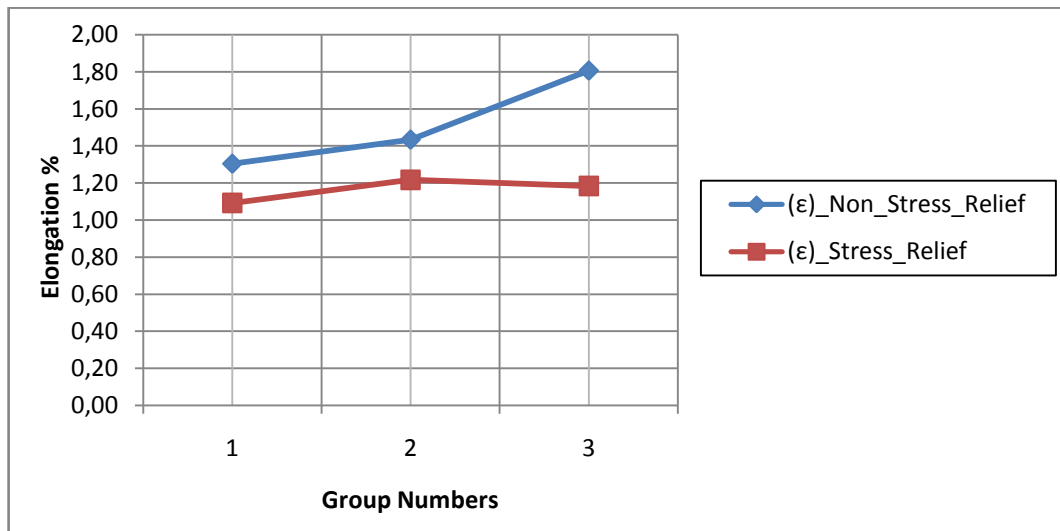


Figure 4.10: Comparing ϵ of $d_0=5$ mm specimens

The 1st group has the lowest grain refiner level and it has the highest SDAS values and the worst UTS, YS and $\epsilon\%$ values compared to other groups. Although the UTS, YS and $\epsilon\%$ values are above the limit, it should be noted that the SDAS values are higher than the desired limit. An increase of UTS, YS and $\epsilon\%$ are expected and obtained in the 2nd and 3rd groups progressively. The 3rd group has the highest grain refiner level and it has the lowest SDAS values and the best UTS, YS and $\epsilon\%$ values compared to other groups. The increase in UTS is higher than that in YS. This result is in agreement with the literature [Zha05]. The increase between UTS and YS in each group can be recognized in Figure 4.9. The increase in UTS is almost two times higher than the increase in YS.

In addition to this, the trends of UTS and YS with SDAS can be seen in Figure 4.11. UTS has a higher rate of increase than that of YS. Likewise, the decreasing of $\epsilon\%$ with the increasing SDAS is explained in Figure 4.12.

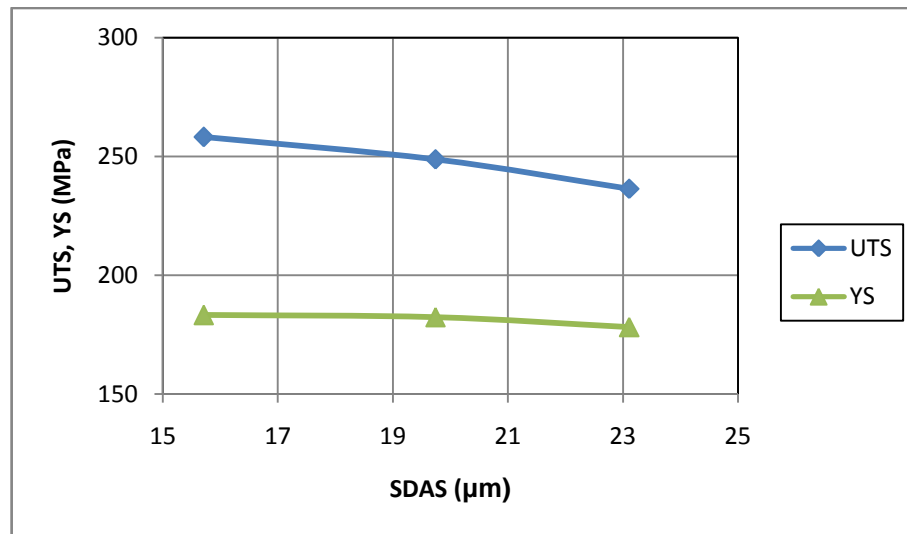


Figure 4.11: UTS/YS-SDAS values of specimens from AISi6Cu4 cylinder heads

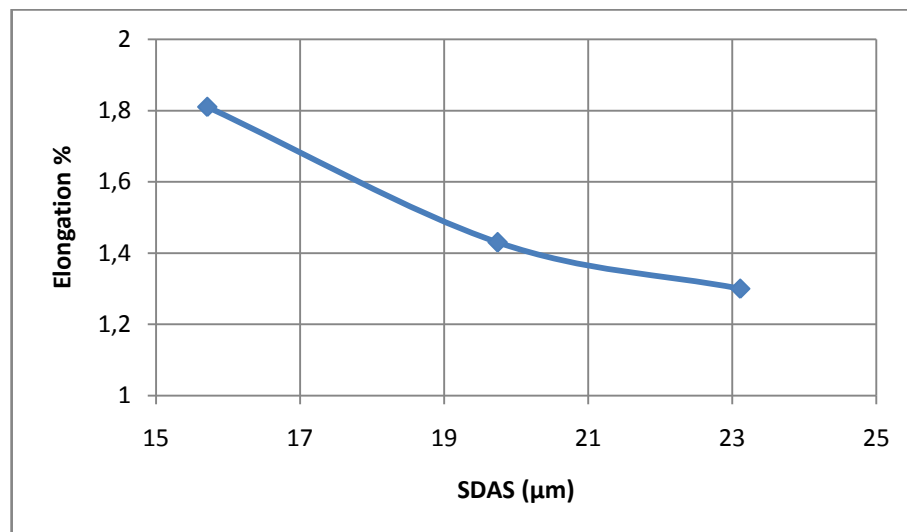


Figure 4.12: Elongation-SDAS values of specimens from AISi6Cu4 cylinder heads

Second, results of tensile test of $d_0=12$ mm specimens are shown in Table 4.13.

Table 4.13: Tensile test results of $d_0=12$ mm specimens which are poured into the tensile test bar mould

Ø12 specimens		UTS (MPa)	YS (MPa)	ϵ (%)
1 st Group	Non Stress Relief	210.25	175.57	0.63
	Stress Relief	220.86	205.69	0.37
2 nd Group	Non Stress Relief	216.57	191.02	0.44
	Stress Relief	231.26	210.15	0.45
3 rd Group	Non Stress Relief	234.09	193.00	1.35
	Stress Relief	247.77	219.34	1.15

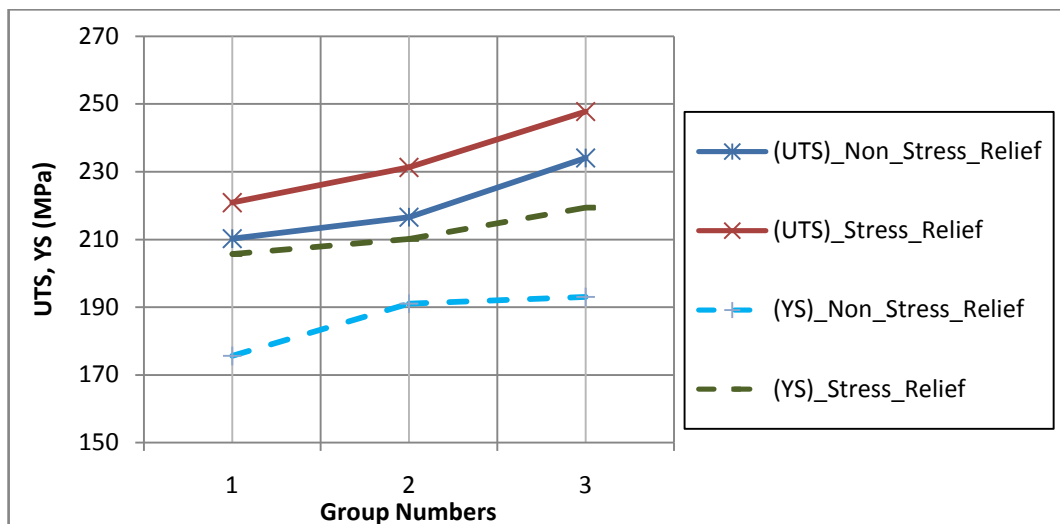


Figure 4.13: Comparing UTS and YS of $d_0=12$ mm specimens

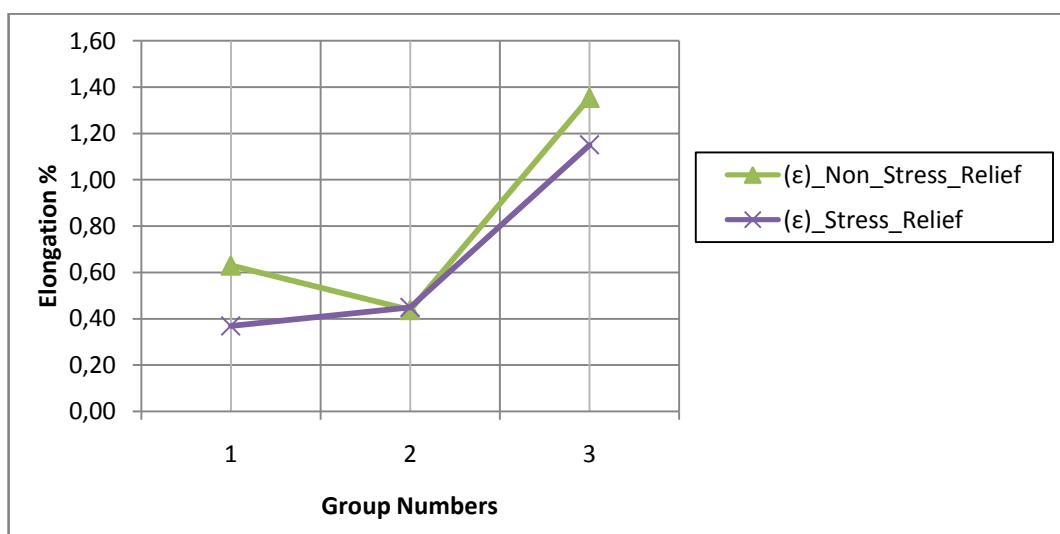


Figure 4.14: Comparing ϵ of $d_0=12$ mm specimens

Table 4.14: The effects of stress relief on the UTS and YS

		UTS (MPa)	YS (MPa)
1st Group	Ø5 specimens	1.92% worse	1.89% better
	Ø12 specimens	5.05% better	17.16% better
2nd Group	Ø5 specimens	10.99% better	23.83% better
	Ø12 specimens	6.78% better	10.01% better
3rd Group	Ø5 specimens	8.47% better	25.71% better
	Ø12 specimens	5.84% better	13.65% better

Except the $d_0=5$ mm specimens of 1st group, other groups give better results. Although the better results of the samples in the 2nd and 3rd group, the 1st group gives unexpected results. The reason of this could be inclusions in the structure or unexpected problems during stress relief process. The SDAS values were 23.11 μm and 20.31 μm and from the practical knowledge, the industry demands around 19-20 μm or less SDAS values. That is the reason why the samples in the 1st group of aluminium cylinder heads cannot be used for industry.

The UTS, YS and $\epsilon\%$ values show differences between $d_0=5$ mm and $d_0=12$ mm specimens. The UTS, YS and $\epsilon\%$ values of $d_0=12$ mm specimens which are poured into the tensile test bar mould are lower compared with those values of $d_0=5$ mm specimens which are extracted from the combustion chamber of cylinder heads. The main reason of this could be different cooling rates of tensile test bar mould and cylinder head mould. The combustion chambers regions of cylinder heads are cooled down very fast in the mould which has water channels in it whereas the tensile test bar mould does not have any extra cooling equipment. Higher cooling rate results in very fine grains and better mechanical properties. Whereas lower cooling rate causes coarse grains and worse mechanical properties. Beside this, the casting into the tensile test bar mould is done by an operator, the labor and experience of the operator may affect the part condition and it may cause different results in the same group of specimens.

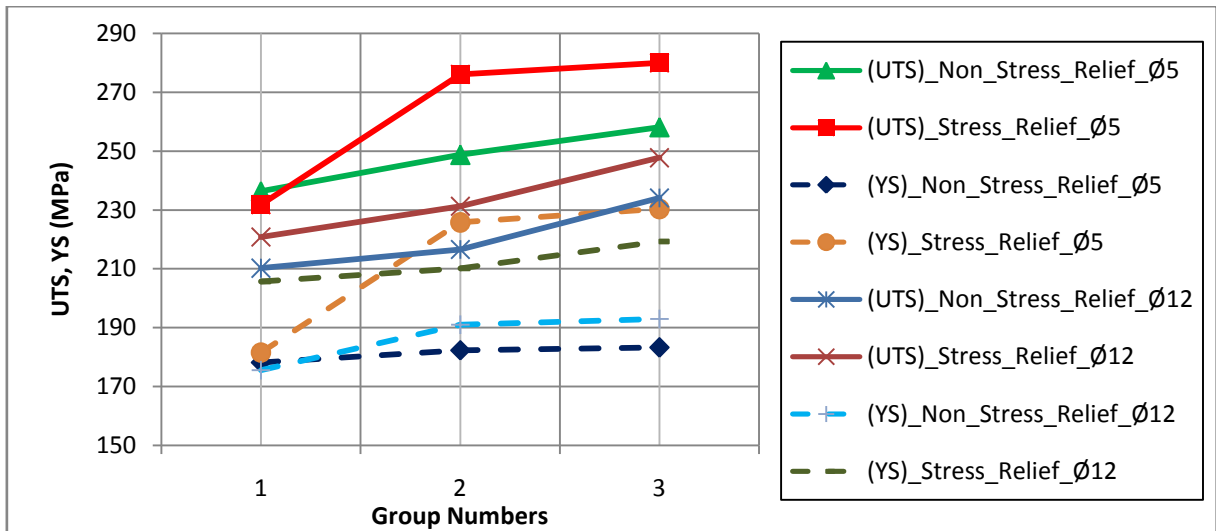


Figure 4.15: Comparing the UTS and YS of $d_0=5$ mm and $d_0=12$ mm specimens

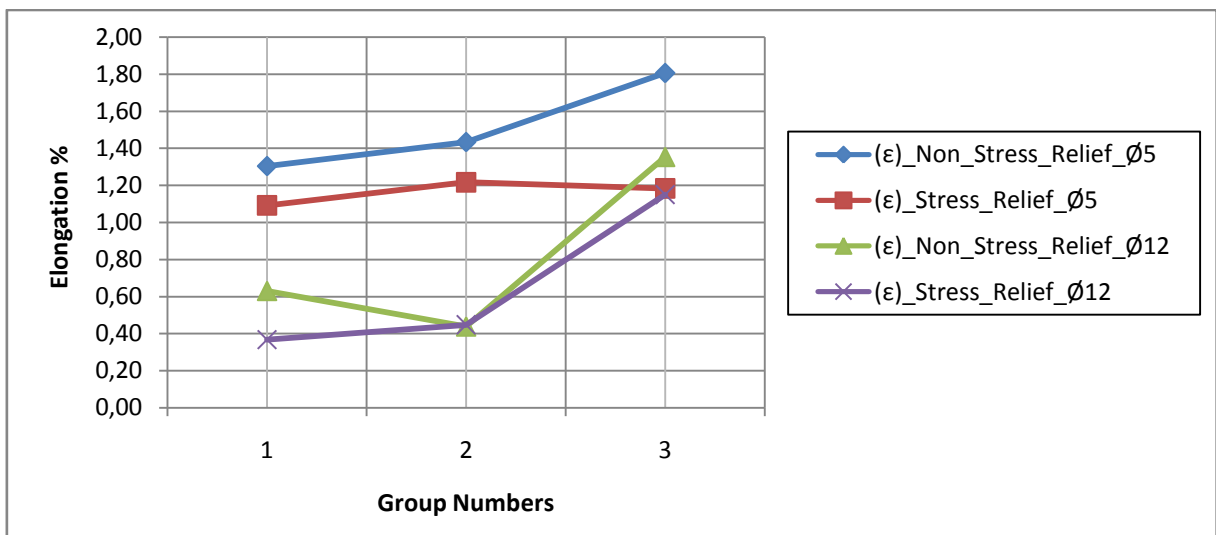


Figure 4.16: Comparing the ϵ of $d_0=5$ mm and $d_0=12$ mm specimens

4.4 Results of fatigue test

Microstructure of the materials affects the fatigue properties directly. SDAS is measured from predetermined critical regions of aluminium cylinder heads and SDAS values can affect the fatigue properties. Also the surface condition of the specimen affects the results. Different surface quality may lead to differences in the results.

Table 4.15: Different fractured samples in different cycle number

Figure	Number of cycles before fracture	Figure	Number of cycles before fracture
4.20	33,450	4.24	142,850
4.21	38,350	4.27	516,150

In Table 4.15, cycle numbers before fracture are given. As seen from the figures, porosities and macro cracks lead to failure. In addition to this, almost all cracks occur on the surface.

The specimen that is shown in Figure 4.17 is fractured with a low cycle number. The porosity in the structure causes the easy propagation for the cracks which occur on the surface.

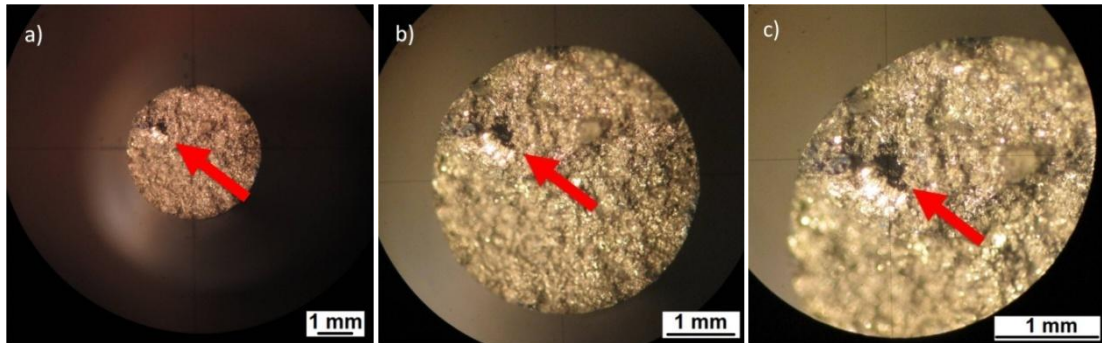


Figure 4.17:Fracture surface a) x20 Magnification, b) x40 Magnification, c) x63 Magnification

The specimen that is shown in Figure 4.18 shows many macro cracks in different regions of the surface.

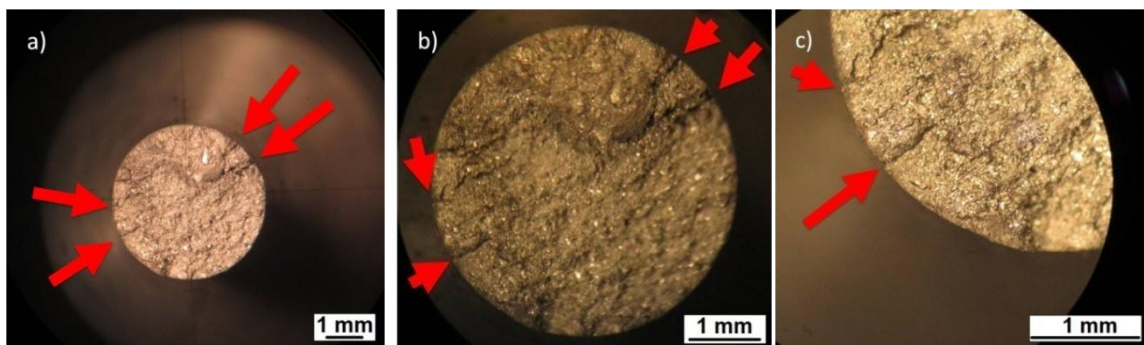


Figure 4.18:Fracture surface a) x20 Magnification, b) x40 Magnification, c) x63 Magnification

Another specimen is shown in Figure 4.19. In this failure, cracks occur in one point and propagate.

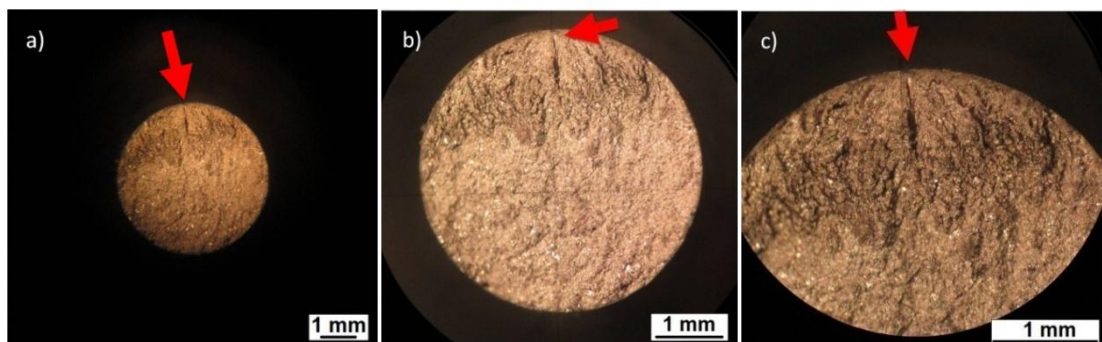


Figure 4.19:Fracture surface a) x20 Magnification, b) x40 Magnification, c) x63 Magnification

Finally, the samples which are fractured in higher cycle numbers are shown in Figure 4.20.

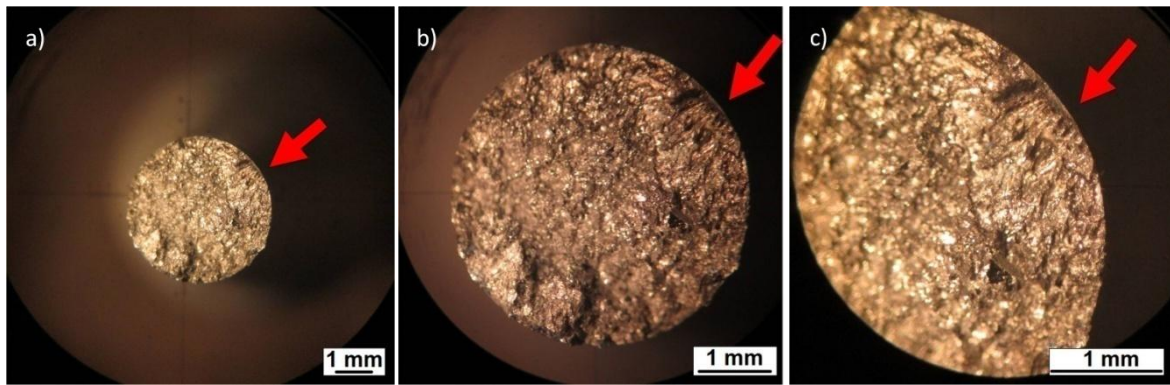


Figure 4.20:Fracture surface a) x20 Magnification, b) x40 Magnification, c) x63 Magnification

As a conclusion, fatigue failure occurs at the stress level less than yield strength. Beside this, there is not any warning on the specimen before fatigue failure. The specimens may fracture unexpectedly. Repeating cyclic loads may lead to failure under yield strength. This situation may cause disastrous results so that fatigue behaviour of the material has to be kept in mind in designing components, development of new materials and methods.

4.4.1 Woehler (S-N) curve

Due to applied loads fracture occurs and this point is marked on the S (stress) – N (Number of cycle) graphs. N (Number of cycle) which is located on X axis is drawn in log.

Stress was controlled during the tests and was kept constant for each test meaning that the stress at any points on the surface of the cantilever varies sinusoidally. The reversal stress is between the limits $\pm\sigma$ and so the stress range is 2σ .

In engineering material fatigue tests, two types of Woehler (S-N) curve may occur. First, there is an endurance limit in the S-N curve. It means, there will be not any failure under the endurance limit. Thus, the material can be evaluated to have an infinite life under the endurance limit. Ferrous alloys and titanium have endurance limits and they can guarantee the infinite life under the endurance limit. On the other hand, there is no endurance limit in the S-N curve for some materials such as aluminium and copper. This means, there will be failure in the structure absolutely. The number of cycle (or time) exceeds to millions or billions but the failure will occur definitely. However, the millions or billions cycles take so much time to test and it is a great disadvantage for practical approach, especially in the industry applications. As a result of this, the limit of the number of cycles has to be defined at which the test will stop. This limit is determined as 10^7 (10 Million cycle) for aluminium in the literature. This limit is especially used for the aluminium alloys for automotive applications.

Figure 4.21.a shows the test under predetermined load. The counter is driven through a reduction gear (1:50). One unit increase on the counter denotes 50 cycles. The test machine has a switch which touches the shaft. When the specimen is fractured, contact between the

switch and shaft is cut. Thus, the power supply of machine is stopped automatically. This equipment makes a test possible which continues for days.

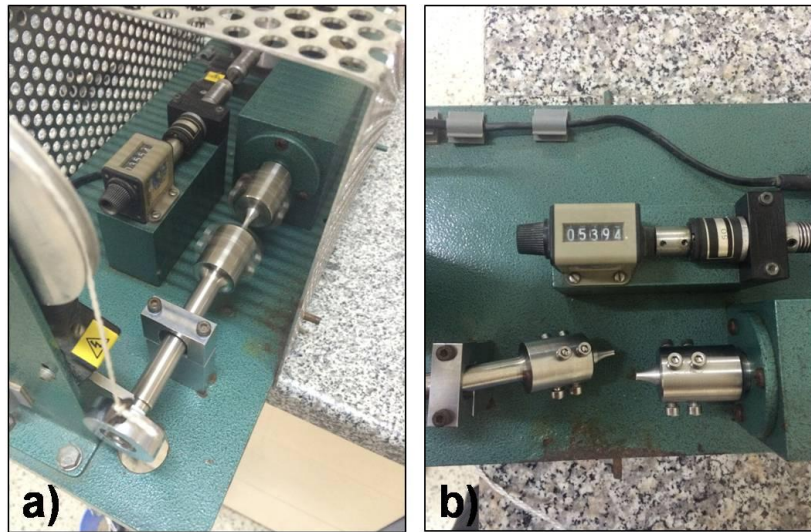


Figure 4.21: a) Rotating bending fatigue test, b) Fractured specimen

Table 4.16: Different failure samples with fractured cycle number

Load (MPa)	1 st Group		2 nd Group		3 rd Group	
	Non-Stress Relief	Stress Relief	Non-Stress Relief	Stress Relief	Non-Stress Relief	Stress Relief
225	8,350	13,950	27,900	28,050	38,350	36,250
200	30,700	33,450	66,950	71,300	88,200	89,200
175	85,250	89,250	142,290	89,200	142,850	147,850
150	147,850	150,650	164,610	166,400	233,150	269,700
125	245,550	259,450	195,300	231,550	464,300	516,150
100	669,600	825,850	901,150	1,076,950	3,208,500	3,646,550
75	4,800,350	7,150,000	>10,000,000	>10,000,000	>10,000,000	>10,000,000
50	>10,000,000	>10,000,000				

Woehler (S-N) curve is drawn by Excel computer software with the values given in Table 4.15. First, S-N curve of the 1st group without and with stress relief is drawn. As seen in Table 4.15 and Figure 4.22., stress relief increases the fatigue strength. However, the difference after stress relief is not remarkable.

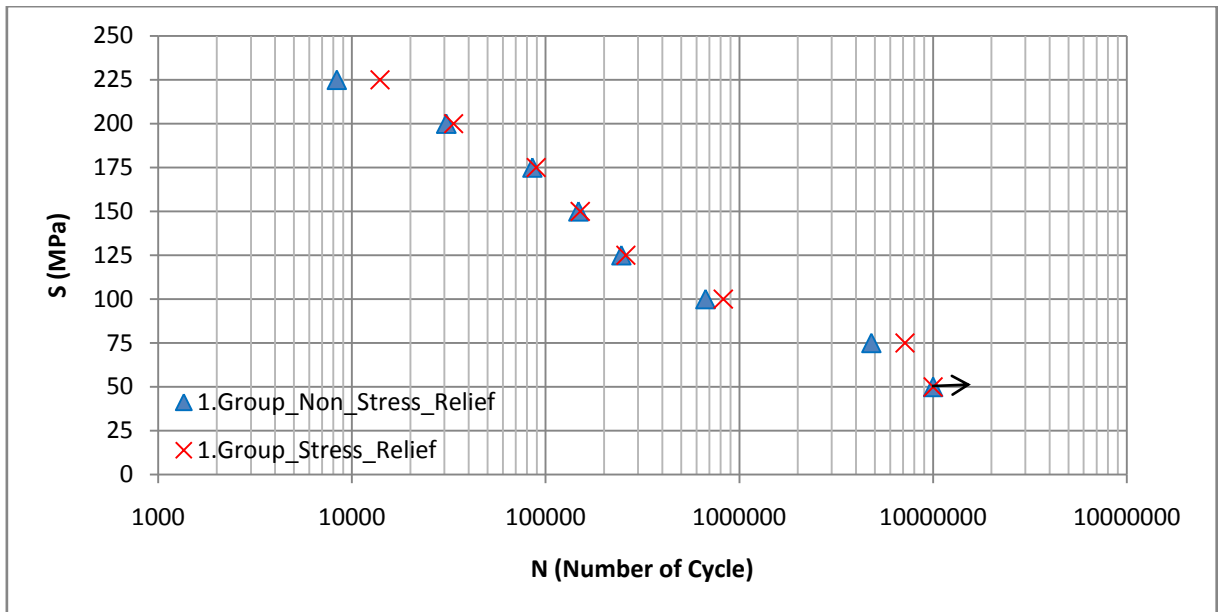


Figure 4.22: S-N values of 1st group with and without stress relief process

Similarly, 2nd group shows improvement on the fatigue strength but the improvement is limited. Beside this, some specimens which are not stress relieved show better results compared to the specimens which are stress relieved.

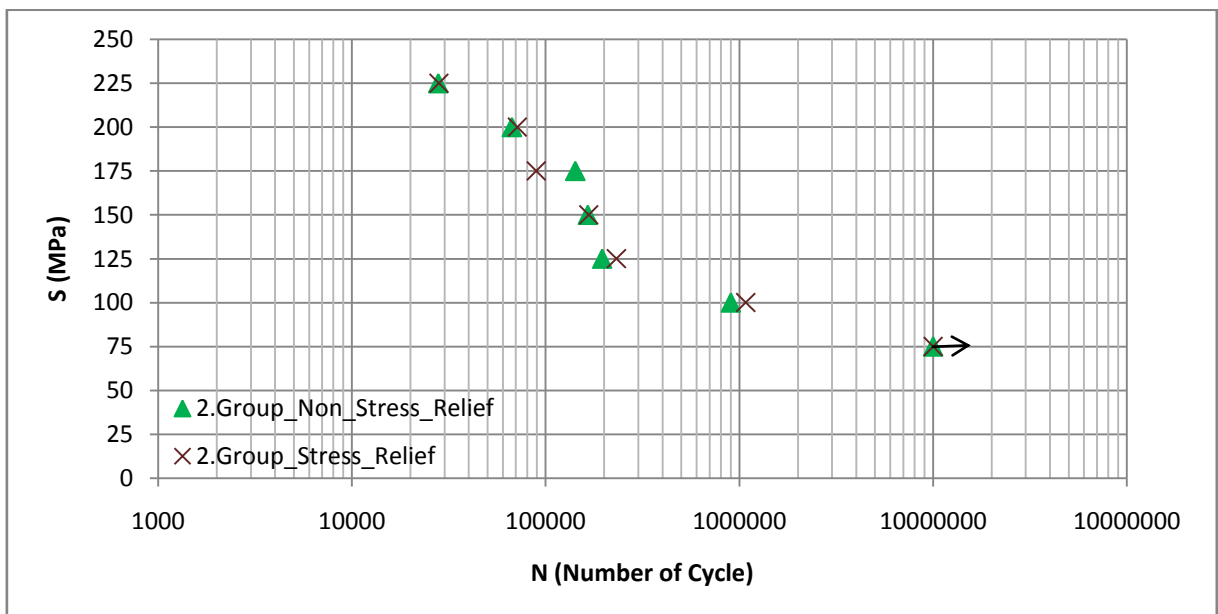


Figure 4.23: S-N values of 2nd group with and without stress relief process

3rd group shows similar results with previous groups.

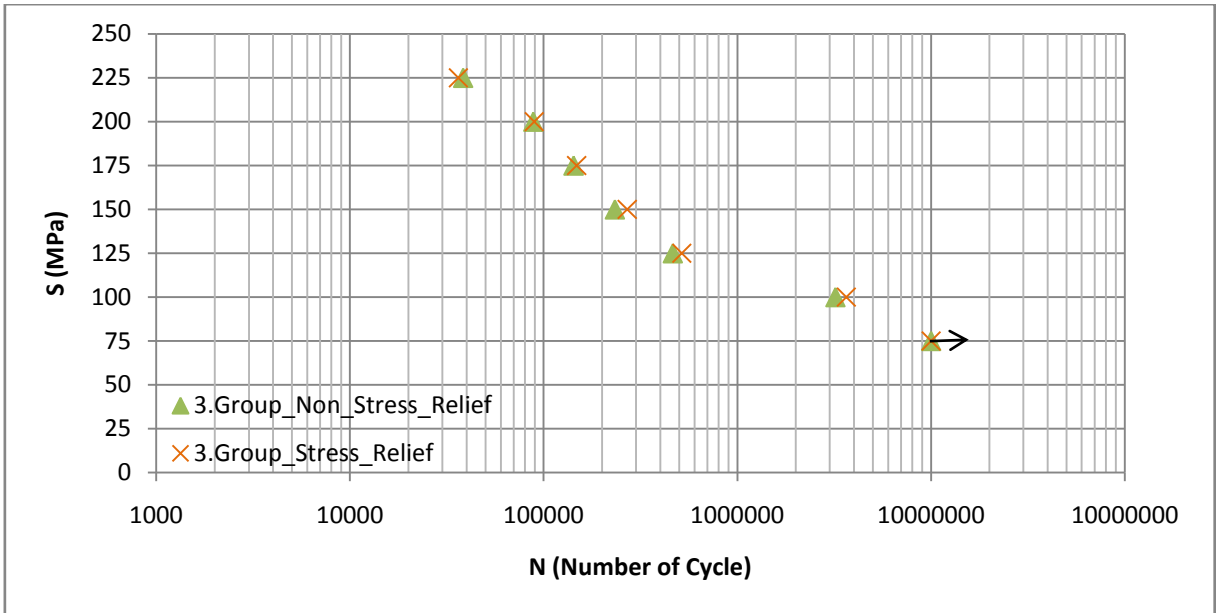


Figure 4.24: S-N values of 3rd group with and without stress relief process

As seen in Figure 4.22-4.24, the best values are obtained in the 3rd group and the worst results are obtained in the 1st group. Stress relief process improves the fatigue properties beside the tensile properties but it is not distinguishable for fatigue properties in each group.

Finally, all groups are compared with each others in Figure 4.25.

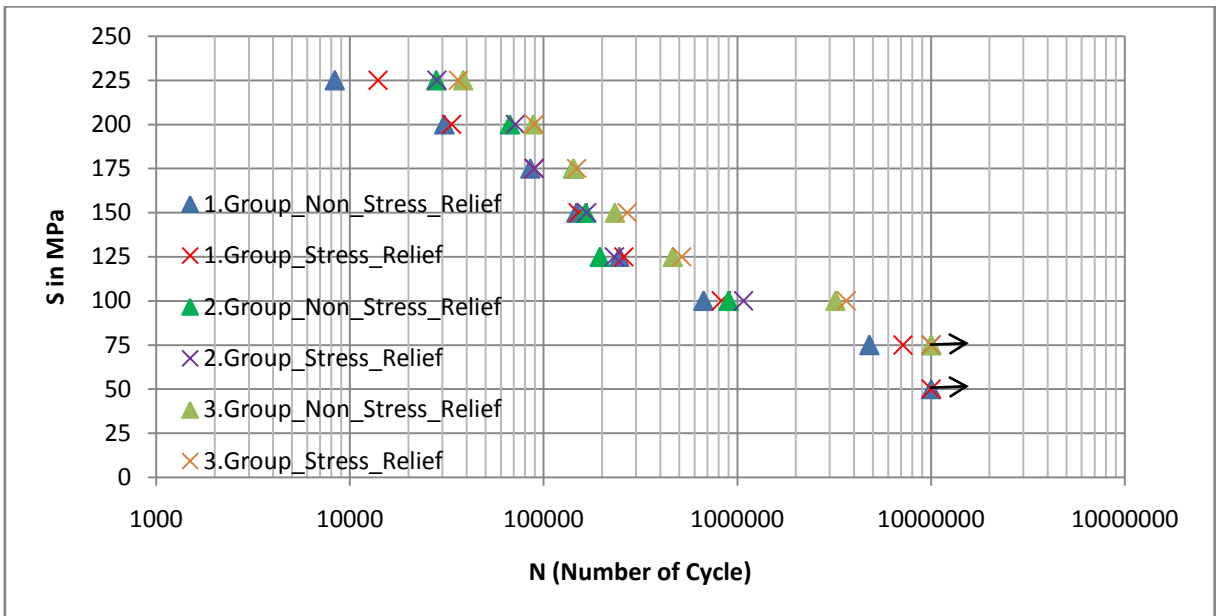


Figure 4.25: S-N values of all groups with and without stress relief process

5 Discussion

This study presents the different grain refinement levels which are new for related aluminium cylinder heads. Three different levels are developed for this type of cylinder heads and first group is determined as insufficient, second is determined as sufficient for today and third is determined as future option. In this view, this study is not only new approach for today but also it is an option for the future. Beside this, the samples are taken from combustion chamber of finished part directly and present the result the related industry directly. This approach gives the originality to this study. Finally, many factors can affect the results, that is why this study gives new results to the literature.

The results show that many parameters such as microstructure and cooling condition. First, the SDAS values were measured and the lowest SDAS values are obtained with higher grain refiner level. Ti and B react with and $TiAl_3$ and TiB_2 occur in the structure. These are plays role as nuclei in the structure. This chemical reaction makes the fine grains and grain boundary area is higher. The grain boundary hinders the dislocations. Dislocation cannot move easily in the structure and the strength of material is improved in fine grained structure. On the other hand, the cooling of part takes low time in higher cooling rate. During this time, grains cannot find time to be a bigger size. Similar to first paragraph, smaller grains give better mechanical properties.

Group with 23.11 SDAS value gives the worst SDAS values. Normally, these SDAS values could be evaluated as adequate when comparing other types of aluminium cylinder heads but it is not sufficient for related aluminium cylinder heads. Group with 19.74 SDAS value gives optimum SDAS values for related cylinder heads. The higher limit is around 19-20 μm for this type of cylinder head. Group with 15.71 SDAS value gives the best SDAS values. Therefore, the samples in the group with 15.71 SDAS value can be evaluated as a good option for future applications. The higher SDAS value limits are determined around 19-20 μm in current applications but it is obvious that this limit will be tightened in the future. Lower grain refinement additive levels of the group with 23.11 SDAS value are the reason of the worst results, so lower levels are not tested. On the other hand, higher grain refinement additive levels within the group with 15.71 SDAS value cannot show distinguishable differences in the group with 15.71 SDAS value. This situation is also noted by Hu and Li in the literature [Hu97]. Stress relief may affect the SDAS values.

The inclusions are extremely dangerous for the structure. In casting, one of the most important inclusions is oxide flake. Oxide flakes may occur in the structure because of high scrap ratio, slag inclusions and sand cores in the mould. The oxide flakes become an even more serious problem when they are big in size. In addition to casting defects, different cooling rates may lead to different mechanical properties. For instance, tensile test bar mould

which has a lower cooling rate shows worst mechanical properties. On the other hand, cylinder head mould which has a higher cooling rate gives better mechanical properties. In addition to this, the lower SDAS values which can be obtained with additional grain refiner lead to better mechanical properties such as UTS, YS and $\epsilon\%$. Although the group with 23.11 SDAS value specimens which are extracted from combustion chamber regions have the necessary UTS, YS and $\epsilon\%$, their SDAS value is above the allowed limit. Group with 19.74 SDAS value and group with 15.71 SDAS values not only have the necessary UTS, YS and $\epsilon\%$ but also comply with the allowed SDAS limit.

Rotating bending fatigue tests are carried out to obtain the Woehler (S-N) curve. Fatigue failures start with softening and hardening in the structure because of stress. Dislocations collapse and cause micro cracks on the surface. These micro cracks propagate to macro cracks and fatigue failure occurs in the structure. The most important point is that specimens do not give any warning before fracture. This situation may cause a disaster in the structure. Aluminium alloys do not have an endurance limit in Woehler (S-N) curve but 10^7 cycle numbers can be accepted as an endurance limit. When the specimens reach this number of cycles, the experiment can be stopped and the specimen can approved as having an infinite life.

In the tests, the group with 15.71 SDAS value which has the lowest SDAS gives the best results whereas group with 23.11 SDAS value which has the highest SDAS gives the worst results. Group with 19.74 SDAS value gives the results between group with 23.11 SDAS value and group with 15.71 SDAS values. Group with 15.71 SDAS value gives the best SDAS values and mechanical properties. However, the higher grain refiner (Ti and B) levels may cause an incremental cost in the long term.

The specimens which are extracted from the critical area (combustion chamber) show sufficient mechanical properties. On the other hand, the specimens which are poured into the tensile test bar mould gives insufficient mechanical properties because of worse cooling condition.

The effect of grain refiner on the mechanical properties is positive. The stress relief process also has a positive effect on the mechanical properties however this effect is not comparable with that of the grain refiner.

In conclusion, the group with 19.74 SDAS value is the optimum solution in today's conditions. However, it should be kept in mind that the limits will be tightened and mechanical demands will be increased in the future such that the group with 15.71 SDAS value is a good candidate for future applications.

6 Summary and Outlook

Microstructural parameters like secondary dendrite arm spacing (SDAS) strongly influence the quasistatic properties and especially, the fatigue properties of aluminium casting. The sizes of these, in turn, depend on different refining elements like Ti and B. To control these microstructural parameters, the influence of grain refinement must be investigated. This study analyzed the influence of grain refinement on the mechanical properties of cast aluminium alloy (AlSi6Cu4) used in automotive industry for cylinder heads.

After literature survey, the current state of the art in the optimum percentage of refining elements is determined and a framework for improving the mechanical properties is developed. Refining elements are added at different levels to check their influences on SDAS values. After grain refinement, stress relief is carried out over half of the specimens, so that the influence of post-refinement stress relief on the mechanical properties is investigated. The specimens are extracted from the cylinder head from the critical areas for mechanical tests. Microscopic analysis is carried out to measure the SDAS values. The optimum percentage of the refining elements for the required SDAS values is determined. Quasistatic mechanical properties as well as fatigue properties are investigated so that optimum percentage of Ti and B can be determined for highest ultimate tensile strength and yield strength values. Woehler (S-N) curves are generated and compared with the predetermined life cycles required for the product for conformance to the performance criteria.

The future expectation of automotive industry about aluminium cylinder head is getting better mechanical properties. Because of this, trying to getting lower SDAS will be continued in the future. First, new cooling water channels can be developed in the cylinder head mould. This approach cannot be possible for this study because present casting line and moulds are used in this study. Costs of new moulds may reach extremely high levels. Another reason of this, the mould design is created by primary producers and the modification of mould cannot be possible in the industry. Second, present casting line can be improved by increasing cooling time of mould before casting. More cooling time may lead to better mechanical properties, but time has a vital importance for automotive industry. Higher cooling time decrease the total number of cast cylinder heads and it could not be acceptable for primary producer. Because of these restrictions, the best solution is improving the present line with studying of grain refiners. For future, different Ti and B levels can be tried to improve the mechanical properties. Although AlTiB master alloys is dominant in the industry, other grain refiners such as zirconium can be tried on the manufacturing line.

7 References

- [Bac83] Backerud, L.: How does a good grain refiner work? *Light Metal Age* (1983) 6-12.
- [Bas07] Bast, J.; Kotova, Y.: Using of the casting simulation system 'PoligonSoft' for analysis of a temperature field of aluminium alloys. *Freiberger Forschungshefte*, ISBN 978-3-86012-319-5 (2007) 107-113.
- [Bec11] Becker, R.: The new 1.0-l three-cylinder MPI engine for the Up! ATZ extra worldwide Vol.16 Issue 3 (2011) 36-43.
- [Bel05] Belov, N.A.; Eskin, D.G.; Aksenov, A.A.: *Multicomponent phase diagrams: Application for commercial aluminum alloys*, 1st Edition. Elsevier Science (2005) 170.
- [Bir08] Birol, Y.; Ebrinç, A. A.: Critical material issues in cast aluminium cylinder heads. *Foundry Trade Journey*. Technical paper (2008) 196-199.
- [Bon99] Bonollo, F.; Tovo, R.: Fatigue in Al casting alloys: Metallurgical aspects. EAA – European Aluminium Association. TALAT Lecture 1254 (1999) 1-16.
- [Bor00] Boromei, I.; Ceschini L.; Morri, Al.; Morri, An.; Nicoletto, G.; Riva, E.: Influence of the solidification microstructure and porosity on the fatigue strength of Al-Si-Mg casting alloys. *Metallurgical Science and Technology*. Vol. 28-2 Ed.2000 (2000) 18-24.
- [Bro99] Brown, J.R.: *Foseco Non-Ferrous Foundryman's Handbook*. Butterworth Heinemann. (1999) 23.
- [Cam94] Campbell, J.; Harding, R.A.: Solidification defects in casting. EAA – European Aluminium Association. TALAT Lecture 3207 (1994) 1-29.
- [Cen80] Center Technique Des Industries De La Fonderie: *Atlas Metallographique De L'a-S5 U3*. Editions Techniques des Industries de la Fonderie. (1980) 1-32.
- [Çol09] Çolak, M.; Kayıkçı, R.: Investigation of grain refining effect of ALTIB master alloy addition on ETIAL 160 casting alloy. 5. International Advanced Technologies Symposium (IATS'09). Turkey (2009) 1-6.
- [Das04] DasGupta, R.; DasGupta, S.; Brown, C.: Factors affecting tensile properties of castings. SAE International, SAE World Congress Detroit, Michigan 2004-01-1021 (2004) 1-9.
- [DIN91] DIN 50125 Standard: Testing of metallic materials; tensile test pieces. With DIN ISO 10002 T 1/04.91 (1991) 1-8.

- [Dju12] Djurdjevič, M.B.; Grzinčič, M.A.: The effect of major alloying elements on the size of the secondary dendrite arm spacing in the as-cast Al-Si-Cu alloys. Archives of Foundry Engineering ISSN (1897-3310) Vol.12 Issue 1/2012, (2012) 19-24.
- [EN10] EN 1706 Standard: Aluminium and aluminium alloys – Casting – Chemical composition and mechanical properties. CEN European Committee for Standardization (2010) 10-16.
- [Fir07] Firouzdor, V.; Rajabi, M.; Nejati, E.; Khomamizadeh, F.: Effect of microstructural constituents on the thermal fatigue life of A319 aluminum alloy. Material Science and Engineering A 454 -455 (2007) 528-535.
- [Gop13] Gopikrishna, S.; Yeldose, B. C.: Study on effects of T6 heat treatment on grain refined A319 alloy with Magnesium and Strontium addition. International Journal on Theoretical and Applied Research in Mechanical Engineering (IJTARME) ISSN: 2319 – 3182, Volume-2, Issue-3 (2013) 59-62.
- [Gra88] Granger, D.A.; Elliott, R.: Solidification of eutectic alloys: Aluminum – Silicon alloys. ASM Handbook Casting. ASM International. Volume 15 (1988) 348-370.
- [Hu97] Hu, B.; Li, H.: Comparison of effects of master alloys containing titanium and/or boron on the grain size and dendrite arm spacing of DIN226S aluminium alloy. Journal of Materials Science 16 (1997) 1750-1752.
- [Hu98] Hu, B.; Li, H.: Grain refinement of DIN226S alloy at lower titanium and boron addition levels. Journal of Materials Processing Technology 74 (1998) 56-60.
- [Kau04] Kaufman, J.G.; Rooy, E.L.: Aluminium alloy castings: Properties, processes, and applications. ASM International (2004) 13-17.
- [Kli12] Kliemt, C.: Thermo-Mechanical fatigue cast aluminium alloys for engine applications under severe conditions. Heriot-Watt University. Doctorate Dissertation (2012)
- [Kni04] Knirsch, S.; Ambos, E.; Todte, M.: Material and process development for cylinder heads of high-performance combustion engines. MTZ worldwide Volume.65 Issue.4 (2004) 14-16.
- [Koh10] Köhler, E.; Klimesch, C.; Bechtle, S.; Stanchev, S.: Cylinder head production with gravity die casting. MTZ Worldwide Vol.71 Issue.9 (2010) 38-41.
- [Kon14] Konečná, R.; Nicoletto, G.; Riva, E.: Influence of microstructure and defect population on the fatigue performance of cast A356-T6 automotive components. Material Science Forum Vol. 782 (2014) 301-305.

- [Kor08] Kores, S.; Zak, H.; Tonn, B.: Aluminium alloys for cylinder heads. RMZ – Materials and Geoenvironment Vol.55 No.3 (2008) 307-317.
- [Mad11] Madlen, D.; Bolibruchova, D.: Influence of antimony on the mechanical properties and gas content of alloys AlSi6Cu4. Archives of foundry engineering. ISSN (1897-3310) Volume 11, Issue1/2011 (2011)73-78.
- [Maj02] Major, J.F.: Porosity control and fatigue behaviour in A356-T61 aluminum alloy. AFS (American Foundry Society) 97-94 (2002) 901-906.
- [Mat10] Mattos, J.J.I.; Uehara, A.Y.; Sato, M.; Ferreira I.: Fatigue properties and micromechanism of fracture of an AlSiMg0.6 cast alloy used in diesel engine cylinder head. Procedia Engineering 2 (2010) 759-765.
- [Mey97] Meyer, Ph.; Massinon, D.; Guerin, Ph.; Wong, L.: Influence of microstructure on the static and thermal fatigue properties of 319 alloys. SAE International, SAE International Congress & Exposition Detroit, Michigan 970705 (1997) 1-10.
- [Mol03] Molina, R.; Leghissa, M.; Mastrogiacomo L.: New developments in high performance cylinder heads: application of LHIP and split cylinder head concept. Metallurgical Science and Technology. A Journal published by Teksid Aluminium. Vol.22 No.2 (2003) 3-8.
- [Nef88] Neff, D.V.: Nonferrous molten metal processes. ASM Handbook Casting. ASM International. Volume 15 (1988) 964-1084.
- [NN02] N.N.; The Aluminium Automotive Manual: European Aluminium Association (2002).
- [NN11] N.N.; The Aluminium Automotive Manual: European Aluminium Association (2011).
- [NN12] N.N.; 1.0 It R3 MPI 4V Cylinder head technical presentation, Cevher Aluminium Foundry (2012) 1-88.
- [NN14] N.N.; Leaflet of hardness measurement regions for VW 404F cylinder heads. Cevher Aluminium Foundry (2014) 1-6.
- [NN15] N.N.; <http://www.cevherdokum.com> Cevher Aluminium Foundry. Retrieved on 30.01.2015.
- [Pav08] Pavlak, L.: Effect of filling conditions on the quality of cast aluminium cylinder heads. Metalurgija-Journal of Metallurgy. Association of Metallurgical Engineers of Serbia AMES. Vol.14 (2008) 31-39.

- [Pav10] Pavlovic-Krstic, J.: Impact of casting parameters and chemical composition on the solidification behaviour of Al-Si-Cu hypoeutectic alloy. Otto von Guericke Universität Magdeburg, Doctorate Dissertation (2010)
- [Per88] Perepezko, J.H.: Nucleation kinetics. ASM Handbook Casting. ASM International. Volume 15 (1988) 212-230.
- [Ran12] Rana, R.S.; Purohit, R.; Das, S.: Reviews on the influences of alloying elements on the microstructure and mechanical properties of aluminum alloys and of aluminum alloys composites. International Journal of Scientific and Research Publications. Vol.2 Issue.6 (2012) 1-7.
- [Ren14] Renault Standard 02-40-110/--H, Aluminium alloys for automobile moulded casting in house bought out, Normalisation Renault Automobiles DQ-EDP/Service (2014).
- [Rie04] Rie, K.T. and Schmidt, R.M.: (Low-Cycle Fatigue) Kurzzeitermüdung unter besonderer Berücksichtigung der Temperatur und des Umgebungsmediums. Ermüdungsverhalten metallischer Werkstoffe. Deutsche Gesellschaft für Metallkunde: Karlsruhe (2004) 397-418.
- [Rob01] Roberts, N.P.; Hart, N.R.: Instruction Manual HSM 19 mk3 Rotating fatigue machine. Hi-Tech Education. (2001) 1-17
- [Row93] Rowley, M.T.: International atlas of casting defects. International Committee of Foundry Technical Associations, American Foundrymen's Society. (1993) 9-40.
- [Ser11] Serbino, E.M.; Cândido, J.; Benedicto, E.R.: Secondary dendrite arm spacing refining in cylinder head by low pressure die casting process. SAE International Brasil, SAE Brasil International Congress and exhibition Sao Paulo, Brasil. 2011-36-0004 (2011) 1-8.
- [Sig07] Sigworth, G.K.; Kuhn, T.A.: Grain refinement of aluminum casting alloys. AFS Transactions. American Foundry Society, Schaumburg, USA 07-067(02) (2007) 1-12.
- [Sme14] Smetan, H.; Rathner, T.; Plank, K.H.: New innovative casting process and its first application in the efficient manufacturing of high-performance aluminum components. Giesserei Rundschau 61 Issue 1/2 (2014) 2-11.
- [Suh07] Suharno, B.; Nanda, I.P.; Harjanto, S.; Lirachandra E.: The influence of grain refiner on dendrite arm spacing of aluminum alloy ADC 12. Indonesian Journal of Materials Science Vol.8 No.2 (2007) 121-124.

- [Wan01] Wang, Q.G.; Apelian, D., Lados, D.A.: Fatigue behaviour of A356/357 aluminum cast alloys. Part II – Effect of microstructural constituents. *Journal of Light Metals* 1 (2001) 85-97.
- [Wic84] Wickberg, A.; Gustafsson, G.; Larsson, L.E.: Microstructural effects on the fatigue properties of a cast Al7SiMg alloy. SAE International, SAE International Congress & Exposition Detroit, Michigan 840121 (1984) 1-11.
- [Yu05] Yu, L.; Liu, X.; Wang, Z.; Bian, X.: Grain refinement of A356 alloy by AlTiC / AlTiB master alloys. *Journal of Materials Science* 40 (2005) 3865-3867.
- [Zha03] Zhang, B.; Garro, M.; Tagliano, C.: Dendrite arm spacing in aluminium alloy cylinder heads produced by gravity semi-permanent mold. *Metallurgical Science and Technology. A Journal published by Teksid Aluminium. Vol.21 No.1* (2003) 3-29.
- [Zha05] Zhang, B.; Garro, M.; Leghissa, M.; Giglio, A.; Tagliano, C.: Effect of dendrite arm spacing on mechanical properties of aluminum alloy cylinder heads and engine blocks. SAE International, SAE World Congress Detroit, Michigan 2005-01-1683 (2005) 1-9.
- [Zhu06] Zhu, X.; Shyam, A.; Jones, J.W.; Mayer, H.; Lasecki, J.V.; Allison, J.E.: Effects of microstructure and temperature on fatigue behaviour of E319-T7 cast aluminum alloy in very long life cycles. *International Journal of Fatigue. 28* (2006) 1566-1571.